

ABSTRACT

SAFAEI, FARINAZ. Characterization and Modeling of Asphalt Binder Fatigue. (Under the direction of Dr. Cassandra Castorena)

Fatigue cracking is a primary distress in asphalt pavements caused by the accumulation of damage under repeated traffic loading. Many factors influence fatigue damage in pavements, including pavement structure, environmental conditions, and asphalt mixture volumetric properties. Asphalt binder is the weakest asphalt concrete constituent and, thus, plays a critical role in determining the fatigue resistance of pavements. Therefore, the ability to characterize and model the inherent fatigue performance of an asphalt binder is a necessary first step to design. A comprehensive understanding and prediction of asphalt binder fatigue performance require a suitable experiment coupled with a model to predict how the binder will perform under various traffic, temperature, and structural conditions encountered in the field.

The simplified viscoelastic continuum damage (S-VECD) model has been used successfully by researchers to predict the damage evolution in asphalt mixtures for various traffic and climatic conditions using limited uniaxial test data. Although the literature shows promise for applying VECD modeling to asphalt binder fatigue, the past efforts have several shortcomings. It has been demonstrated that flow and adhesion loss can impede DSR fatigue test results. Thus, definition of test conditions (e.g., temperature) where cyclic DSR tests are appropriate for fatigue characterization of binders is necessary. In addition, the applicability of the model to predict fatigue performance under varying loading and thermal history has not been rigorously evaluated. Furthermore, the effects of material nonlinearity have been largely neglected in past modeling efforts for simplicity. In addition, past efforts have

employed the parallel plate DSR geometry for the fatigue characterization of asphalt binders. In the parallel plate geometry, the strain depends on the radial distance from the specimen center. Therefore, the material will fail at different rates as a function of radial location. Past efforts have neglected the radial strain gradient, using the apparent shear stress at the sample edge to infer fatigue damage and derive S-VECD model parameters. Apparent edge stress is calculated using linear mapping to the total torque, which is erroneous in the presence of material or geometric nonlinearities (such as cracking). This study seeks to overcome the aforementioned shortcomings of past efforts to improve the ability to characterize and predict asphalt binder fatigue.

© Copyright 2017 by Farinaz Safaei

All Rights Reserved

Characterization and Modeling of Asphalt Binder Fatigue

by
Farinaz Safaei

A doctoral dissertation submitted to the Graduate Faculty of
North Carolina State University
in partial fulfillment of the
requirements for the Degree of
Doctor of Philosophy

Civil Engineering

Raleigh, North Carolina

2017

APPROVED BY:

Cassandra Castorena, Assistant Professor
Chair of Advisory Committee

Murthy N. Guddati, Professor

Y. Richard Kim, Professor

Akhtarhusein Tayebali, Professor

Wenqiao Yuan, Professor

DEDICATION

This is dedicated to my parents, Ahmadreza Safaei and Betty Jamalifar, and my brother, Arsalan Safaei, who have always loved me and supported me unconditionally. I am truly blessed to have them in my life.

BIOGRAPHY

Farinaz Safaei was born in Esfahan, Iran on June 21, 1989 in a family whose members were oriented towards science. Her father, Ahmadreza Safaei, who is a well-known civil engineer, used to take her to his project sites and describe the challenges involved in each one. Under his care, Farinaz was brought into the world of civil engineering into which not many female students are prepared to venture. She attended the Farzanegan High school for exceptional talented students and graduated in 2007. She managed to rank among the top 0.1% of contestants in the math-physics area of Iran's nationwide university entrance exam in 2007. In 2007, she enrolled at Sharif University of Technology (SUT) to pursue a degree in Civil Engineering. During her undergraduate years, Farinaz became involved in research through an undergraduate research assistantship with Dr. Nader Tabatabaee. Following graduation, she moved to United States to continue her path while pursuing a Doctorate of Philosophy degree in Transportation Materials under the guidance of Dr. Cassie Castorena at North Carolina State University (NCSU). This document presents the culmination of the study and knowledge gained during this time at North Carolina State University.

ACKNOWLEDGMENTS

First, I would like to sincerely thank my adviser, Dr. Cassie Castorena, for her continuous guidance and support. Dr. Castorena challenged me with different aspects of research through all the years of PhD.

In addition, I would like to thank my advisory committee members, Dr. Richard Kim, Dr. Murthy N. Guddati, Dr. Akhtar A. Tayebali and Dr. Wenqiao Yuan for agreeing to serve and their assistance.

TABLE OF CONTENTS

LIST OF FIGURES	ix
LIST OF TABLES	xiv
CHAPTER 1 INTRODUCTION	1
1.1 Background	1
1.2 Objectives	4
1.3 Outline.....	4
CHAPTER 2 LINKING ASPHALT BINDER FATIGUE TO ASPHALT MIXTURE FATIGUE PERFORMANCE USING VISCOELASTIC CONTINUUM DAMAGE MODELING	7
2.1 Introduction.....	8
2.2 Background	11
2.2.1 Asphalt Binder Fatigue Testing in the DSR.....	11
2.2.2 Simplified Viscoelastic Continuum Damage Model Applied to Asphalt Binders	14
2.2.3 Linear Viscoelastic Modeling	26
2.3 Experimental Plan.....	28
2.3.1 Materials and Experimental Methods for Developing the S-VECD Model .	28
2.3.2 Use of Data from Past Studies to Evaluate the Linkage between Binder S- VECD Modeling and Mixture Performance	29
2.4 Results.....	31
2.4.1 Verification of Elastic-Viscoelastic Correspondence Principle	31
2.4.2 S-VECD Model Verification.....	33
2.4.3 Failure Criteria	37
2.4.4 Model Verification and Validation Using Binder Test Results	39
2.5 Linking Asphalt Binder S-VECD Results to Mixture and Field Performance	42
2.5.1 Linking Asphalt Binder and Mixture S-VECD Damage Characteristic Curves	42
2.5.2 Linking Asphalt Binder S-VECD Model Results to Field Performance	44
2.6 Conclusion	48
CHAPTER 3 IMPLICATION OF WARM MIX ASPHALT ON LONG TERM OXIDATIVE AGING AND FATIGUE PERFORMANCE OF ASPHALT BINDERS AND MIXTURES	50
3.1 Introduction.....	50
3.2 Objectives	51
3.3 Experimental Program	51
3.3.1 Materials and mix design	51

3.3.2	Laboratory aging methods.....	53
3.3.3	Asphalt binder testing.....	53
3.3.4	Asphalt mixture testing	54
3.4	Analysis methods	54
3.4.1	Linear viscoelasticity.....	54
3.4.2	Viscoelastic continuum damage analysis	56
3.5	Discussion of Results	60
3.5.1	Material-level results.....	60
3.5.2	Fatigue failure definition.....	67
3.5.3	Fatigue performance analysis.....	69
3.6	Conclusions.....	73
CHAPTER 4 TEMPERATURE EFFECTS IN LINEAR AMPLITUDE SWEEP		
TESTING AND ANALYSIS..... 75		
4.1	Introduction.....	75
4.2	Objectives	77
4.3	Developing Improved Specification for Selection of LAS Test Temperature	77
4.4	Incorporation of Temperature Effects into S-VECD Modeling of LAS Test	
Results	78
4.4.1	Simplified Viscoelastic Continuum Damage Modeling.....	78
4.4.2	Performance Prediction	80
4.5	Experimental Plan.....	84
4.5.1	Materials and Test Methods	84
4.5.2	Pavement Temperature Analysis.....	86
4.6	Results.....	87
4.6.1	Effect of Temperature on LAS Failure Mechanism and Relation to Binder Modulus	87
4.6.2	Application of Time-Temperature Superposition to S-VECD Damage Curves	88
4.6.3	Failure Criteria	91
4.6.4	Model Validation.....	92
4.6.5	Pavement Temperature Analysis.....	93
4.7	Conclusions.....	95
CHAPTER 5 MATERIAL NONLINEARITY IN ASPHALT BINDER FATIGUE		
TESTING AND ANALYSIS..... 97		
5.1	Introduction.....	97
5.2	Objective	101
5.3	Materials and Methods.....	102
5.3.1	Materials.....	102
5.3.2	Experimental Methods	102

5.4	Experimental Plan.....	107
5.5	S-VECD Modeling.....	107
5.5.1	Linear Viscoelastic Modeling	107
5.5.2	Simplified Viscoelastic Continuum Damage Modeling.....	108
5.6	Fatigue Life Prediction	110
5.7	Results.....	112
5.7.1	Repeated Stress Sweep (RSS) Test.....	112
5.7.2	Incremental Stress Sweep Test (ISS)	114
5.7.3	TS S-VECD Damage Characteristic Curves.....	116
5.7.4	Back-calculation of $ G^*/_{NLVE}$ in LAS tests using S-VECD Modeling.....	119
5.7.5	Comparison between $ G^*/_{NLVE}$ Values Determined from RSS Tests and Back Calculation using S-VECD Model.....	122
5.7.6	Implications of Nonlinearity on Failure Criteria.....	123
5.7.7	Validation of the $ G^*/_{NLVE}$ Back-calculation using S-VECD Modeling.....	124
5.7.8	Implications of Nonlinearity on Fatigue Life Predictions.....	127
5.8	Conclusions.....	130
Chapter 6 IMPROVED INTERPRETATION OF ASPHALT BINDER PARALLEL		
PLATE DYNAMIC SHEAR RHEOMETER (DSR) CYCLIC FATIGUE TESTS 132		
6.1	Introduction.....	132
6.2	Objectives	135
6.3	Theory.....	136
6.3.1	Parallel Plate Geometry.....	136
6.3.2	Cone and Plate Geometry.....	137
6.3.3	Linear Viscoelasticity.....	137
6.3.4	Nonlinear Viscoelasticity	138
6.3.5	Simplified Viscoelastic Continuum Damage Modeling.....	140
6.3.6	Accounting for the Nonlinear Radial Stress Gradient in Parallel Plate Fatigue Tests	142
6.4	Materials and Methods.....	146
6.5	Results.....	147
6.5.1	Mastercurves	147
6.5.2	RSS Test Results	149
6.5.3	Cone and Plate Fatigue Test Results.....	150
6.5.4	Prediction of Parallel Plate Torque Evolution S-VECD Calibrated using Cone and Plate (Forward Analysis)	156
6.5.5	Use of Parallel Plate Torque Evolution to Calibrate S-VECD Model (Backwards Analysis).....	158
6.6	Conclusions.....	161
Chapter 7 CONCLUSIONS 162		

REFERENCES..... 164

LIST OF FIGURES

Figure 2-1. PG64-22 binder monotonic test results.....	13
Figure 2-2. Schematic of asphalt binder master curve.....	19
Figure 2-3. Schematic representation of released and stored pseudo strain energy in the LAS test.....	24
Figure 2-4. Schematic depiction of determination of “A” for time sweep test.....	25
Figure 2-5. (a) Stress –Strain (b) Stress-pseudo strain relationship for selected cycles that correspond to time sweep testing of PG 64-22 binder at 3 percent strain amplitude and 15°C.	32
Figure 2-6. Time sweep damage characteristic curves shifted to a reference temperature of 20°C with $\alpha = 1/m$ for (a) PG64-22, (b) PG64-28, (c) PG58-28, and (d) PG70-22.	34
Figure 2-7. Time sweep damage characteristic curves shifted to a reference temperature of 20°C with $\alpha = 1+1/m$ for (a) PG 64-22, (b) PG 64-28, (c) PG 58-28, and (d) PG 70-22.....	35
Figure 2-8. LAS damage characteristic curves shifted to a reference temperature of 20°C with $\alpha = 1+1/m$ for (a) PG 64-22, (b) PG 64-28, (c) PG 58-28, and (d) PG 70-22.	36
Figure 2-9. Comparison of binder damage characteristic curves from (a) time sweep tests and (b) LAS tests.	37
Figure 2-10. GR vs. Nf failure criteria for (a) PG 64-22, (b) PG 64-28, (c) PG 58-28, and (d) PG 70-22.	38
Figure 2-11. Comparison of fatigue life measured in time sweep tests and predicted using S-VECD model calibrated using time sweep test results.	39
Figure 2-12. Comparison of fatigue life measured in time sweep tests and predicted by S-VECD model calibrated using LAS test results.....	41

Figure 2-13. Damage characteristic curves corresponding to: (a) binder STA, (b) mixture STA, (c) binder LTA1, (d) mixture LTA1, (e) binder LTA3, and (f) mixture LTA3. 43

Figure 2-14. Comparison between ALF (a) binder and (b) mixture damage characteristic curves. 44

Figure 2-15. Comparison between mixture and binder predictions of fatigue life using a binder-to-mix strain ratio of 80 (Safaei et al. 2014). 46

Figure 2-16. Comparison between measured field fatigue life and binder prediction of fatigue life using a binder-to-mix strain ratio of 80 (Wang et al. 2015). 48

Figure 3-1. STA master curves for (a) binders (b) mixtures, damage characteristic curves at a reference temperature of 19°C for (c) binders (d) mixtures. 62

Figure 3-2. LTA1 master curves for (a) binders (b) mixtures, damage characteristic curves at a reference temperature of 19°C for (c) binders (d) mixtures. 63

Figure 3-3. LTA3 master curves for (a) binders (b) mixtures, damage characteristic curves at a reference temperature of 19°C for (c) binders (d) mixtures. 64

Figure 3-4. Trends in aging index property. 65

Figure 3-5. $|E^*|$ ratio ($|E^*|$ after long-term aging / $|E^*|$ after short-term aging) values at 10 Hz loading frequency. 66

Figure 3-6. Fatigue failure definitions for (a) asphalt mixtures and (b) asphalt binders. 67

Figure 3-7. Fatigue failure definitions for (a) asphalt mixtures and (b) asphalt binders. 68

Figure 3-8. C at failure values for (a) mixtures and (d) binders. 68

Figure 3-9. Fatigue performance analysis results for asphalt mixtures: (a) HMA, (b) Foam WMA, (c) Evotherm WMA, and (d) Fatigue life comparison of the mixtures. 71

Figure 3-10. Comparison between mixture and binder fatigue life. 73

Figure 4-1. Depiction of (a) failure definition (b) calculation of released PSE.....	81
Figure 4-2. LAS failure mechanisms.....	87
Figure 4-3. Comparison of LAS damage characteristic curves before application of time-temperature superposition (TTS) for (a) PG64-22 (c) PG64-28 (e) PG58-28 (g) PG70-22 and after application of TTS for (b) PG64-22 (d) PG64-28 (f) PG58-28 (h) PG70-22.....	90
Figure 4-4. GR vs. Nf for (a) PG64-22 (b) PG64-28 (c) PG58-28 (d) PG70-22.....	91
Figure 4-5. Comparison between measured and LAS predicted fatigue lives with (a) delineation by binder type and (b) delineation by test temperature.....	93
Figure 4-6. Average of mean temperatures of representative locations for all the tested binders for 24 and peak hours of spring and annual.	94
Figure 5-1.(a) RSS loading history schematic, and (b) example RSS results (Underwood and Kim 2015).	104
Figure 5-2. Illustration of ISS test: (a) applied stress (b) strain responses (Branco 2008)...	106
Figure 5-3. RSS test results for PG 58-28 at 20°C.	113
Figure 5-4. $/G^*/_{NLVE}$ relationship with strain for (a) PG 64-22 (b) PG 64-28 (c) PG 58-28 (d) PG 70-22 at 20°C.....	114
Figure 5-5. ISS strain response at (a) 20°C, (b) 15°C, and (c) 10°C.	115
Figure 5-6. Comparison of $/G^*/_{NLVE}$ values determined using ISS and RSS method for PG 70-22 at 20°C.....	116
Figure 5-7. S-VECD damage characteristic curves for TS at the reference temperature of 20°C for (a) PG 64-22 (b) PG 64-28 (c) PG 58-28 (d) PG 70-22.....	117
Figure 5-8. LVE vs. NLVE TS damage curves for (a) PG 64-22 (b) PG 64-28 (c) PG 58-28 (d) PG 70-22 at 20°C.	118

Figure 5-9. Measured vs. predicted C^* vs. N for TS test for PG 64-22 at 20°C, 4% strain. 121

Figure 5-10. Comparison of measured and predicted shear stress for PG 64-28 at 20°C (a) before optimization (b) after optimization (c) back calculated $|G^*|_{NLVE}$ relationship with strain..... 122

Figure 5-11. Comparison of $|G^*|_{NLVE}$ values determined using RSS and back calculation method for PG 70-22 at 20°C..... 123

Figure 5-12. G^R vs. N_f using linear vs. nonlinear S-VECD for (a) PG 64-22 (b) PG 64-28 (c) PG 58-28 (d) PG 70-22. 124

Figure 5-13. Back calculated $|G^*|_{NLVE}$ for standard LAS and LAS with 0.00008 s^{-1} CSR at 20°C for (a) PG 64-22 (b) PG 64-28 (c) PG 58-28 (d) PG 70-22. 125

Figure 5-14. Nonlinear S-VECD damage characteristic curves for (a) PG 64-22 (b) PG 64-28 (c) PG 58-28 (d) PG 70-22..... 126

Figure 5-15. Comparison of measured and predicted fatigue lives for LAS test with CSR value of 0.00008 s^{-1} using nonlinear S-VECD. 127

Figure 5-16. Comparison of measured and predicted fatigue lives when using LAS test results within (a) linear S-VECD log scale (b) nonlinear S-VECD log scale (c) linear S-VECD linear scale (d) nonlinear S-VECD linear scale. 129

Figure 6-1. Parallel plate geometry..... 133

Figure 6-2. Parallel plate failure surface..... 133

Figure 6-3. Cone and plate geometry..... 134

Figure 6-4. Comparison of the mastercurves at 1 percent strain amplitude for CP and PP geometries for a) PG 64-22 b) PG 70-22 c) PG 58-28. 148

Figure 6-5. Comparison of modified parallel plate and cone and plate $/G^*/_{NLVE}$ for (a) PG 64-22 (b) PG 70-22 (c) PG 58-28 at 20°C.	150
Figure 6-6. Failure surface cone and plate geometry.....	151
Figure 6-7. Determination of failure point for PG 64-22 TS at 20°C at 4% strain amplitude.	152
Figure 6-8. S-VECD damage characteristic curves for TS at the reference temperature of 20°C for (a) PG 64-22 (b) PG 70-22 (c) PG 58-28.....	153
Figure 6-9. G^R vs. N_f for (a) PG 64-22 (b) PG 70-22 (c) PG 58-28.....	154
Figure 6-10. Measured vs. predicted C^* vs. N for TS test for PG 64-22 at 20°C, 4% strain.	155
Figure 6-11. Comparison of measured and predicted fatigue lives using S-VECD model derived from the cone and plate geometry.....	156
Figure 6-12. Shear stress distribution within parallel plate geometry for TS PG 58-28 at 20°C and 3% strain.....	157
Figure 6-13. Comparison of measured and predicted torque 20°C for (a) PG 64-22 TS 4% strain (b) PG 70-22 TS 3% strain (c) PG 58-28 TS 4% strain.....	158
Figure 6-14. Comparison of damage curves from cone and plate and damage curves at the edge of parallel plate for a) PG 64-22 TS 4% strain b) PG 70-22 TS 3% strain c) PG 58-28 TS 4% strain at 20°C.	159
Figure 6-15. Comparison of predicted fatigue lives using corrected shear stress in parallel plate versus measured fatigue lives in cone and plate using nonlinear S-VECD.	161

LIST OF TABLES

Table 2-1. Experimental plan.....	29
Table 2-2. m value for tested binders.....	35
Table 3-1. Asphalt Mixture and Binder S-VECD Analysis Frameworks.....	59
Table 4-1. Experimental Plan.	85
Table 4-2. Relationship between $ G^* LVE$, Test Temperature, and Failure Mechanism.	88
Table 4-3. Comparison between Average Spring Pavement Temperature and Climatic PG. 95	
Table 5-1. Experimental Plan.	107
Table 6-1. Experimental Plan	147

CHAPTER 1 INTRODUCTION

1.1 Background

Asphalt pavements constitute a major component of civil infrastructure. Over 90% of the roads in the United States have an asphaltic surface, resulting in the consumption of 30 million tons of asphalt binder annually (FHWA 2006). Increases in traffic volumes in recent years have led to aging and deterioration of the nation's roadways (FHWA 2006). Asphalt binder plays a critical role in pavement performance. Therefore, the ability to characterize and model the performance of an asphalt binder is a necessary first step to design mixtures and pavements that are not susceptible to premature failure.

Fatigue cracking is a primary distress in asphalt pavements caused by the accumulation of damage under repeated traffic loading. Many factors influence fatigue damage in pavements, including pavement structure, environmental conditions, and asphalt mixture volumetric properties. Visual observation of fracture surfaces from laboratory fatigued asphalt mixture specimens indicate failure generally occurs cohesively, in the absence of moisture (Lee and Kim 2014). Therefore, the inherent fatigue resistance of the asphalt binder contained within the pavement is also expected to affect pavement fatigue performance. Therefore, the ability to characterize and model the inherent fatigue performance of an asphalt binder is a necessary first step to design mixtures and pavements that are not susceptible to premature fatigue failure. A comprehensive understanding and prediction of asphalt binder fatigue performance require a suitable experiment coupled with a model to predict how the binder will perform under various traffic, temperature, and structural conditions encountered in the field.

In the current Superpave Performance Graded (PG) specifications for asphalt binders, a single point parameter measured within the linear viscoelastic regime at a single temperature is used to evaluate fatigue performance (Bahia et al. 2001). Research has shown that this parameter is not a good indicator of damage resistance, particularly in the case of modified asphalts because it does not consider the effects of repeated traffic loading (Soenen and Eckmann 2000).

Therefore, alternative approaches have been proposed to quantify binder resistance to damage which utilize repeated cyclic loading in the Dynamic Shear Rheometer (DSR). These DSR-based fatigue tests include the time sweep (TS) and Linear Amplitude Sweep (LAS) test (AASHTO TP 101). The TS test consists of applying sinusoidal loading at fixed amplitude and frequency. The LAS test is also consists of sinusoidal loading at fixed frequency. However, the strain amplitude is systematically increased in the LAS test to accelerate fatigue tests and improve practicality for specification. In both the TS and LAS tests, the reduction in loading resistance with increasing number of loading cycles is used to infer fatigue damage.

One of the more widely used mechanistic models for predicting the fatigue performance of asphalt concrete is the viscoelastic continuum damage (VECD) model, e.g., (Lee and Kim 1998, Daniel and Kim 2002, Kutay et al. 2008, Underwood et al. 2010, Sabouri and Kim 2014, Norouzi and Kim 2015). The continuum damage modeling approach ignores complicated microscale behavior. Rather, continuum damage modeling quantifies the damage evolution based on the effective stiffness reduction, which comprises the net effect of the growth of microdefects. The VECD model further allows for differentiating viscoelasticity from the effect of damage on measured macroscale stiffness using Schapery's extended elastic-viscoelastic correspondence principle (Schapery 1984). The VECD model allows a constitutive relationship with damage to be derived based on a path-independent damage characteristic curve, which can be obtained

using relatively limited uniaxial tests of asphalt concrete mixtures. Furthermore, a simplified procedure to derive the VECD model based on uniaxial cyclic direct tension testing, termed the simplified VECD model, i.e., the S-VECD model, has been formalized into a standard procedure (AASHTO TP 107-14).

The VECD modeling approach has recently been extended to asphalt binders tested using the TS and LAS test methods (Johnson et al. 2009, Wen and Bahia 2009, Hintz et al. 2011, Underwood 2016). Although the literature shows promise for applying VECD modeling to asphalt binder fatigue, the past efforts have several shortcomings. It has been demonstrated that flow and adhesion loss can impede DSR fatigue test results (Hintz and Bahia 2013, Safaei et al. 2016). Thus, definition of test conditions (e.g., temperature) where cyclic DSR tests are appropriate for fatigue characterization of binders is necessary. In addition, the applicability of the model to predict fatigue performance under varying loading and thermal history has not been rigorously evaluated. Furthermore, the TS and LAS test include strain amplitudes that are expected to exceed the linear viscoelastic limit of the material (Underwood 2016). However, the effects of material nonlinearity have been largely neglected in past modeling efforts for simplicity. In addition, past efforts have employed the parallel plate DSR geometry for the fatigue characterization of asphalt binders (Bahia et al. 2001, Safaei et al. 2016, Underwood 2016, Shan et al. 2017). In the parallel plate geometry, the strain depends on the radial distance from the specimen center. Therefore, the material will fail at different rates as a function of radial location. Past efforts have neglected the radial strain gradient, using the apparent shear stress at the sample edge to infer fatigue damage and derive S-VECD model parameters. Apparent edge stress is calculated using linear mapping to the total torque, which is erroneous in the presence of material or geometric nonlinearities (such as cracking). This study seeks to overcome the

aforementioned shortcomings of past efforts to improve the ability to characterize and predict asphalt binder fatigue.

1.2 Objective and Tasks

The main objective of this research is to improve the fatigue testing and modeling of asphalt binder to enable the accurate prediction of fatigue performance under variable temperatures and loading conditions which reflect asphalt mixtures and pavements. To achieve this overarching objective, five specific tasks were undertaken as follows:

1. Develop and validate an S-VECD modelling framework that is applicable to asphalt binders subjected to cyclic fatigue loading in the DSR.
2. Establish the appropriate test conditions for asphalt binder fatigue characterization in the DSR.
3. Evaluate the ability of asphalt binder fatigue test results coupled with S-VECD modeling to reflect asphalt mixture fatigue performance.
4. Develop an approach to separate material nonlinearity from damage in asphalt binder DSR fatigue test results.
5. Develop a methodology to account for the nonlinear radial gradient in shear stress when interpreting parallel plate DSR fatigue tests.

1.3 Outline

This document consists of seven chapters, organized as follows:

- Chapter 1 provides the introduction and motivation for the research conducted. The objective and required tasks are stated and an outline for the remaining dissertation is presented.
- Chapter 2 describes the derivation and assessment of S-VECD modeling framework that can be applied to asphalt binder fatigue test results. The ability of asphalt binder fatigue tests coupled with S-VECD analysis to reflect asphalt mixture fatigue performance is demonstrated. This chapter has been accepted for publication as: Safaei, F., Castorena, C. and Kim, Y.R. “Linking Asphalt Binder Fatigue to Asphalt Mixture Fatigue Performance Using Viscoelastic Continuum Damage Modeling” in the Journal of Mechanics of Time-Dependent Materials, 2016, doi:10.1007/s11043-016-9304-1.
- Chapter 3 validates that the S-VECD model applied to asphalt binder DSR results reflects asphalt mixture fatigue performance. This chapter has been published as: Safaei, F., Lee, J., Nascimento, L. A. H., Hintz, C, and Kim, Y.R. “Implications of Warm-Mix Asphalt on Long Term Oxidative Aging and Fatigue Performance of Asphalt Binders and Mixtures: in Journal of Association of Asphalt Paving Technology, Vol 15, 2015, pp 45–61.
- Chapter 4 describes a study undertaken to develop a framework to select asphalt binder fatigue test temperature to avoid confounding effects of adhesion loss and flow while also reflecting critical climatic conditions. The applicability of time-temperature superposition to the S-VECD model is also demonstrated. This chapter has been published in Transportation Research Record as: Safaei, F., and Castorena,

- C. “Temperature Effects in Linear Amplitude Sweep Testing and Analysis” in the Journal of Transportation Research Record, 2016.
- Chapter 5 describes an effort undertaken to develop an approach to separate the effects of nonlinearity from fatigue damage in cyclic DSR test results. This chapter has been prepared for consideration of publication in the Materials and Design: Safaei, F., and Castorena, C. “Material Nonlinearity in Linear Amplitude Sweep Testing and Analysis”, 2017.
 - Chapter 6 describes the use of S-VECD modeling to account for the nonlinear change in stress with radial distance from the specimen center. This chapter has been prepared for consideration of publication in the Journal of Materials in Civil Engineering: Safaei, F., and Castorena, C. “Improved Interpretation of Asphalt Binder Parallel Plate Dynamic Shear Rheometer Fatigue Tests”, 2017.
 - Chapter 7 summarizes the main findings and contributions of this research.

CHAPTER 2 LINKING ASPHALT BINDER FATIGUE TO ASPHALT MIXTURE FATIGUE PERFORMANCE USING VISCOELASTIC CONTINUUM DAMAGE MODELING¹

Fatigue cracking is a major form of distress in asphalt pavements. Asphalt binder is the weakest asphalt concrete constituent and, thus, plays a critical role in determining the fatigue resistance of pavements. Therefore, the ability to characterize and model the inherent fatigue performance of an asphalt binder is a necessary first step to design mixtures and pavements that are not susceptible to premature fatigue failure. The simplified viscoelastic continuum damage (S-VECD) model has been used successfully by researchers to predict the damage evolution in asphalt mixtures for various traffic and climatic conditions using limited uniaxial test data. In this study, the S-VECD model, developed for asphalt mixtures, is adapted for asphalt binders tested under cyclic torsion in a dynamic shear rheometer. Derivation of the model framework is presented. The model is verified by producing damage characteristic curves that are both temperature- and loading history-independent based on time sweep tests, given that the effects of plasticity and adhesion loss on the material behavior are minimal.

The applicability of the S-VECD model to the accelerated loading that is inherent of the linear amplitude sweep test is demonstrated, which reveals reasonable performance predictions, but with some loss in accuracy compared to time sweep tests due to the confounding effects of nonlinearity imposed by the high strain amplitudes included in the test. The asphalt binder S-

¹ This chapter has been published as: Safaei, F., Castorena, C. and Kim, Y.R. "Linking Asphalt Binder Fatigue to Asphalt Mixture Fatigue Performance Using Viscoelastic Continuum Damage Modeling" *Journal of Mechanics of Time-Dependent Material*, 2016,20(3), 299-323.

VECD model is validated through comparisons to asphalt mixture S-VECD model results derived from cyclic direct tension tests and Accelerated Loading Facility performance tests. The results demonstrate good agreement between the asphalt binder and mixture test results and pavement performance, indicating that the developed model framework is able to capture the asphalt binder's contribution to mixture fatigue and pavement fatigue cracking performance.

2.1 Introduction

Fatigue damage is a critical distress in asphalt pavements and is caused by the accumulation of damage under repeated traffic loading. The fatigue cracking resistance of an asphalt pavement is dictated by the structure (layer thickness), mixture type and volumetrics, and inherent fatigue cracking resistance of the asphalt binder. Asphalt binder is the weakest asphalt concrete constituent and, thus, fatigue cracks initiate and propagate cohesively through the binder phase of the mix and / or at the asphalt – aggregate interface.

Visual observation of fracture surfaces from laboratory fatigued asphalt mixture specimens indicate failure generally occurs cohesively, in the absence of moisture (Lee and Kim 2014). Therefore, the ability to characterize and model the inherent fatigue performance of an asphalt binder is a necessary first step to design mixtures and pavements that are not susceptible to premature fatigue failure. Comprehensive understanding and prediction of asphalt binder fatigue performance require a suitable experiment coupled with a model to predict how the binder will perform under various traffic, temperature, and structural conditions encountered in the field.

A great deal of attention has been given to characterizing and modeling the complex fatigue behavior of asphalt mixtures. However, relatively little attention has been given to

characterizing and modeling asphalt binder fatigue performance. Traditionally, asphalt concrete fatigue performance has been modeled using empirical approaches that utilize predictive schemes that employ a power law relationship between some input parameter (e.g., stress, strain) and the number of cycles to failure (Monismith et al. 1970). Deriving such a power law relationship requires extensive testing at multiple loading amplitudes. The empiricism and extensive testing requirements of the traditional approach for fatigue analysis have prompted many researchers to apply mechanistic models to characterize the fatigue of asphalt concrete.

One of the more widely used mechanistic models for predicting the fatigue performance of asphalt concrete is the viscoelastic continuum damage (VECD) model, e.g., (Lee and Kim 1998, Daniel and Kim 2002, Kutay et al. 2008, Underwood et al. 2010, Sabouri and Kim 2014, Norouzi and Kim 2015). The continuum damage modeling approach ignores complicated microscale behavior. Rather, continuum damage modeling quantifies the damage evolution based on the effective stiffness reduction, which comprises the net effect of the growth of microdefects. The VECD model further allows for differentiating viscoelasticity from the effect of damage on measured macroscale stiffness using Schapery's extended elastic-viscoelastic correspondence principle (Schapery 1984). The VECD model allows a constitutive relationship with damage to be derived based on a path-independent damage characteristic curve, which can be obtained using relatively limited uniaxial tests of asphalt concrete mixtures. In addition, Chehab et al. (2002) demonstrated that time-temperature superposition remains valid during micro-cracking, and hence, the effects of temperature can easily be modeled using the VECD approach.

Furthermore, a simplified procedure to derive the VECD model based on uniaxial cyclic direct tension testing, termed the simplified VECD model, i.e., the S-VECD model, has been formalized into a standard procedure (AASHTO TP 107-14). A recently developed failure

criterion has been incorporated into the S-VECD model framework to allow for the accurate prediction of fatigue failure under any loading condition of interest (Sabouri and Kim 2014). The S-VECD model also has been incorporated successfully into pavement structural analyses for performance prediction (Norouzi and Kim 2015).

The VECD modeling approach has recently been extended to asphalt binders tested using torsional loading in a dynamic shear rheometer (DSR). Wen and Bahia (2009) first investigated the applicability of the VECD model to asphalt binders under monotonic constant strain-rate shear loading in the DSR. They found that the relationship between material integrity and internal damage is independent of the strain rate for neat binders. However, the model was found to be inapplicable for monotonic test results of polymer-modified binders that display two-phase behavior in monotonic tests (Johnson et al. 2009). At a low strain level, the binder dominates the response to loading. However, at a high strain level, the binder yields and the polymer network is activated, leading to distinct changes in behavior that cannot be captured using a continuum damage approach (Johnson et al. 2009).

Therefore, Johnson (2010) proposed an application of a VECD-based model to asphalt binders subjected to cyclic loading in a DSR whereby the excessively high strains associated with monotonic testing were avoided. In this effort, Johnson (2010) introduced the linear amplitude sweep (LAS) test, which utilizes systematically increasing strain amplitudes to accelerate damage and was later formalized in (AASHTO TP 101). However, Johnson (2010) did not rigorously evaluate the validity of the extended elastic-viscoelastic correspondence principle and demonstrated that, although the VECD modeling of the LAS test results gave a reasonable ranking of the materials, the fatigue life predictions were inaccurate.

Hintz et al. (2011) followed the VECD model framework proposed by Johnson (2010) and showed promising correlations between the binder performance predictions and pavement performance data. Later, Safaei et al. (2014) refined the VECD model approach proposed by Johnson (2010) to better reflect the underlying VECD theory and current S-VECD asphalt mixture model. Their results demonstrated promising agreement between the asphalt binder and mixture fatigue performance predictions. Wang et al. (2015) incorporated an energy-based failure criterion to improve the predictive capabilities of the binder VECD model. Safaei and Castorena (2016) recently demonstrated the applicability of the time-temperature superposition principle to the VECD modeling of asphalt binders subjected to cyclic loading in the DSR.

Although the literature shows promise for applying VECD modeling to asphalt binder fatigue, past studies have failed to justify and validate the selected model framework in a rigorous manner. This study presents a rigorous derivation and assessment of the S-VECD model for asphalt binder fatigue, including assessment of the model's ability to capture the effects of loading history, temperature, and loading mode. The developed framework is validated through comparison to asphalt mixture S-VECD model results derived from cyclic direct tension tests and measured pavement performance obtained from the Federal Highway Administration (FHWA 2006) Accelerated Loading Facility (ALF).

2.2 Background

2.2.1 Asphalt Binder Fatigue Testing in the DSR

Current asphalt binder specifications dictate that the parameter $|G^*| \cdot \sin \delta$ is measured in a DSR at a small strain level over a limited number of load cycles to evaluate fatigue resistance. This procedure lacks the ability to characterize damage resistance, and thus, VECD models

cannot be applied directly to these specification test results. However, several damage-inducing tests can be implemented in a DSR. Bahia et al. (2001) introduced the time sweep test as a means to characterize the fatigue resistance of asphalt binders in the DSR.

The time sweep test consists of repeated cyclic loading in the DSR in either stress- or strain-controlled mode, which is similar to many fatigue tests for characterizing asphalt mixture fatigue. However, the time sweep test poses some challenges for routine use because it is time-consuming and a strain or stress amplitude must be selected that will produce failure in a reasonable amount of time. Such selection is not possible without a priori knowledge of the binder's fatigue resistance.

Therefore, two alternative procedures have been proposed under the assumption that their results can be input into a VECD model to derive fatigue responses under any loading history of interest with limited but efficient material characterization. These two test methods are monotonic tests (Wen and Bahia 2009) and the LAS test (AASHTO TP 101). The monotonic test consists of subjecting asphalt binder to constant strain rate loading (i.e., noncyclic loading) in a DSR. In contrast, the LAS test (AASHTO TP 101) includes an oscillatory strain amplitude sweep that consists of linearly increasing strain amplitudes from 0.1 percent to 30 percent over the course of just five minutes. The LAS test has been found to induce significant damage in all binders, irrespective of their fatigue resistance (e.g., modified versus unmodified).

As discussed previously, monotonic testing has been demonstrated to give rise to problems when testing modified asphalt. Nevertheless, monotonic tests were evaluated for this study, and further problems were identified when using the test to characterize asphalt binder damage resistance. Representative monotonic test results for a neat PG 64-22 asphalt binder are shown in Figure 2-1, including both shear and normal (compressive) stress evolutions with time.

Note that the results presented in Figure 2-1 represent typical trends, irrespective of binder type, strain rate, or test temperature. Typically, in DSR tests, only the shear results are considered. However, normal forces also can be monitored using a DSR. The results presented in Figure 2-1 demonstrate the significant development of normal stresses within the sample in addition to shear. These stresses are speculated to be the result of the Weissenberg effect, which can lead to the development of normal stresses in viscoelastic materials subjected to shear (Weissenberg 1947). Such normal stresses are not observed in cyclic tests, which impose much lower shear strains than monotonic tests. Normal stresses will affect the resultant damage growth, which precludes their use in calibrating the S-VECD model. Therefore, the primary focus of this study is to apply the S-VECD model to asphalt binders subjected to cyclic loading.

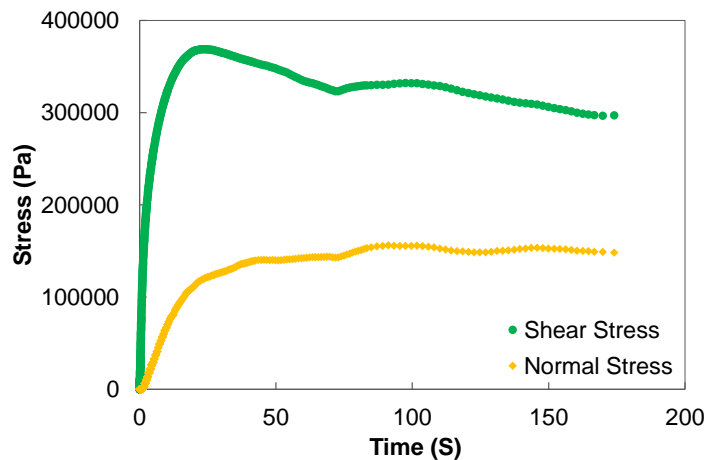


Figure 2-1. PG64-22 binder monotonic test results.

In tests where the asphalt binder is subjected to damage-inducing cyclic loading in the DSR, failure will occur via the formation of radial cracks that start at the sample periphery (where strain levels are the highest) and grow inward, assuming that adhesion loss and plastic flow are avoided (Hintz and Bahia 2013). This process is distinct from that of uniaxial tests that

are used to develop asphalt mixture S-VECD models. In uniaxial testing, there is a uniform stress state, and thus, distributed microcracks develop throughout the sample. Safaei and Castorena (2016) demonstrated that cohesive cracking failure occurs in cyclic asphalt binder DSR tests when the initial sample's dynamic shear modulus value is between 12 MPa and 60 MPa at the given test temperature and frequency based on visual observations of sample geometry and morphology following fatigue testing and adherence of results to the S-VECD model. Adhesion loss between the sample and the DSR plates is likely to occur when the modulus value of the sample exceeds 60 MPa, and edge flow impedes the results if the sample modulus value is lower than 12 MPa. When cohesive cracking is the failure mechanism, the formation of radial cracks within the sample will lead to a reduction in the effective area over which the stresses are distributed. This process results in a macroscale measure of loss in material stiffness, which can be used within the VECD model to quantify damage growth.

2.2.2 Simplified Viscoelastic Continuum Damage Model Applied to Asphalt Binders

The S-VECD model is comprised of four primary components: (1) Schapery's extended elastic-viscoelastic correspondence principle for separating the effects of damage and viscoelasticity on measured stiffness, (2) Schapery's work potential theory for modeling the effects of damage on macroscopic constitutive behavior, (3) the time-temperature superposition principle for modeling the temperature effects on damage growth, and (4) a failure criterion for modeling the effects of loading and temperature history on ultimate fatigue failure. Each of the S-VECD model components is assessed rigorously herein in the context of asphalt binder fatigue. First, a brief introduction to each model component is presented. Next, an assessment of the applicability of each component to the asphalt binder test results is presented. Finally, the

model is verified and validated using asphalt mixture fatigue test results and observed pavement performance.

2.2.2.1 Elastic – Viscoelastic Correspondence Principle

Schapery's extended elastic-viscoelastic correspondence principle allows for the elimination of the effects of viscoelasticity on measured macroscale stiffness and consequently reduces a viscoelastic problem to the form of the corresponding elastic case by replacing the physical strain with pseudo strain (Schapery 1984). Pseudo strain is defined in Equation (2.1).

$$\gamma^R = \frac{1}{G_R} \int_0^{t_R} G(t_R - \xi) \frac{d\gamma}{d\xi} d\xi \quad (2.1)$$

where $G(t)$ is the relaxation modulus, t_R is the reduced time, ξ is a time variable of integration, and G_R is an arbitrary reference modulus, selected to be one. Given the definition of linear viscoelastic stress (τ) shown in Equation (2.2), it can be seen that the definition of linear viscoelastic stress can be reduced to the form of Hooke's law for elastic materials, shown in Equation (2.3). Note that if G_R is selected to be one, which is the case herein, the magnitude of the pseudo strain is equivalent to the linear viscoelastic stress response to a given loading history.

$$\tau = \int_0^{t_R} G(t_R - \xi) \frac{d\gamma}{d\xi} d\xi \quad (2.2)$$

$$\tau(t) = G_R \cdot \gamma^R \quad (2.3)$$

The pseudo strain concept allows for calculation of the pseudo stiffness (C), which is a function of the damage level (S) as given in Equation (2.4).

$$C(S) = \frac{\tau}{\gamma^R} \quad (2.4)$$

Pseudo stiffness is an indicator of material integrity, which accounts for the viscoelasticity effects on the measured stress response. Because pseudo strain is equivalent to the linear viscoelastic stress response, Equation (2.4) implies that C will be one if the material is behaving in a linear viscoelastic manner and will decrease as the stress deviates from linear viscoelasticity because of damage.

In the case of cyclic loading applied in the DSR with zero mean strain, the peak pseudo strain in a given cycle can be approximated using Equation (2.5).

$$\gamma_p^R = \frac{1}{G_R} \left(\gamma_p \cdot |G^*|_{LVE}(\omega_R) \right) \quad (2.5)$$

where γ_p^R is the peak pseudo strain in a given cycle, and $|G^*|_{LVE}(\omega_R)$ is the linear viscoelastic dynamic shear modulus at the reduced frequency (ω_R) of testing. Correspondingly, the peak pseudo stiffness (C^*) in a given cycle can be determined as defined in Equation (2.6).

$$C^*(S) = \frac{\tau_p}{\gamma_p^R \times DMR} \quad (2.6)$$

where τ_p is the peak stress in the cycle of interest and DMR is the dynamic modulus ratio. The DMR is a parameter that is used to account for specimen-to-specimen variability and is taken to be the finger print dynamic shear modulus value of the specimen subjected to fatigue testing, measured at low strain amplitude, divided by the linear viscoelastic dynamic shear modulus value measured from frequency sweep testing. For each fatigue test, the DMR value should be between 0.9 and 1.0 to ensure good repeatability. Similar to Equation (2.4), Equation (2.6) implies that C^* will be one if the material is behaving in a linear viscoelastic manner and will decrease as the stress deviates from linear viscoelasticity because of damage. Equation (2.5) is

used for analysis herein rather than using the full time histories of the strain and stress to determine the pseudo stiffness values, which would require significant computational effort and can lead to problems (Underwood et al. 2010). Because the peak pseudo stiffness is used for analysis rather than full time history data, the VECD model proposed herein is referred to as the ‘simplified’ VECD model, i.e., the S-VECD model.

2.2.2.2 Schapery’s Work Potential Theory

Schapery’s work potential theory (Schapery 1984), which is based on thermodynamic principles of irreversible processes, is the basis for the S-VECD model. The work potential theory for viscoelastic media is given in Equation (2.7).

$$\frac{dS}{dt} = \left(-\frac{\partial W^R}{\partial S} \right)^\alpha \quad (2.7)$$

where S is an internal state variable representing damage, W^R is the stored pseudo strain energy, t is time, and α is the damage evolution rate. Stored pseudo strain energy, for the case of cyclic loading, is defined in Equation (2.8):

$$W^R = \frac{1}{2} C^*(S) (\gamma_p^R)^2 \quad (2.8)$$

Note that past researchers have also used pseudo dissipated energy as the basis for VECD modeling (e.g., (Johnson 2010)), which considers changes in phase angle during fatigue.

However, while the effects of damage on pseudostiffness is intuitive, the effects damage on phase angle is less clear. Phase angle may increase due to a nonlinear response associated with the increase in localized strain, internal heating, or appear to increase only as an artifact of distortion of the stress waveform associated with damage. Therefore, pseudostrain energy

density has been selected as the basis for S-VECD modeling herein which is consistent with asphalt mixture S-VECD modeling (AASHTO TP 107-14).

The parameter, α , is material-dependent and was introduced when Schapery's initial work potential theory for elastic material was extended to viscoelastic media, which he found was able to demonstrate rate-dependent damage growth. Schapery (1990) suggested that α can be calculated using the slope of the relaxation modulus mastercurve in log space, m . According to Schapery's crack growth theory for viscoelastic media, if a material's fracture energy and fracture stress are constant, then $\alpha=1+1/m$, whereas if the fracture energy and fracture process zone size are constant, then $\alpha=1/m$. For application to uniaxial testing of asphalt mixtures, Lee and Kim (1998) found that α should be defined as $1+1/m$ for displacement-controlled tests and $1/m$ for load-controlled tests in order to obtain path-independent damage characteristic curves. For application to asphalt mixtures, m is taken to be the maximum slope of the sigmoidal-shaped relaxation modulus mastercurve in log space. For asphalt binders, which are viscoelastic fluids rather than solids, the mastercurves are parabolic rather than sigmoidal in shape, and therefore, the definition of α used for asphalt mixtures cannot be extrapolated directly for asphalt binders. Furthermore, DSR testing is torsional, whereas asphalt mixture testing is generally uniaxial. Therefore, suitable definitions for α are investigated in this study on the basis of the steady-state dynamic shear modulus mastercurve in log space as depicted in Figure 2-2, because investigations of asphalt binders indicate the steady-state slopes of the dynamic shear modulus and relaxation modulus curves are equivalent (Johnson 2010).

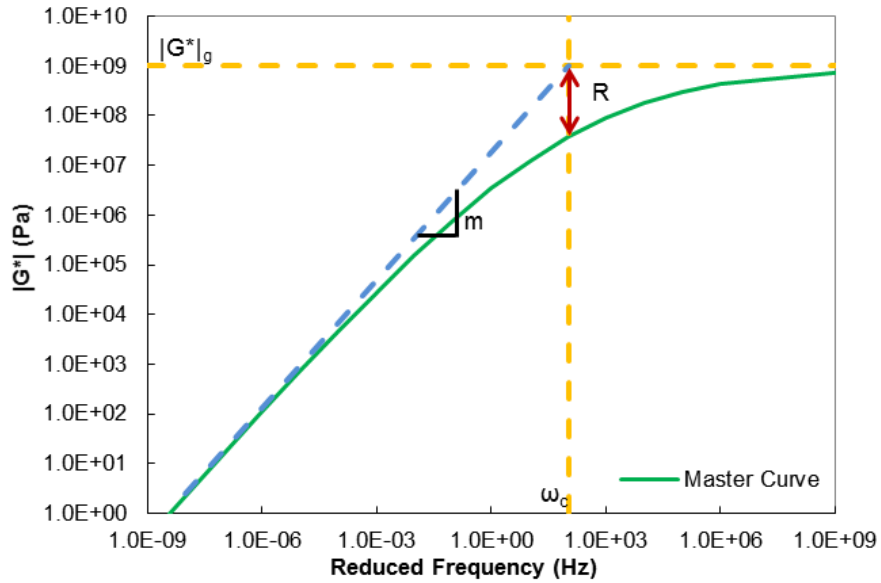


Figure 2-2. Schematic of asphalt binder master curve.

The internal state variable that represents damage, S , is derived as a function of time by combining Equations (2.6) and (2.7) using numerical integration. The solution is given in Equation (2.9).

$$S = \sum_{i=1}^N \left[\frac{DMR}{2} (\gamma_{p,i}^R)^2 (C_{i-1}^* - C_i^*) \right]^{\frac{\alpha}{\alpha+1}} \cdot [\Delta t]^{\frac{1}{1+\alpha}} \quad (2.9)$$

where t is time and i refers to the cycle number. The crux of the S-VECD model is the relationship between C^* and S (termed the *damage characteristic curve*) that has been shown to be independent of loading history and temperature for asphalt mixtures, which allows the prediction of the damage response to any given loading history of interest using limited test results. It should be noted that the S-VECD model for asphalt mixtures differs slightly from the framework presented for asphalt binders. First, the application of the S-VECD model to asphalt mixtures tested under cyclic uniaxial tension requires the rigorous calculation of pseudo strain and damage in the first loading path (using equations that are analogous to Equations (2.1) and (2.4)), as a significant amount of damage occurs the first time the mixture is subjected to tension

(Underwood et al. 2010). Asphalt binders are tested in shear mode, and the first loading path has been found not to induce significant damage. Therefore, only cycle-to-cycle calculations of damage are necessary for asphalt binder modeling.

In addition, in asphalt mixture S-VECD modeling, it is assumed that damage grows only during the period within each loading cycle when the mixture is subjected to tension. Thus in damage calculations, time is reduced to the time when mix is under tension using a shape factor. Underwood (2011) proposed Equation (2.10) to describe the stress history regardless of input condition to determine the tensile time:

$$\frac{\sigma(t)}{\sigma_{0,ta}} = (\beta - \cos(\omega t)) \cdot \frac{1}{\beta + 1} \quad (2.10)$$

where $\sigma_{0,ta}$ is the tension stress amplitude.

Underwood (2011) assessed the tensile time in a given stress history by the definition of β for each cycle as follows:

$$\beta_i = \frac{(\sigma_{peak})_i + (\sigma_{valley})_i}{|\sigma_{peak}|_i + |\sigma_{valley}|_i} \quad (2.11)$$

where σ_{peak} and σ_{valley} are the largest and smallest values in cycle i respectively. The value of 1 for β means that the entire stress history is in tension whereas $\beta=0$ means that σ_{peak} and σ_{valley} are equal in value and only half of the time mix is under tension. Therefore to calculate damage based on the time where mix is under tension, Equation (2.9) changes as follows:

$$S = \sum_{i=1}^N \left[\frac{DMR}{2} (\gamma_{p,i}^R)^2 (C_{i-1}^* - C_i^*) \right]^{\frac{\alpha}{\alpha+1}} \cdot [\Delta t \times B]^{\frac{1}{1+\alpha}} \quad (2.12)$$

$$B = f_R \int_{\xi_i}^{\xi_f} |f(\xi)|^{2\alpha} d\xi \quad (2.13)$$

$$f(\xi) = -\frac{1}{2} \cos(\omega\xi) + \frac{(\tau_{peak})_i + (\tau_{valley})_i}{2[(\tau_{peak})_i - (\tau_{valley})_i]} \quad (2.14)$$

The times in the integral of Equation (2.13) are the start and end time of tensile loading in a cycle duration and can be obtained as:

$$\xi_i = \frac{\cos^{-1}(\beta)}{\omega} \quad (2.15)$$

$$\xi_f = \frac{2\pi - \cos^{-1}(\beta)}{\omega} \quad (2.16)$$

For the case of asphalt mixture the amount of shape factor was 0.77 and 0.7 for controlled crosshead and controlled stress tests respectively. In order to assess shape factor for asphalt binder for different test protocols, controlled strain time sweep at 3 and 4% strain amplitudes and LAS tests were performed at two different temperatures for binder PG70-22 and PG64-22 and the raw data were collected. Factor β was found during three stages: start of the test (before evolution of damage), middle of test ($C=0.6$) and at the time of failure. It was found that β value was almost zero for all the cases. By implementing this value into above equations, the shape factor for the case of asphalt binder was found to be 0.74 which is close to the finding for asphalt mixture.

2.2.2.3 Time-Temperature Superposition with Growing Damage

Temperature effects have been incorporated into the S-VECD model for asphalt mixtures through the use of time-temperature superposition (Chehab et al. 2002, Underwood et al. 2006). Chehab et al. (2002) demonstrated that the replacement of actual time with the reduced time determined using linear viscoelastic time-temperature shift factors allows temperature effects to be incorporated into the S-VECD modeling of asphalt mixtures. In the case of the S-VECD

model framework for the binders presented, time-temperature superposition is incorporated by replacing time with reduced time, t_R , in calculating the damage. Reduced time is used in the damage calculation in order to shift the damage characteristic curves to the reference temperature using time-temperature shift factors determined from linear viscoelastic characterization. Corresponding definitions of reduced time and damage that allow the S-VECD model to be extended to capture the temperature effects are given in Equations (2.17) and (2.18), respectively.

$$t_R = \frac{T}{a_T} \quad (2.17)$$

where t is temperature and a_T is the linear viscoelastic time-temperature shift factor.

$$S(t) = \sum_{i=1}^N \left[\frac{DMR}{2} (\gamma_p^R)^2 (C_{i-1} - C_i) \right]^{1+\alpha} \cdot [t_{Ri} - t_{Ri-1}]^{\frac{1}{1+\alpha}} \quad (2.18)$$

2.2.2.4 Failure Definition and Criterion

A clear means to define fatigue failure in asphalt binder fatigue tests is an important component of fatigue characterization. In addition, a corresponding failure criterion is needed to predict when failure will occur under loading and thermal conditions other than those used in fitting the model. That is, the failure criterion allows for predicting the damage level at which failure will occur for any given loading or temperature history.

The peak in the C^* times N ($C^* \times N$, where N is the number of load cycles) versus N curve is used to define fatigue failure in time sweep tests based on the recommendations of (Wang et al. 2015). The peak in the $C^* \times N$ versus N curve has been shown to correspond to a marked change in the rate of material integrity loss and, hence, is considered a reasonable means for defining failure in time sweep tests (Wang et al. 2015). The peak in the $C^* \times N$ versus N curve is

not suitable for LAS tests where the strain amplitude increases with increasing load cycles. Rather, Wang et al. (2015) demonstrated that the peak in the stored pseudo strain energy versus N curve is a suitable definition of failure for LAS tests. Initially in LAS tests, the stored pseudo strain energy increases with each cycle, indicating that the material is able to store additional energy as the strain amplitude (and hence input energy) increases. However, once the material fails, the binder loses its ability to store additional energy with the increase in strain amplitude, and thus, the stored pseudo strain energy will decay.

Sabouri and Kim (2014) developed a failure criterion for asphalt mixtures that can be incorporated into S-VECD modeling for improved performance predictions. Sabouri and Kim (2014) failure criterion is the relationship between fatigue life in terms of number of cycles to failure (N_f) and the average released pseudo strain energy until failure, denoted as G^R . Sabouri and Kim (2014) demonstrated that the relationship between N_f and G^R is independent of loading history and temperature and thus can be captured using results from several fatigue tests conducted with different loading histories.

Wang et al. (2015) expanded on the work of Sabouri and Kim (2014) by applying the G^R -based failure criterion to asphalt binder fatigue test results obtained from DSR testing. Similar to the case for asphalt mixtures, Wang et al. (2015) demonstrated that a unique relationship exists between N_f and G^R for asphalt binders that is independent of the loading history. Safaei and Castorena (2016) further demonstrated the temperature independence of the failure criterion. G^R is defined in Equation (2.19).

$$G^R = \frac{\overline{W}_r^R}{N_f} = \frac{A}{N_f^2} \quad (2.19)$$

where W_r^R is the average released pseudo strain energy. The released pseudo strain energy represents the difference between total pseudo strain energy (undamaged response) and stored pseudo strain energy (damaged response). The total pseudo strain energy (W_{total}^R) is determined according to Equation (2.20).

$$W_{total}^R = \frac{1}{2} \tau_{pundamaged} \cdot \gamma_p^R = \frac{1}{2} (\gamma_p^R)^2 \quad (2.20)$$

Given the definition of stored pseudo strain energy (Equation (2.8)), the released pseudo strain energy is calculated using Equation (2.21). A schematic illustration of stored and released pseudo strain energy in terms of the stress-pseudo strain space is provided in Figure 2-3.

$$W_r^R = W_{total}^R - W_s^R = \frac{1}{2} (1 - C^*) (\gamma_p^R)^2 \quad (2.21)$$

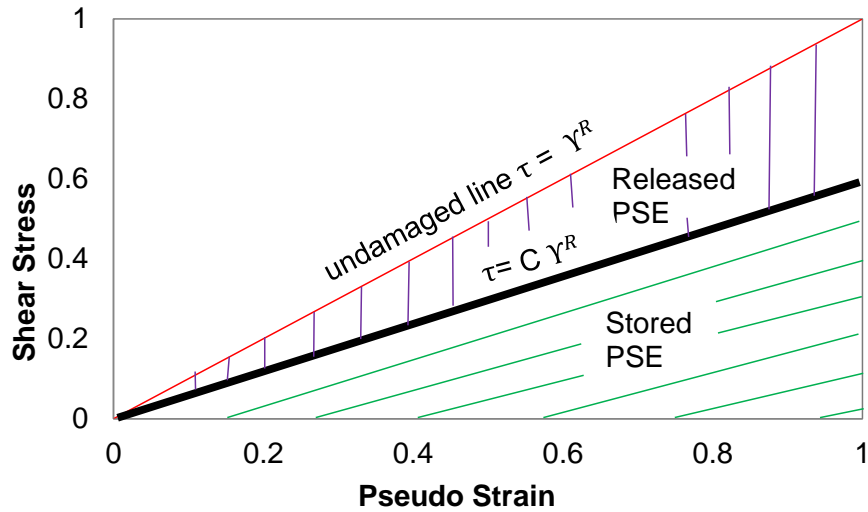


Figure 2-3. Schematic representation of released and stored pseudo strain energy in the LAS test.

To calculate the G^R using experimental data, the total released pseudo strain energy up to failure is determined using the area under the W_r^R curve until failure (i.e., A in Equation (2.19)), as depicted in Figure 2-4 for a time sweep test and normalized by N_f .

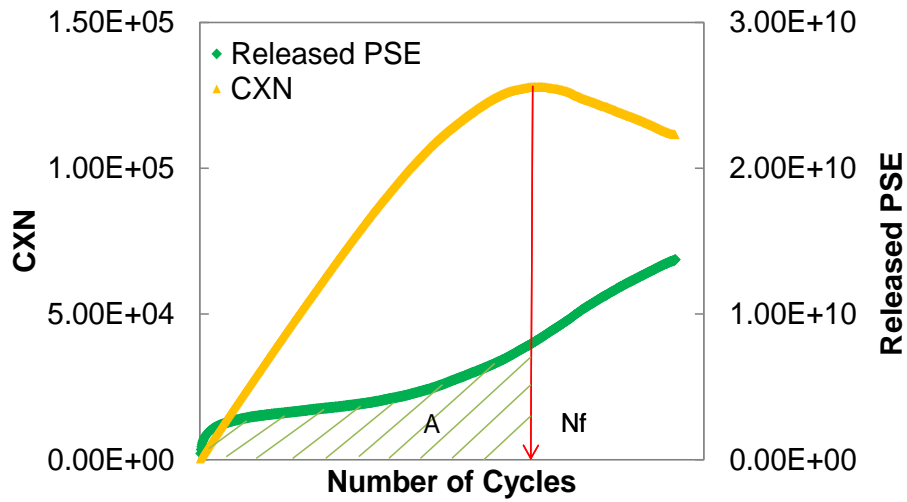


Figure 2-4. Schematic depiction of determination of “A” for time sweep test.

2.2.2.5 Fatigue Life Prediction

The S-VECD model and failure criterion can be combined to enable fatigue life predictions. To incorporate the S-VECD model so that it can be used in fatigue life predictions, a power law model (Equation (2.22)) is fitted to the damage characteristic curve $C^*(S)$.

$$C^* = 1 - C_1(S)^{C_2} \quad (2.22)$$

where C_1 and C_2 are optimized fitted coefficients. Similarly, a power law model (Equation (2.23)) is fitted to G^R versus N_f .

$$G^R = a(N_f)^b \quad (2.23)$$

Equations (2.6), (2.7), and (2.8) can be combined to derive parameter A in Equation (2.19) as a function of strain and N_f , as shown in Equation (2.24).

$$\begin{aligned}
A &= \int_0^{N_f} W^R_r dN = \left[\frac{1}{2} \cdot C_1 \cdot \left(|G^*|_{LVE} (\omega_R) \right)^2 \cdot q^{\left(\frac{-C_2}{p} \right)} \cdot \frac{1}{\frac{C_2}{p} + 1} \right] \cdot (\gamma)^{2+2\alpha \left(\frac{C_2}{p} \right)} (N_f)^{\frac{C_2+1}{p}} \\
&= k \cdot (\gamma)^{2+2\alpha \left(\frac{C_2}{p} \right)} (N_f)^{\frac{C_2+1}{p}}
\end{aligned} \tag{2.24}$$

where p , k , and q are combined constants with definitions given in Equations (2.25) through (2.27).

$$p = 1 - \alpha \cdot C_2 + \alpha \tag{2.25}$$

$$q = \frac{f_R \cdot 2^\alpha}{(1 - \alpha \cdot C_2 + \alpha)(C_1 \cdot C_2)^\alpha \left(|G^*|_{LVE} (\omega_R) \right)^{2\alpha}} \tag{2.26}$$

$$k = \frac{1}{2} \cdot C_1 \cdot \left(|G^*|_{LVE} (\omega_R) \right)^2 \cdot q^{(-C_2/p)} \cdot \frac{1}{(C_2/p) + 1} \tag{2.27}$$

The relationship between N_f and the applied strain amplitude (γ) can then be derived by substituting the definition of A given in Equation (2.24) into Equation (2.26), combining with Equation (2.23), and solving for N_f .

$$N_f = \left[\frac{k}{a} \cdot (\gamma)^{2+2\alpha \left(\frac{C_2}{p} \right)} \right]^{\frac{1}{b+1 - \frac{C_2}{p}}} \tag{2.28}$$

2.2.3 Linear Viscoelastic Modeling

In addition to S-VECD modeling, the modeling of linear viscoelasticity was necessary in this study to verify that Schapery's extended elastic-viscoelastic correspondence principle is applicable to asphalt binders subjected to cyclic loading in the DSR. To verify the extended elastic-viscoelastic correspondence principle, the pseudo strain was calculated rigorously and compared to the measured stress responses for a subset of conducted experiments. In order to

calculate the pseudo strain rigorously, modeling the linear viscoelastic responses was necessary. Dynamic shear modulus and phase angle mastercurves were first constructed using frequency sweep test results through simultaneous time-temperature shifting and fitting to the Christensen-Anderson-Marasteanu (CAM) model (Christensen and Anderson 1992) given in Equations (2.29) and (2.30).

$$|G^*|(\omega_R) = |G^*|_g \left[1 + \left(\frac{\omega_c}{\omega_R} \right)^v \right]^{-\frac{w}{v}} \quad (2.29)$$

$$\delta(\omega_R) = \frac{90 \cdot w}{\left[1 + \frac{\omega_R}{\omega_c} \right]^v} \quad (2.30)$$

Model parameters are graphically depicted in Figure 2-2: ω_R is reduced frequency; $|G^*|_g = |G^*|$ as $f \rightarrow \infty$: glassy dynamic modulus, equal to 1 GPa for asphalt binder; ω_c is the cross-over frequency (reduced frequency where $\delta = 45^\circ$); and m and $v = \log(2)/R$ are the shape parameters, dimensionless. The time-temperature shift factors were fitted to the model given in Equation (2.31).

$$\log a_T = \alpha_1 T^2 + \alpha_2 T + \alpha_3 \quad (2.31)$$

where a_T is the shift factor at temperature T and, α_1 , α_2 and α_3 are coefficients.

The CAM model then was used to predict the storage modulus over a broad range of frequencies. The generated storage modulus data were fitted to the Prony series model shown in Equation (2.32) using the collocation method.

$$G'(\omega) = \sum_{i=1}^N G_i \frac{\omega^2 \rho_i^2}{1 + \omega^2 \rho_i^2} \quad (2.32)$$

where G_i and ρ_i represent the stiffness and relaxation time for the i^{th} component of the material, respectively, and ω is the angular frequency. The Prony series can be recast in terms of the relaxation modulus, as shown in Equation (2.33).

$$G(t) = \sum_{i=1}^N G_i e^{-\frac{t}{\rho_i}} \quad (2.33)$$

Equation (2.33) was used as input to Equation (2.1) to calculate the pseudo strain. The rigorous calculation of the pseudo strain was accomplished using numerical integration within a developed MATLAB routine.

2.3 Experimental Plan

2.3.1 Materials and Experimental Methods for Developing the S-VECD Model

Four binders with different performance grades (PGs) were subjected to DSR testing in this study to evaluate the applicability of S-VECD modeling to asphalt binders subjected to cyclic loading in a DSR. Experimental details are provided in Table 2-1. Note that the PG 64-28 binder is polymer-modified asphalt whereas the other binders evaluated in this study are unmodified. All binders were aged in a rolling thin-film oven and pressure aging vessel prior to testing. All tests were conducted in a TA AR-G2 DSR with an 8-mm parallel plate set-up. Linear viscoelastic characterization was conducted, which was necessary for determining the pseudo strain and α in the S-VECD model. In addition, both time sweep and LAS tests were performed to characterize the binders' fatigue resistance. To determine the linear viscoelastic properties of each binder, frequency sweep tests were performed using 1 percent shear strain amplitude at temperatures of 35°C, 20°C, and 5°C over frequencies ranging from 0.1 to 30 Hz. Time-temperature superposition was applied to the frequency sweep test results to form dynamic shear

modulus and phase angle mastercurves. Displacement (strain) -controlled time sweep tests were conducted for all the study binders. The strain amplitudes used in the time sweep tests were selected such that failure occurred within a reasonable time (i.e., 30 minutes to 4 hours). To evaluate the effect of strain amplitude on the test results, two initial strain values were considered at one test temperature. In addition, to evaluate the loading mode independency of the damage characteristic curves, stress-controlled time sweep tests were run for the PG 64-22 and PG 70-22 binders. Test temperatures were chosen to ensure failure by cohesive cracking based on the recommendations of Safaei and Castorena (2016) who prescribe testing at a temperature frequency combination such that the linear viscoelastic dynamic shear modulus value is between 12 MPa and 60 MPa.

Table 2-1. Experimental plan.

Binder	Test Method				
	LAS	Strain Controlled Time Sweep 3%	Strain Controlled Time Sweep 4%	Stress Controlled Time Sweep	Frequency Sweep
	Test Temperatures (°C)				
PG 70-22	15,20,25	15,20,25	25	20 (700 KPa)	5,20,35
PG 64-28	10,15,20	10,15,20	15	-	5,20,35
PG 64-22	15,20,25	15,20,25	20	20 (500 KPa)	5,20,35
PG 58-28	10,15,20	10,15,20	20	-	5,20,35

2.3.2 Use of Data from Past Studies to Evaluate the Linkage between Binder S-VECD

Modeling and Mixture Performance

Data from past studies, which include both asphalt binder and asphalt mixture test results, were utilized (Safaei et al. 2014, Wang et al. 2015) to validate that the S-VECD model applied to asphalt binder DSR results reflects asphalt mixture fatigue performance. Safaei et al. (2014)

evaluated the effect of age hardening on the fatigue resistance of warm-mix asphalt (WMA) binders and mixtures compared to hot mix asphalt (HMA) binders and mixtures. All mixtures produced were constructed using the same gradation, volumetrics, and asphalt binder. Two WMA technologies were considered: foaming by water injection and Evotherm modification. Short-term aging (STA) in the oven was applied to the HMA mix at 135°C for four hours according to (AASHTO R 3) prior to compaction. STA was applied to both WMA mixtures at 117°C for two hours according to NCHRP 9-43 recommendations (Bonaquist 2011). In order to simulate the long-term aging (LTA) of the HMA and WMA mixtures using AASHTO R 3, the cored and cut samples were conditioned at 85°C for two days and at 85°C for eight days as LTA Level 1 (LTA1) and Level 3 (LTA3), respectively (Zapata and Houston 2008). The asphalt binders were extracted and recovered from the produced asphalt mixture specimens. The asphalt mixtures and extracted binders were subjected to linear viscoelastic and fatigue characterization following aging. Because oxidative aging occurs within the asphalt binder phase of asphalt concrete, Safaei et al. (2014) study allowed a unique opportunity to study the isolated influence of the binder on the fatigue performance of the mixture. Cyclic direct tension tests were used to measure the fatigue resistance of the asphalt mixtures, and LAS tests were used to measure the fatigue resistance of the binders. Fatigue tests of both the binders and the mixtures were conducted at 20°C. S-VECD analysis was performed to interpret the fatigue test results and predict the fatigue performance of the binders (using the model developed herein) and mixtures using a pavement structural model.

Wang et al. (2015) measured the fatigue resistance of four asphalt binders from the FHWA-ALF pooled fund study TPF-5 (019) using LAS and time sweep tests at 19°C. These binders are referred to as Control (PG 70-22), CR-TB (PG 76-28), Terpolymer (PG 70-28), and

SBS-LG (PG 70-28). The FHWA-ALF study focused on evaluating modified asphalt pavements (Nelson et al.) . The study included lanes that were constructed with identical structures but different asphalt concrete mixtures. The different mixtures were prepared using the same aggregate source and gradation, same air void content, and same asphalt content, but with different binders, allowing for isolating the binder effects on the fatigue resistance. The facility was kept at a constant temperature of 19°C during the fatigue evaluation. The mixture performance test results obtained from both the cyclic direct tension tests and field performance data were available for the ALF mixtures. Thus, the relationship between the S-VECD modeling of the asphalt binder data using the model framework developed herein and the mixture and field performance could be evaluated.

2.4 Results

2.4.1 Verification of Elastic-Viscoelastic Correspondence Principle

In order to verify the applicability of Schapery's extended elastic-viscoelastic correspondence principle to asphalt binders tested under cyclic loading in a DSR, raw stress and strain time history data from displacement-controlled time sweep tests were analyzed in this study. The raw data collection involved collecting 100 data points per load cycle. The strain and time raw data histories were coupled with the linear viscoelastic Prony series model in order to calculate the full time history of the pseudo strain rigorously using Equation (2.1).

Representative results of the pseudo strain analysis that correspond to the test results of the PG 64-22 binder tested using a constant strain amplitude of three percent at 15°C are shown in Figure 2-5. Figure 2-5 (a) presents the stress versus strain relationship and Figure 2-5 (b) presents the stress versus pseudo strain relationships for selected load cycles. Recall that,

according to the extended elastic-viscoelastic correspondence principle, the replacement of strain with pseudo strain in analysis is supposed to be in the form of an elastic problem. That is, the relationship between stress and pseudo strain should be linear. The results presented in Figure 2-5 show that this is the case, with only minor hysteretic behavior observed in Figure 2-5 (b) compared to Figure 2-5 (a). Furthermore, Figure 2-5 shows that in the first cycle of loading, the stress and pseudo strain are close in magnitude, indicating that the binder is undamaged and behaving in a linear viscoelastic manner, as expected. The measured stress exceeds pseudo strain slightly, which can be attributed to sample-to-sample variability. (DMR of the sample is 1.10). Thus, the slope of the stress-pseudo strain curve (i.e., pseudo stiffness) is near one in the first load cycle. As the number of load repetitions increases, the slope of the stress-pseudo strain curve decreases, indicating decay in the stress response due to damage. However, the relationship between the stress and pseudo strain remains linear (i.e., analogous to the stress-strain relationship for elastic materials), indicating the validity of the extended elastic-viscoelastic correspondence principle and the corresponding use of pseudo stiffness to capture material integrity. Note that similar trends were observed for all the binders and test conditions evaluated, but these are not included herein for brevity.

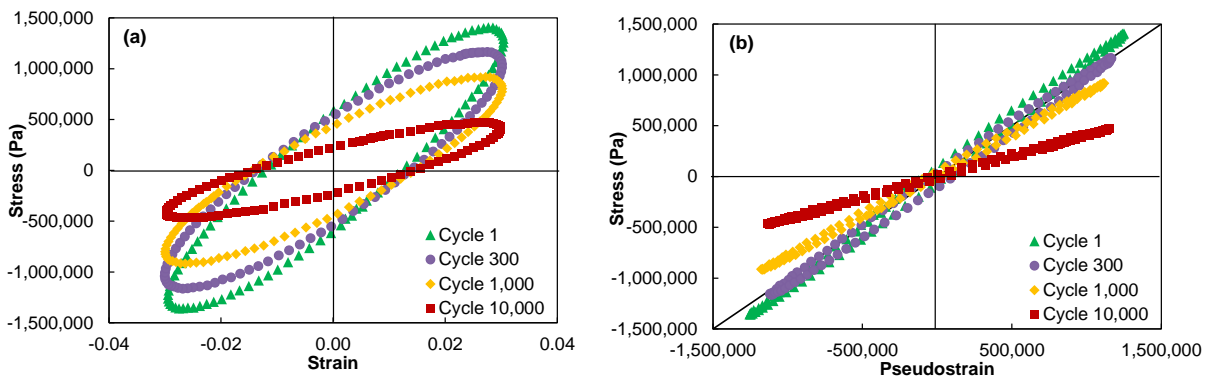


Figure 2-5. (a) Stress –Strain (b) Stress-pseudo strain relationship for selected cycles that correspond to time sweep testing of PG 64-22 binder at 3 percent strain amplitude and 15°C.

2.4.2 S-VECD Model Verification

2.4.2.1 Applicability of S-VECD Model to Time Sweep Test Results and Selection of α Definition

To evaluate the applicability of the S-VECD model to the asphalt binders tested under cyclic loading in the DSR in this study, only the time sweep test results were considered initially, because the LAS test includes more complicated loading histories and high strain amplitudes than the time sweep test. Damage characteristic curves were determined for a reference temperature of 20°C for all the binders and were constructed using the two commonly utilized definitions of the damage evolution rate parameter α , i.e., $1/m$ and $1+1/m$, where m is the dynamic shear modulus mastercurve in log space. The m values for each binder are shown in Table 2-2. The linear viscoelastic time-temperature shift factors determined from the frequency sweep tests were used to shift the time sweep data collected at temperatures other than 20°C to the reference temperature.

The damage characteristic curves that correspond to the use of $\alpha = 1/m$ and $\alpha = 1+1/m$ are shown in Figure 2-6 and Figure 2-7, respectively. Figure 2-6 demonstrates that when α is defined as $1/m$, the damage characteristic curves exhibit temperature and loading history dependence. However, Figure 2-7 demonstrates that the damage characteristic curves are the same, irrespective of temperature and loading history (loading amplitude and loading mode), when α is defined as $1+1/m$. These results demonstrate the applicability of S-VECD modeling to the asphalt binder time sweep test results and establish that α should be defined as $1+1/m$.

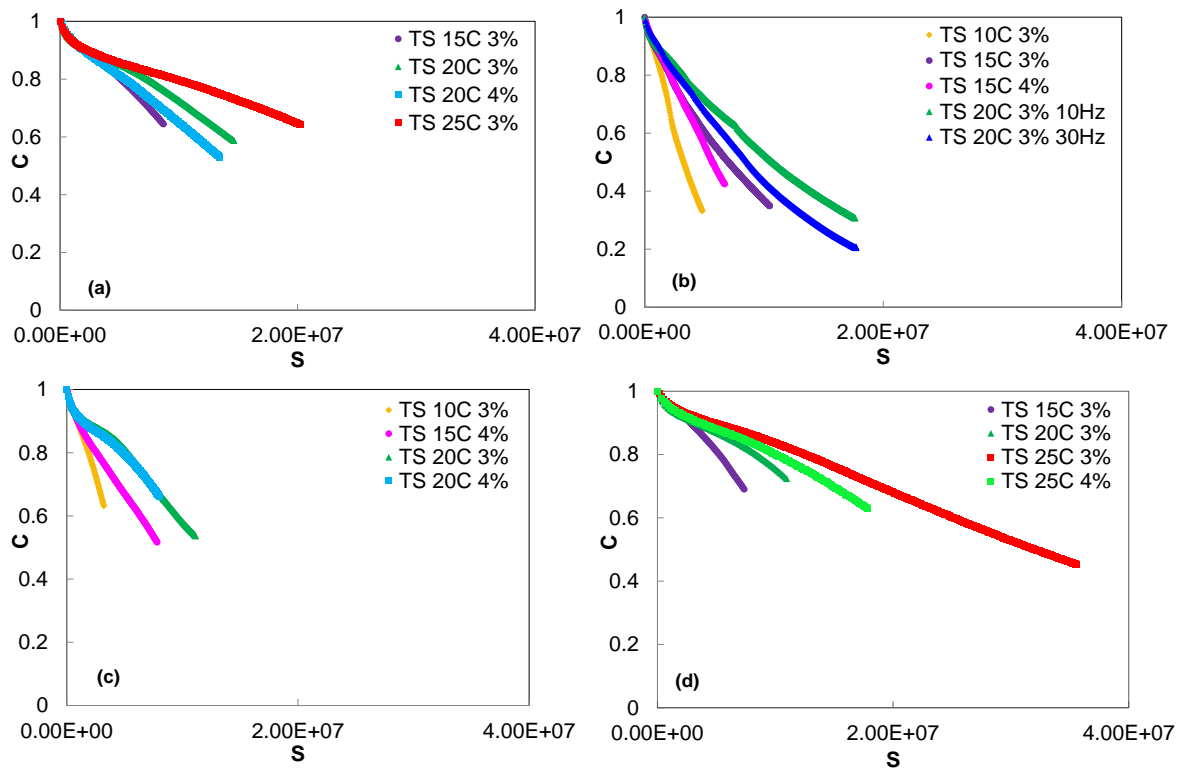


Figure 2-6. Time sweep damage characteristic curves shifted to a reference temperature of 20°C with $\alpha = 1/m$ for (a) PG64-22, (b) PG64-28, (c) PG58-28, and (d) PG70-22.

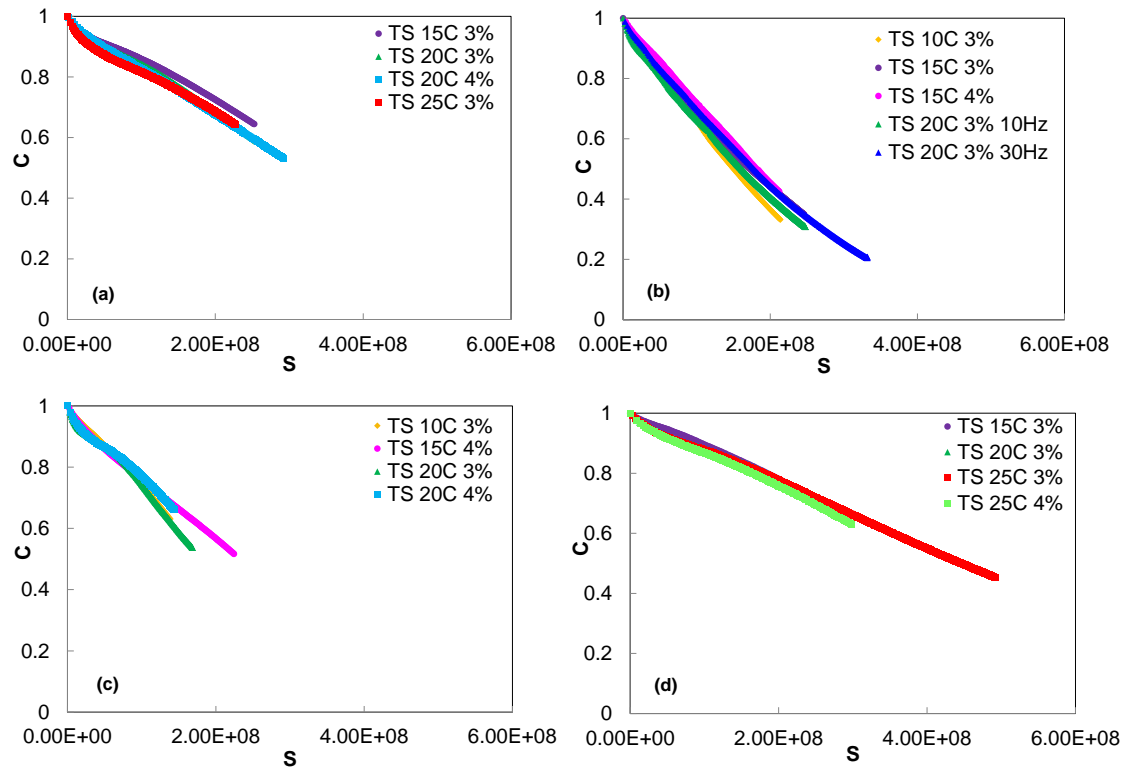


Figure 2-7. Time sweep damage characteristic curves shifted to a reference temperature of 20°C with $\alpha = 1+1/m$ for (a) PG 64-22, (b) PG 64-28, (c) PG 58-28, and (d) PG 70-22.

Table 2-2. m value for tested binders

Binder	m
PG70-22	1.02
PG64-28	1.01
PG64-22	1.01
PG58-28	1.01

2.4.2.2 Applicability of S-VECD Model to LAS Test Results

Once the S-VECD model was verified for the time sweep tests, the applicability of the model to the LAS test results was evaluated. Note that the LAS test includes linearly increasing strain amplitudes ranging from 0.1 percent to 30 percent. Thus, the LAS test is distinguished from time sweep tests in two ways: (1) variable amplitude loading history and (2) use of high strain levels, likely in the nonlinear range.

The damage characteristic curves obtained from the LAS tests conducted at different temperatures are shown in Figure 2-8 for each binder tested. Note that α is defined as $1+1/m$ based on the time sweep test results. A reference temperature of 20°C was used for each binder in generating the damage characteristic curves. For LAS test temperatures other than 20°C, the data were shifted to the reference temperature using linear viscoelastic time-temperature shift factors obtained through frequency sweep testing. The results demonstrate that the LAS damage characteristic curves are unique to the test temperature, indicating the validity of time-temperature superposition for modeling the LAS test results.

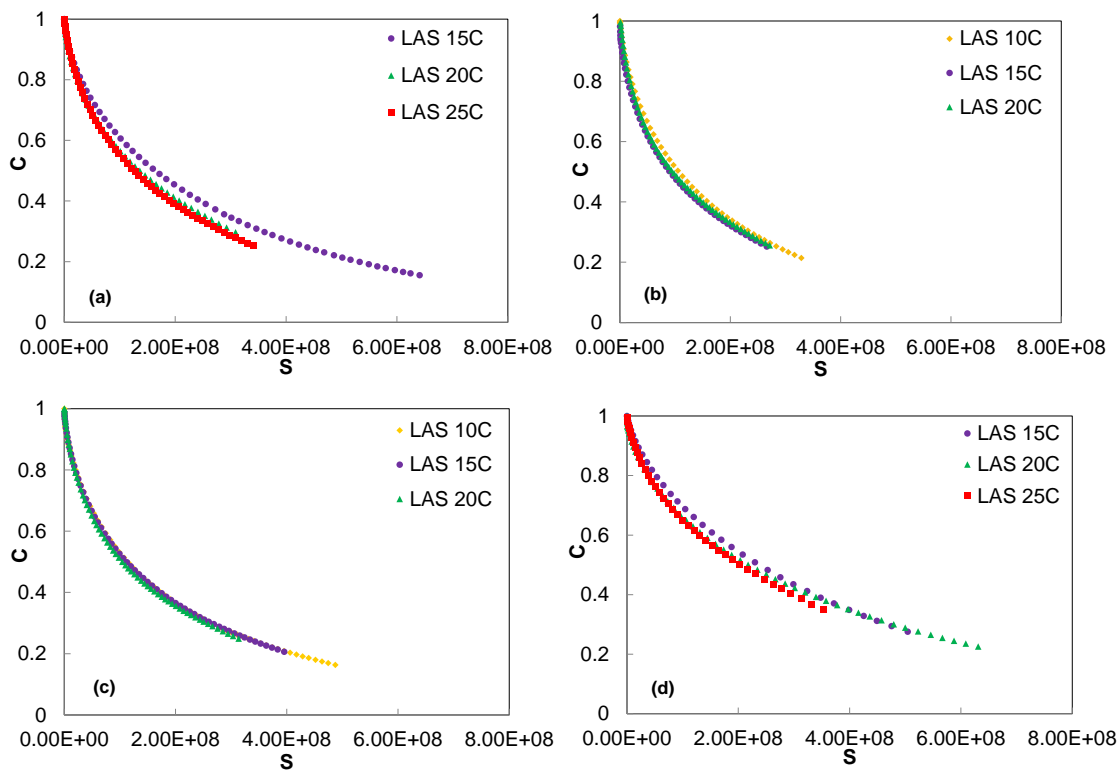


Figure 2-8. LAS damage characteristic curves shifted to a reference temperature of 20°C with $\alpha = 1+1/m$ for (a) PG 64-22, (b) PG 64-28, (c) PG 58-28, and (d) PG 70-22.

However, the damage characteristic curves obtained from the LAS test results differ somewhat from those generated from the time sweep test results, as shown in Figure 2-9.

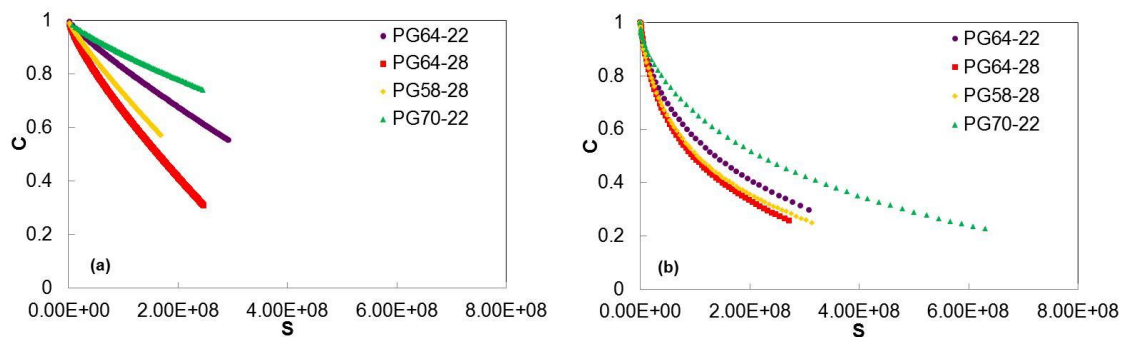


Figure 2-9. Comparison of binder damage characteristic curves from (a) time sweep tests and (b) LAS tests.

Figure 2-9 shows that the time sweep test-derived damage characteristic curves are generally more linear and lie higher than the LAS test-generated damage characteristic curves. The reason that the LAS curves fall below the corresponding time sweep damage characteristic curves is the material nonlinearity that is imposed by the high strain amplitudes used in LAS testing. Material nonlinearity will contribute to the loss in material integrity (i.e., pseudo stiffness) in addition to damage. However, in the S-VECD analyses conducted, all material loss is attributed to damage for the sake of simplicity. Separating nonlinearity and damage is very challenging and beyond the scope of this research. Although the damage characteristic curves derived from the time sweep and LAS tests differ somewhat, the relative position of the damage characteristic curves for the different binders evaluated is consistent among those derived from LAS and time sweep testing. Thus, the LAS damage curves were given further consideration for performance predictions herein.

2.4.3 Failure Criteria

The G^R versus N_f failure criterion, derived from time sweep and LAS tests at different temperatures, is shown in Figure 2-10 for each binder tested. It is observed that a unique

relationship exists between G^R and N_f that is independent of loading history and temperature. These results suggest that G^R versus N_f is a fundamental relationship for a given material, which is consistent with the asphalt mixture findings. Interestingly, although the LAS damage characteristic curves differ somewhat from the time sweep damage characteristic curves, the failure criterion is consistent between the two test methods. These results suggest that several time sweep or LAS tests conducted at different temperatures or with different loading histories can be used to derive the failure criterion efficiently. The failure criterion is a critical component of performance prediction as it allows for the damage at failure to be dependent on the loading history.

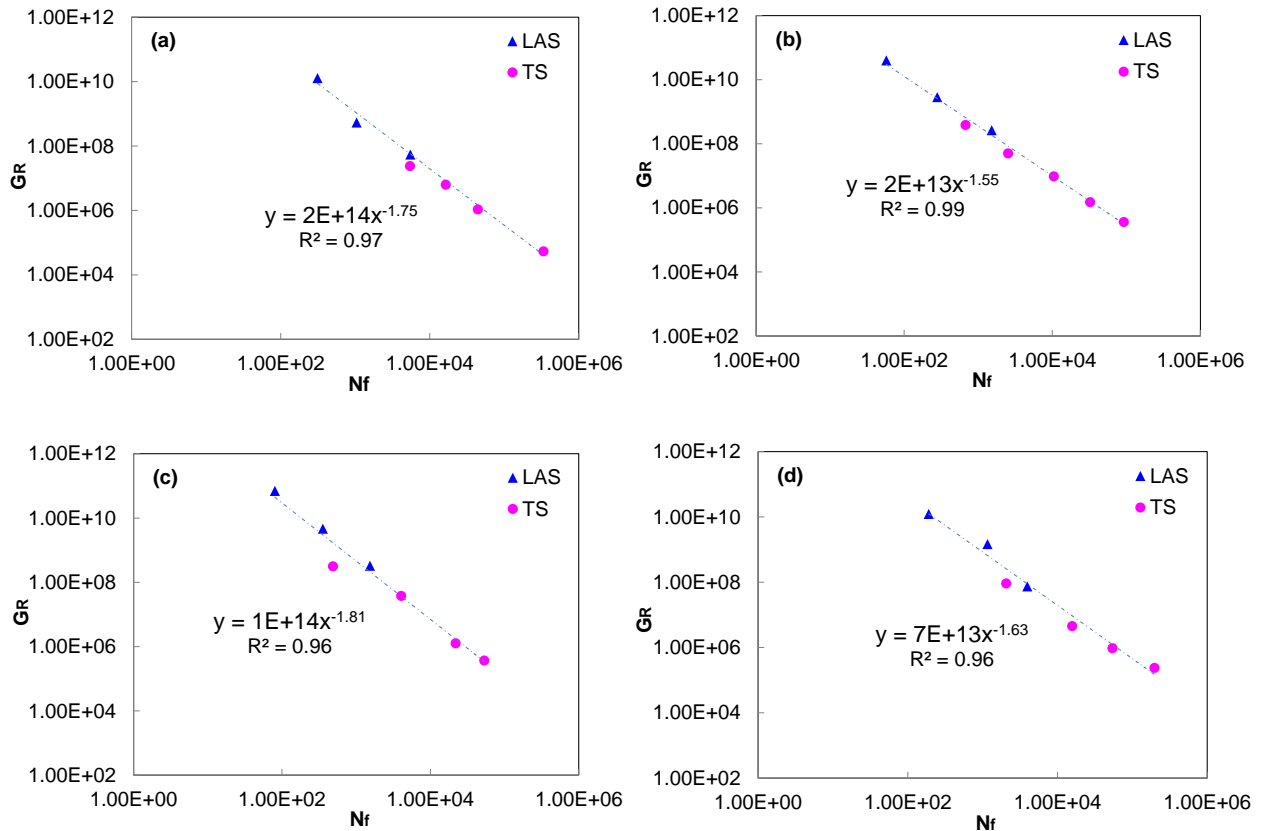


Figure 2-10. G^R vs. N_f failure criteria for (a) PG 64-22, (b) PG 64-28, (c) PG 58-28, and (d) PG 70-22.

2.4.4 Model Verification and Validation Using Binder Test Results

2.4.4.1 Model Verification Using Time Sweep Test Results

In order to verify the S-VECD model for performance predictions, the results from the time sweep tests were used to fit the damage characteristic curves and failure criterion models given in Equations (2.15) and (2.16), respectively. Optimized model coefficients were input into Equation (2.21) in order to predict the fatigue life that corresponds to the strain amplitude and temperatures of the time sweep tests. The comparison between measured and predicted fatigue life data is shown in Figure 2-11. The results demonstrate good agreement between the measured and predicted fatigue life ($R^2 = 0.97$), thus providing verification that the S-VECD model coupled with time sweep tests results can be used as a tool to predict binder fatigue life.



Figure 2-11. Comparison of fatigue life measured in time sweep tests and predicted using S-VECD model calibrated using time sweep test results.

2.4.4.2 Model Validation Using LAS Test Results

Despite the observed differences in the damage characteristic curves obtained from the time sweep and LAS tests, the performance prediction ability of the S-VECD model as derived using the LAS test results was evaluated. The ability to use the LAS test results for the S-VECD model calibration is of great interest, as the LAS test is easier to implement than the time sweep test. To assess the performance prediction capability of the LAS tests, the results were used to fit the damage characteristic curves and failure criterion models given in Equations (2.15) and (2.16), respectively. Optimized model coefficients were input into Equation (2.21) in order to predict the fatigue life data that correspond to the strain amplitudes and temperatures of the time sweep tests.

The comparison between the fatigue life data measured from the time sweep tests and those predicted using the S-VECD modeling of the LAS test results are shown in Figure 2-12. These results indicate relatively good agreement between the measured and predicted fatigue life data. At conditions that correspond to long term fatigue (i.e., low strain and high temperature), the LAS test results tend to under-predict the fatigue life somewhat. However, the rankings of the predicted fatigue life data amongst the various materials and test conditions remain in good agreement with the measured trends from the time sweep tests, indicating that the LAS test can still be used to assess the relative fatigue performance of binders under various loading and thermal conditions.

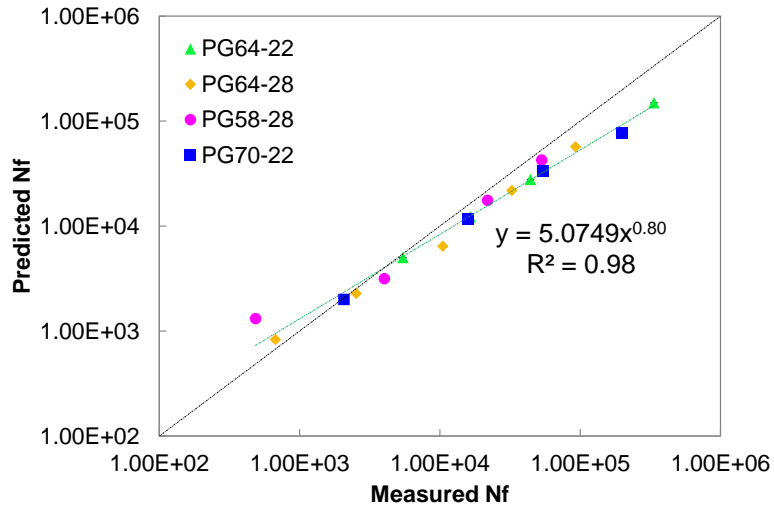


Figure 2-12. Comparison of fatigue life measured in time sweep tests and predicted by S-VECD model calibrated using LAS test results.

It is speculated that the under-prediction is the result of the material nonlinearity that is associated with the high strain amplitudes used in the LAS test, which are neglected in the analyses for simplicity, as previously stated. Separating nonlinearity and damage is very challenging and would require much more extensive testing than the quick LAS test. Thus, although it is recommended that future research quantifies the effects of nonlinearity on LAS test results, given the relatively good agreement between the fatigue life data predicted by the LAS test and the measured fatigue life data, it is recommended that the LAS test protocol coupled with S-VECD modeling should still be considered as a practical and efficient tool for assessing the fatigue performance of asphalt binders.

2.5 Linking Asphalt Binder S-VECD Results to Mixture and Field Performance

2.5.1 Linking Asphalt Binder and Mixture S-VECD Damage Characteristic Curves

As an initial assessment of the linkage between the asphalt binder and mixture S-VECD model results, the damage characteristic curves obtained for the binders and mixtures were compared. Figure 2-13 presents the comparison between the binder and mixture damage characteristic curves that correspond to the data collected by Safaei et al. (2014) to evaluate the effects of aging on the fatigue resistance of WMA and HMA mixtures. In Figure 2-13, the left-hand column displays the binder damage characteristic curves of the three mixtures evaluated at each age level, where the curves that correspond to each aging level are shown in separate rows. The right-hand column shows the corresponding asphalt mixture damage characteristic curves. The results demonstrate strong agreement in the trends amongst the binder and mixture damage characteristic curves at each age level considered.

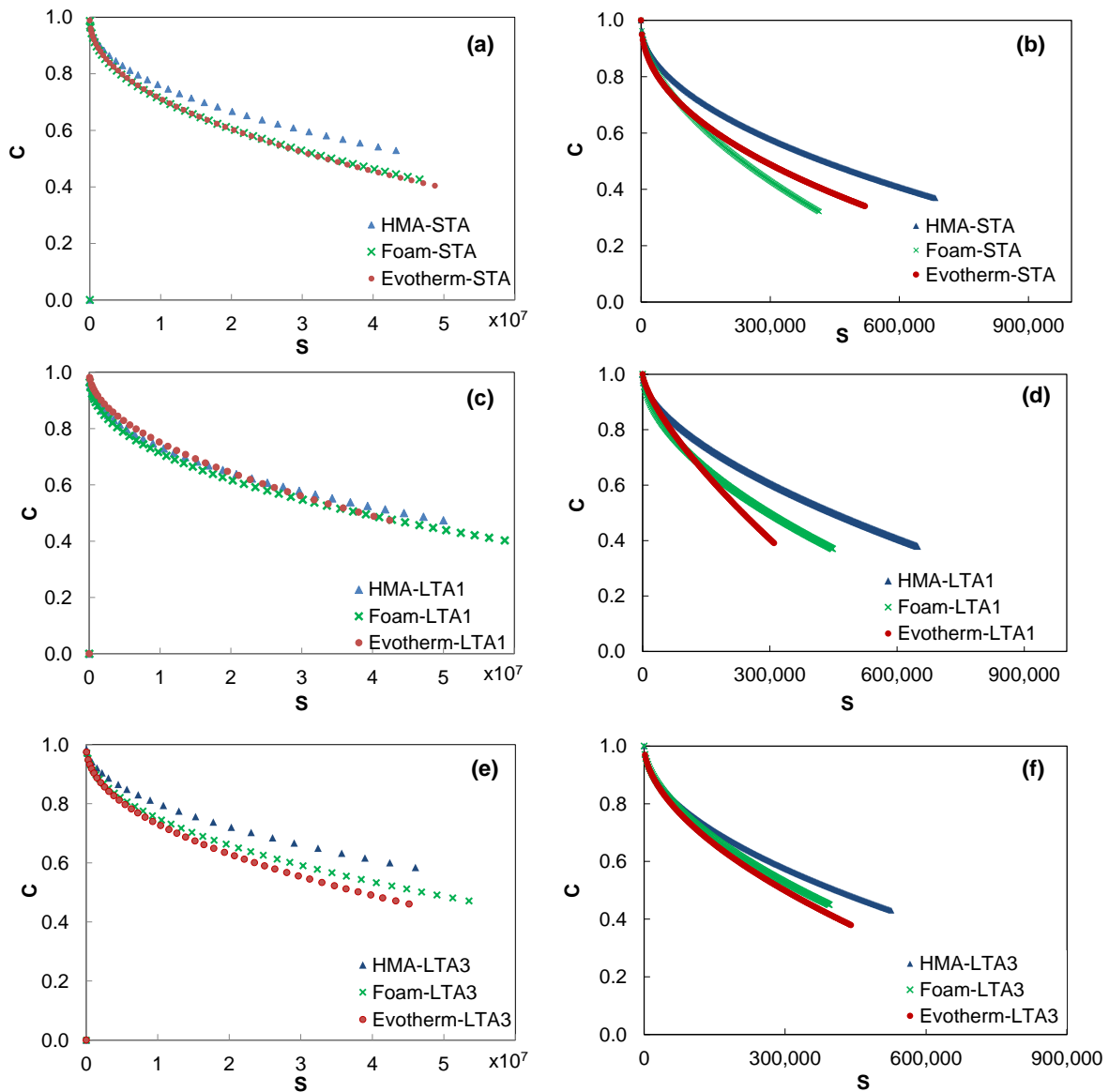


Figure 2-13. Damage characteristic curves corresponding to: (a) binder STA, (b) mixture STA, (c) binder LTA1, (d) mixture LTA1, (e) binder LTA3, and (f) mixture LTA3.

Figure 2-14 presents a comparison between the binder and mixture damage characteristic curves that correspond to those of the ALF materials tested by Wang et al. (2015). Figure 2-14 shows similar rankings of the materials in terms of the S-VECD damage characteristic curves. These results provide promising evidence that the binder S-VECD model reflects mixture fatigue

resistance and highlight the importance of the binder in determining mixture fatigue performance.

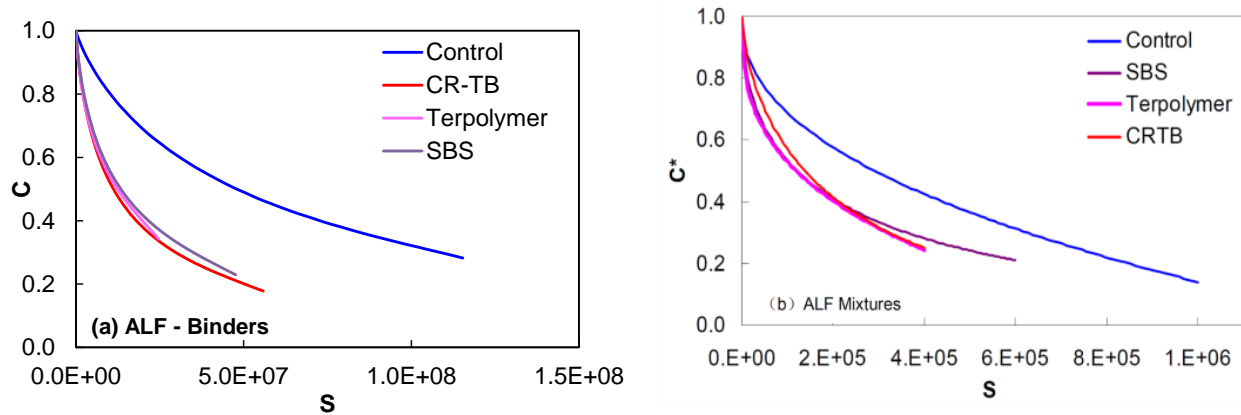


Figure 2-14. Comparison between ALF (a) binder and (b) mixture damage characteristic curves.

2.5.2 Linking Asphalt Binder S-VECD Model Results to Field Performance

Given the promising similarity between the binder and mixture S-VECD damage characteristic curves, the ability of the binder S-VECD model to capture mixture performance in a field setting was evaluated. The fatigue performance of pavements is a function of both the asphalt concrete's ability to resist cracking and the strain that the material experiences as dictated by the pavement structure. Thus, these two factors must be taken into account in establishing a link between binder and field performance. Therefore, in evaluating the ability to link the asphalt binder to mixture performance using the S-VECD model in a realistic scenario, a layered viscoelastic analysis (LVEA) model (Kim and Underwood 2010) was applied to determine the strain kernel at the bottom of the asphalt layer in a representative pavement structure subjected to a moving wheel load. Asphalt mixture dynamic modulus test results were input into the LVEA model along with tire pressure and speed in order to predict the tensile strain response at the bottom of the asphalt layer. For use in asphalt binder S-VECD modeling, the strain obtained

from LVEA must be scaled, as the binder experiences a much greater strain than the bulk mixture. Therefore, for asphalt binder fatigue life predictions, the peak tensile strain value obtained from the strain kernel analysis was multiplied by 80. This strain ratio of 80 was selected based on previous findings that suggest that this strain ratio results in equivalent binder and corresponding mixture fatigue life data (Safaei et al. 2014) and is also consistent with findings obtained from multiscale modeling (Underwood 2011).

2.5.2.1 Aging Study (Safaei et al. 2014)

No field performance data were available for the aging study conducted by Safaei et al. (2014). However, an evaluation of the performance of the different materials studied within a pavement structure was deemed critical, because mixture stiffness (which increases with age) can have a significant effect on the resultant strain within the mix when loaded in a pavement structure. Therefore, although oxidative aging is generally assumed to decrease the material's fatigue resistance, the reduction in deflection due to mixture stiffening will reduce the strain, which has a beneficial effect on fatigue resistance. Thus, the combined effect of changes in the material's fatigue resistance and pavement deflection must be considered when evaluating the implications of aging on fatigue.

Therefore, a relatively simple thin pavement structure that is assumed to produce bottom-up cracking was used in performance prediction analyses that use binder and mixture S-VECD models. The developed pavement structural model includes a four-inch thick asphalt layer over subgrade with an elastic modulus value of 70 MPa. A single moving wheel load with contact pressure of 758 kPa, contact area of 0.3 m x 0.18 m, and velocity of 26.8 m/sec was utilized at 19°C for LVEA. The strain kernels obtained were input into the mixture S-VECD model for

fatigue life prediction. In addition, the peak tensile strain value from the strain kernel was multiplied by 80 and input into the binder S-VECD fatigue life prediction model (Equation (2.21)). Figure 2-15 presents the correlation between the binder and mixture predictions of fatigue life using S-VECD modeling. The results demonstrate reasonable agreement (R^2 of 0.84) between the mixture and binder fatigue life predictions.

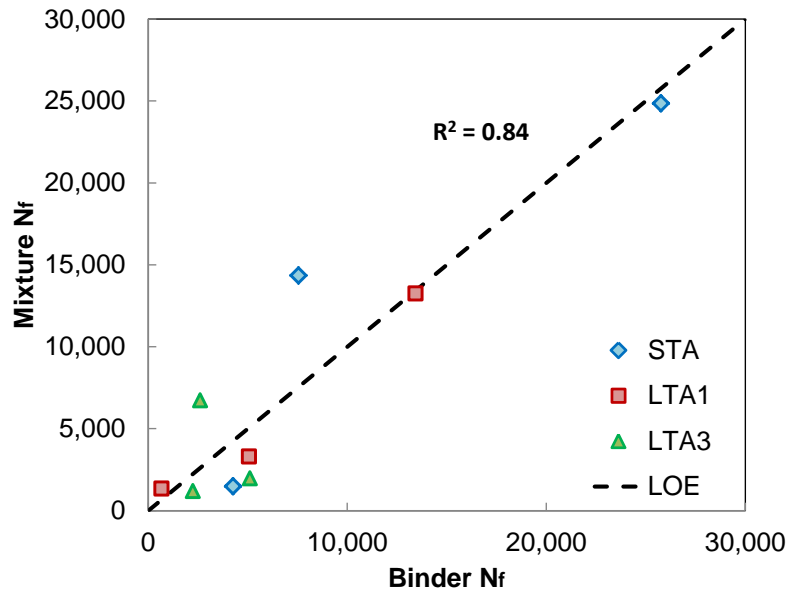


Figure 2-15. Comparison between mixture and binder predictions of fatigue life using a binder-to-mix strain ratio of 80 (Safaei et al. 2014).

2.5.2.2 FHWA ALF Study (Wang et al. 2015)

The FHWA-ALF study is an ideal performance study for evaluating the effect of the binder on the pavement’s fatigue performance, because the test lanes were constructed using equivalent structures and mixture compositions with the exception of different binder types (Nelson et al.). The ALF test sections were exposed to isothermal conditions at 19°C during the fatigue evaluation. The wheel loading consisted of 71-kN loads applied using tires inflated to 827 kPa. These loading conditions along with the known wheel speed, pavement structure, and

mixture dynamic modulus values were input into the LVEA model in order to determine the strain kernel at the bottom of the asphalt mixture for each lane. The maximum tensile strain values obtained from the analysis were multiplied by 80 and input into the S-VECD-based fatigue life prediction models derived for each binder. The fatigue life predictions were compared to the ALF-measured fatigue life data, defined as the number of wheel passes required to reach a crack length of 25 m (Gibson 2010).

The comparison between the binder predictions of fatigue life and field-measured fatigue life is shown in Figure 2-16, excluding the CR-TB binder. CR-TB was excluded from Figure 2-16 because this binder demonstrated the longest binder predicted fatigue life but relatively poor field performance. Considering only the binders, it is not surprising that the CR-TB material performed the best, because it contains both terminal blend ground tire rubber and styrene-butadiene-styrene, thereby including more modification than the other binders under consideration (Kluttz et al. 2014). Thus, the CR-TB binder may affect the aggregate structure formation or exhibit a unique interaction with the aggregate, which cannot be captured using a binder test alone.

With the exception of the CR-TB binder, a high correlation is evident between the measured and binder predicted fatigue life data, thereby providing validation that binder S-VECD modeling can be used effectively to predict the binder's effect on the pavement's fatigue performance. However, the results of this study should be verified in the future using a larger data set.

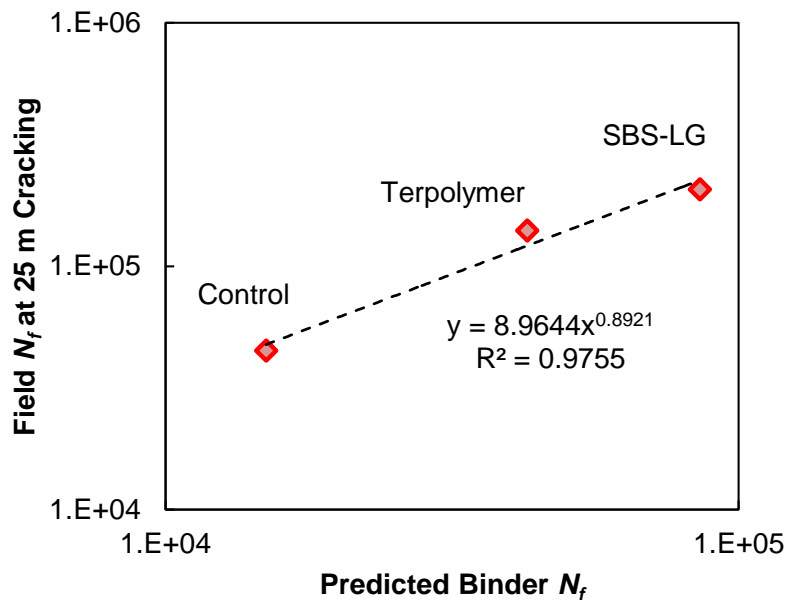


Figure 2-16. Comparison between measured field fatigue life and binder prediction of fatigue life using a binder-to-mix strain ratio of 80 (Wang et al. 2015).

2.6 Conclusion

The following points summarize the findings of this study:

- Schapery's extended elastic-viscoelastic correspondence principle applies to asphalt binders subjected to cyclic loading in a DSR.
- S-VECD modeling can be applied to asphalt binder time sweep test results, thereby producing a damage characteristic curve that is independent of loading mode, loading amplitude, and temperature. Use of the model for fatigue life predictions was verified in this study.
- S-VECD modeling allows a damage characteristic curve to be derived that is independent of temperature, based on LAS testing (AASHTO TP 101). However, the damage characteristic curves differ from those obtained from time sweep tests, but nonetheless retain a consistent material ranking. Furthermore, although fatigue life

predictions using the S-VECD model calibrated using LAS tests are less accurate than for time sweep tests, the predictions are still deemed reasonable, especially considering the efficiency gains associated with the use of the LAS test over the time sweep test.

- The pseudo strain energy-based failure criterion (G^R) is independent of temperature, loading mode, and loading history. This failure criterion is equivalent for time sweep and LAS tests and can be derived using test results obtained from three or more conditions (i.e., temperature or loading history) to define the G^R function.
- The use of the S-VECD model to model the binder DSR results in order to predict the binder's contribution to mixture and pavement fatigue performance was demonstrated using data from two studies. Although promising, it is suggested that the findings be confirmed using a broader data set.
- It should be noted that the developed framework only related to cohesive binder failure within asphalt concrete mixtures. Future research should also seek to quantify the impact of asphalt – aggregate adhesive failure on fatigue resistance of asphalt concrete.

CHAPTER 3 IMPLICATION OF WARM MIX ASPHALT ON LONG TERM OXIDATIVE AGING AND FATIGUE PERFORMANCE OF ASPHALT BINDERS AND MIXTURES²

3.1 Introduction

Warm mix asphalt (WMA) represents a group of technologies that can be used to produce asphalt pavement mixtures at temperatures 30°F to 100°F lower than those used to produce traditional hot mix asphalt (HMA) (Haggag et al. 2011). The primary benefits of using WMA are reduced energy consumption and emissions, which improves sustainability and worker conditions. In addition, lower production temperatures allow for improved compaction, longer transport (in terms of both times and distances) and, hence, construction at remote locations, an extended paving season, and the ability to open the site to traffic sooner, thereby reducing user-delay costs.

Despite the advantages of using WMA, the long-term performance implications of WMA compared to HMA remain largely unknown. Reduced production temperatures used for WMA compared to HMA lead to reduced oxidation and volatilization during production, which has been speculated to lead to less long-term aging. However, the extent to which reduced production temperatures affect long-term aging and the implications of this reduced aging on fatigue performance merits further study, as previous studies have shown mixed results (Koenders et al.

² This chapter has been published as: Safaei, F., Lee, J., Nascimento, L. A. H., Hintz, C, and Kim, Y.R (2015). “Implications of Warm-Mix Asphalt on Long Term Oxidative Aging and Fatigue Performance of Asphalt Binders and Mixtures” *Journal of Association of Asphalt Paving Technologies*, 15, 45–61.

2000, Kvasnak et al. 2010, Haggag et al. 2011). This study compares the performance of WMA and HMA mixtures subjected to varying levels of laboratory long-term oven aging according to (AASHTO PP) to gain a better understanding of the implications of reduced short-term aging in WMA on long-term performance. Because asphalt binder is the asphalt mixture constituent that undergoes aging, this study focuses on evaluating trends in the properties of WMA and HMA binders extracted and recovered from laboratory-aged mixtures in comparison to the bulk properties of their respective mixtures.

Extracted and recovered asphalt binders and mixtures were subjected to dynamic modulus and fatigue testing. The simplified viscoelastic continuum damage (S-VECD) model was applied to interpret the fatigue performance results and was combined with layered linear viscoelastic analysis to predict the fatigue performance of the WMA and HMA materials.

3.2 Objectives

The objectives of this study are to:

1. Evaluate the implications of reduced short-term aging in WMA compared to HMA in terms of long-term fatigue performance and
2. Compare the fatigue performance of WMA and HMA binders with regard to their respective mixtures.

3.3 Experimental Program

3.3.1 Materials and mix design

The mix design for the HMA and WMA mixtures considered in this study is consistent, that is, the same gradation and binder content were used for both types of mixtures. The mix

used is a fine 9.5 mm nominal maximum aggregate size (NMAS) mix comprised of 19% RAP and 6.7% (5.2% from virgin binder and 1.5% from RAP) PG 70-22 binder from the Superpave mix design ($N_{des} = 75$ gyrations).

Two WMA technologies, Evotherm 3G and foaming, are used in this study to evaluate the effects of WMA on long-term fatigue performance. Evotherm 3G is a chemical surfactant that reduces the internal friction of the asphalt binder and increases the compatibility of the asphalt binder and aggregate, resulting in improved workability and allowing for mixing and compacting at reduced temperatures. The foaming technology is the injection of water into hot asphalt binder through a nozzle. Upon coming into contact with the hot binder, the water turns to steam, forming small bubbles throughout the asphalt, which leads to a volume expansion of the asphalt binder and consequently improves its workability with the aggregate.

For this study, the Evotherm 3G additive was added to the asphalt binder at 157°C at a rate of 0.5% by weight of total asphalt. No anti-stripping agent was used for the Evotherm mixture. For the foamed mix, an anti-stripping agent of 0.7% by weight of total asphalt was added to the pure asphalt binder at 135°C. Then, 2% water by weight of total asphalt was injected into the asphalt binder at 157°C using the PTI foaming machine. Based on a curing time project that investigated a Double Barrel Green foamed mixture, lab-compacted foamed WMA specimens were cured at the ambient temperature for at least 12 days prior to long-term aging conditioning or any testing (Kim 2012). The temperatures of the aggregate, RAP and binder for both of the WMA mixes (Evotherm and foamed) at the time of mixing were 135°C, 110°C, and 157°C, respectively. The temperature for both the aggregate and the binder of the HMA mix was 157°C and that of the RAP was 110°C at the time of mixing.

3.3.2 Laboratory aging methods

All laboratory aging was conducted in a forced draft convection oven. Short-term oven aging (STA) was applied to the HMA mix at 135°C for four hours according to AASHTO R 30 prior to compaction. Short-term aging was applied to both WMA mixtures at 117°C for two hours according to NCHRP 9-43 recommendations (Bonaquist 2011). A Servopac Superpave gyratory compactor was used to compact the test specimens to a height of 178 mm and a diameter of 150 mm. The compacted specimens were cored and cut to a height of 150 mm and a diameter of 75 mm to ensure uniformly distributed air void samples. In order to simulate the long-term aging (LTA) of the HMA and WMA mixtures using (AASHTO R 3), the cored and cut samples were conditioned at 85°C for two days and at 85°C for eight days as the LTA Level 1 (LTA1) and Level 3 (LTA3), respectively. All cored and cut samples were wrapped with wire mesh to avoid slump in the samples during aging. Following the short-term and long-term aging processes, the binders were extracted and recovered to allow for mechanical testing and analysis.

3.3.3 Asphalt binder testing

The mechanical testing of the asphalt binders was conducted using a TA AR-G2 dynamic shear rheometer (DSR) with 8 mm parallel plate set-up. The linear viscoelastic characterization consisted of measuring the dynamic shear modulus ($|G^*|$) of the asphalt binders using frequency sweep tests at 1% shear strain amplitude at 64°C, 50°C, 30°C, 20°C, and 5°C and a range of 0.1 to 30 Hz loading frequency. The fatigue characterization of the asphalt binders was measured using linear amplitude sweep (LAS) tests at 19°C. The LAS test, (AASHTO TP 101 (2014)) , is an oscillatory strain sweep test consisting of linearly increasing strain from 0.1% to 30% effective strain amplitude at a constant frequency of 10 Hz over the course of 310 seconds. A

VECD framework can be applied to predict the fatigue life at any strain amplitude from the LAS test results (Hintz et al. 2011, Hintz et al. 2011).

3.3.4 Asphalt mixture testing

Dynamic modulus and controlled crosshead (CX) cyclic direct tension tests were used to evaluate the linear viscoelastic properties and fatigue of the asphalt mixtures in this study.

Dynamic modulus testing was performed in load-controlled mode in axial compression following the protocol given in (AASHTO PP 61-09 (2009)) using the Asphalt Mixture Performance Tester (AMPT). Tests were completed for all mixtures at 5°C, 20°C, and 40°C and at frequencies of 25, 10, 5, 1, 0.5, and 0.1 Hz. Load levels were determined by a trial and error process so that the resulting strain amplitudes were between 50 and 75 microstrain to prevent damage to the specimens. Cyclic and direct tension tests were carried out in CX mode in axial tension using a closed-loop servo-hydraulic material test system (MTS) to measure the fatigue resistance of the asphalt mixtures. All tests were performed at three different strain levels, causing failure at approximately 1,000, 10,000, and 50,000 cycles at 19°C and 10 Hz loading frequency.

3.4 Analysis methods

3.4.1 Linear viscoelasticity

Mastercurves were constructed using the dynamic modulus values. For the mixtures, uniaxial dynamic modulus values were measured in compression, and for the asphalt binders, dynamic shear modulus values were measured using the DSR. For the asphalt mixtures, the mastercurves for the dynamic moduli were fitted to the sigmoidal function, Equation (3.1), and

the time-temperature shift factor function, i.e., Equation (3.2), by employing an optimization process. To transform to the time domain, a Prony series was then fitted to the data, which takes the analytical form in terms of the relaxation modulus ($E(t)$), given in Equation (3.3).

$$\log |E^*| = a + \frac{b}{1 + \frac{1}{e^{d+g \log f_R}}} \quad (3.1)$$

$$\log a_T = \alpha_1 T^2 + \alpha_2 T + \alpha_3 \quad (3.2)$$

$$E(t) = E_\infty + \sum_{i=1}^m E_i * e^{-t/\rho_i} \quad (3.3)$$

$$\sigma = \int_0^t E(t-\tau) \frac{\partial \varepsilon}{\partial \tau} d\tau \quad (3.4)$$

Where f_R = reduced frequency; a , b , c , d , g = fitting coefficients of the sigmoidal function; a_T = the time-temperature shift factor; α_1 , α_2 , α_3 = fitting coefficients of the time-temperature shift factor function; T = temperature; E_∞ = long-term equilibrium modulus; E_i = modulus of Prony term number i ; t = time; ρ_i = relaxation time of Prony term i ; τ = integration term; and ε = strain.

The asphalt binder dynamic shear modulus and phase angle mastercurves were constructed through time-temperature shifting (Equation (3.2)) and fitting to the Christensen-Anderson-Marasteanu (CAM) model (Christensen and Anderson 1992) given in Equations (3.5) and (3.6).

$$|G^*|(f_R) = |G^*|_g \left[1 + \left(\frac{f_c}{f} \right)^k \right]^{-\frac{m_e}{k}} \quad (3.5)$$

$$\delta(f_R) = \frac{90}{\left[1 + \left(\frac{f_c}{f}\right)^k\right]} \quad (3.6)$$

Where f_R = reduced frequency (Hz); $|G^*|_g = |G^*|$ as $f \rightarrow \infty$: glassy dynamic modulus, equal to 1 GPa for asphalt binder; f_c = location parameter with dimensions of frequency; and k , m_e = shape parameters, dimensionless.

3.4.2 Viscoelastic continuum damage analysis

The fatigue test results were interpreted using the simplified viscoelastic continuum damage (S-VECD) model. VECD-based frameworks have been used extensively to characterize the complex behavior of asphalt mixtures (Kim and Little 1990, Park et al. 1996, Underwood et al. 2006, Underwood et al. 2010) and more recently have been applied to binders (Hintz et al. 2011). Details about the S-VECD model development are provided elsewhere (Underwood et al. 2010); however, a brief overview is provided herein. VECD modeling of asphalt materials is based on Schapery's work potential theory that utilizes an internal state variable, S , to quantify damage as a result of microstructural changes that lead to a reduction in effective stiffness. The internal state variable that represents damage is derived from the following damage evolution law:

$$\frac{dS}{dt} = \left(-\frac{\partial W^R}{\partial S} \right)^\alpha \quad (3.7)$$

Where W^R is the pseudo strain energy density, and α is a material-dependent constant. Because asphalt mixture testing is conducted in uniaxial tension and binder testing is conducted in torsion, there are some differences between the binder and mixture analyses. The S-VECD framework for the binders used in this research was developed to best match the corresponding

framework that is applied to the asphalt mixtures. For the asphalt mixtures, α is defined as $1 + 1/m$, where m is the maximum slope of the relaxation modulus mastercurve in log space (Underwood et al. 2010). For the asphalt binders, which are viscoelastic fluids, the mastercurves have a parabolic rather than sigmoidal shape, and therefore, the definition of α used for the asphalt mixtures cannot be extrapolated directly to the binders. For the work herein, α for the binders is defined as $1/m$, where m is the steady-state slope of the dynamic shear modulus mastercurve in log space, which is equivalent to the m_e parameter of the CAM model defined in Equation (3.5).

Effectively, the pseudo strain is equivalent to the linear viscoelastic stress response to the loading history of interest divided by an arbitrary reference modulus. Thus, the replacement of stress with pseudo strain eliminates the hysteretic behavior associated with viscoelasticity and reduces the stress-strain relationship to an equation resembling the linear elastic Hooke's law.

Table 3-1 provides a summary of the analytical frameworks applied to the asphalt mixtures and binders in this study. Within the VECD framework, Schapery's elastic-viscoelastic correspondence principle is used to separate the time effects associated with viscoelasticity from damage by replacing measured strain with pseudo strain (defined in Table 3-1). The equations for pseudo strain, provided in Table 3-1, resemble the equations for linear viscoelastic stress, with the exception of the inclusion of a reference modulus (i.e., E_R and G_R for mixture and binder, respectively). The reference modulus is a constant of arbitrary value, which is most often chosen to be one, in which case pseudo strain is equivalent to the undamaged linear viscoelastic stress for a given loading history.

The equations provided in Table 3-1 for pseudo strain energy density and S are functions of pseudo stiffness, $C(S)$, which is a material integrity parameter. The value of pseudo stiffness

with no damage is one, and then the pseudo stiffness decreases as material integrity is lost. The dynamic modulus ratio (DMR) in the (S) and S calculations is a parameter that is used to account for specimen-to-specimen variability. For the mixtures, this parameter is taken as the ratio between the measured dynamic modulus value, which is obtained from a fingerprint test at a low loading amplitude on the fatigue test specimen prior to the start of fatigue loading, to the measured linear viscoelastic dynamic modulus value obtained from the dynamic modulus test. Similarly, for asphalt binders, the DMR is taken to be the dynamic shear modulus value, $|G^*|$, at the start of the LAS test (which starts at a very low loading amplitude) to the dynamic shear modulus value measured from frequency sweep testing. The equation for S is derived through numerically solving Equation (3.1).

One noteworthy difference between the mixture and binder frameworks presented in Table 3-1 is that the mixture analysis involves performing a rigorous calculation of pseudo strain and damage during the first loading cycle, whereas the binder framework does not. This rigorous calculation is necessary because a significant amount of damage is observed during the first tensile loading path during CX mixture testing, whereas relatively small increments of damage are observed within subsequent cycles, and damage can be estimated reasonably by considering only the changes between peak C values (i.e., C^*) from consecutive cycles. In the LAS binder testing, the initial strain amplitude is relatively small, and thus, no significant damage is observed during the first loading path; hence, no rigorous calculation of damage is necessary. Additionally, in the mixture testing, damage is found to grow only when in a state of tension, and thus, a shape factor (K_1) must be applied to reduce the total time to the time only when damage grows. In the torsional testing of the binders, damage is assumed to grow during all loading times, and thus, no shape factor is necessary.

The power of the S-VECD model is that the relationship between C(S) and S is unique and can be used to back-calculate the damage behavior of the asphalt binder or mixture under any loading conditions of interest as long as the viscoplastic strain is insignificant in the loading condition of interest.

Table 3-1. Asphalt Mixture and Binder S-VECD Analysis Frameworks.

Property	Mixture (Uniaxial Cyclic Direct Tension)	Binder (Cyclic Torsion in DSR)
Pseudo strain, ε^R ; γ^R	$\varepsilon^R = \frac{1}{E_R} \int_0^t E(t-\tau) \frac{\partial \varepsilon}{\partial \tau} dt \quad \text{for } t < t_p$ $\varepsilon_{pp}^R = \frac{1}{E_R} (\varepsilon_{pp_i} \cdot E^* _{LVE}) \quad \text{for } t > t_p$	$\gamma_{pp}^R = \frac{1}{G_R} (\gamma_{pp_i} \cdot G^* _{LVE})$
Pseudo strain energy density, W^R	$W^R = \frac{1}{2} C(S) (\varepsilon^R)^2$	$W^R = \frac{1}{2} C(S) (\gamma^R)^2$
Pseudo stiffness, $C(S)$	$C(S) = \frac{\sigma}{\varepsilon^R \cdot DMR} \quad \text{for } t < t_p$ $C^*(S) = \frac{\sigma_{pp}}{\varepsilon_{pp}^R \cdot DMR} \quad \text{for } t > t_p$	$C^*(S) = \frac{\tau_{pp}}{\gamma_{pp}^R \cdot DMR}$
Damage, S	$S = \sum_{i=1}^N \left[\frac{DMR}{2} (\varepsilon^R)^2 (C_{i-1} - C_i) \right]^{\frac{\alpha}{1+\alpha}} [t_i - t_{i-1}]^{\frac{1}{1+\alpha}}$ <p>for $t < t_p$</p> $S = \sum_{i=1}^N \left[\frac{DMR}{2} (\varepsilon_{pp}^R)^2 (C_{i-1}^* - C_i^*) \right]^{\frac{\alpha}{1+\alpha}} [(t_i - t_{i-1}) \cdot K_1]^{\frac{1}{1+\alpha}}$ <p>for $t > t_p$</p>	$S = \sum_{i=1}^N \left[\frac{DMR}{2} (\gamma_{pp}^R)^2 (C_{i-1}^* - C_i^*) \right]^{\frac{\alpha}{1+\alpha}} [(t_i - t_{i-1})]^{\frac{1}{1+\alpha}}$
Parameter definitions	E_R = arbitrary reference modulus selected to be 1	

Table 3-1. Continued.

<p>$E(t)$ = relaxation modulus</p> <p>τ = time variable of integration</p> <p>ε = strain</p> <p>ε_{pp}^R = peak pseudo strain in a given cycle</p> <p>ε_{pp} = peak strain in a given cycle</p> <p>$E^* _{LVE}$ = linear viscoelastic dynamic modulus</p> <p>t_p = time to peak tensile stress in first loading cycle</p> <p>DMR = dynamic modulus ratio =</p> $\frac{ E^* _{fingerprint}}{ E^* _{LVE}}$	<p>G_R = arbitrary reference modulus selected to be 1</p> <p>$G(t)$ = shear relaxation modulus</p> <p>γ_{pp}^R = peak pseudo strain in a given cycle</p> <p>γ_{pp} = peak shear strain in a given cycle</p> <p>$G^* _{LVE}$ = linear viscoelastic dynamic shear modulus</p> <p>DMR = dynamic modulus ratio =</p> $\frac{ G^* _{fingerprint}}{ G^* _{LVE}}$
--	---

3.5 Discussion of Results

3.5.1 Material-level results

Figure 3-1 presents the dynamic modulus and VECD damage characteristic curves for the binders and mixtures after short-term aging. As expected, Figure 3-1 (a) and (b) show that the HMA binder and corresponding mix are stiffer than both the WMA binders and mixtures (foam and Evotherm) due to reduced short-term aging. Note that for WMA, the short-term aging consisted of two hours of conditioning at 117°C prior to compaction, whereas for HMA, short-term aging consisted of four hours of conditioning at 135°C. It also can be observed that the binder mastercurves and damage characteristic curves for both WMA technologies are very similar. These results indicate little effect of the Evotherm additive on the binder mechanical response since the foamed WMA mixtures contain neat asphalt and both WMA mixtures were

subjected to the same aging conditions. However, there is some difference in the Evotherm and foam WMA mixture master curves, indicating some difference in effect of the two technology on the binder interaction with aggregate from either the surfactant effect of the Evotherm additive and/or the presence of steam in the asphalt during production of foamed mixtures. Also noteworthy is that the discrepancy between the HMA and WMA binder mastercurves appears to be greater than for the asphalt mixtures. This finding implies that a unit change in the binder dynamic shear modulus does not lead to a unit change in the mixture dynamic modulus, which is expected as the mixture dynamic modulus also is affected by aggregate properties and, thus, is not as sensitive to changes in levels of aging as are the binder properties.

The trends observed in the binder and mixture damage characteristic curves following short-term aging (Figure 3-1 (c) and (d)) are in good agreement, indicating that binder plays an important role in determining the fatigue resistance of asphalt mixtures. As said before, because of the binder-aggregate interactions in mixture we can never expect the exact same behavior for binder and mixture however; we can look for the same ranking for binders as their corresponding mixtures. It can be seen for both binders and mixtures that the HMA C versus S curves fall above those of the foam and Evotherm WMA mixtures. The foam and Evotherm C versus S curves are similar, indicating that foaming versus Evotherm additive makes little difference to fatigue performance.

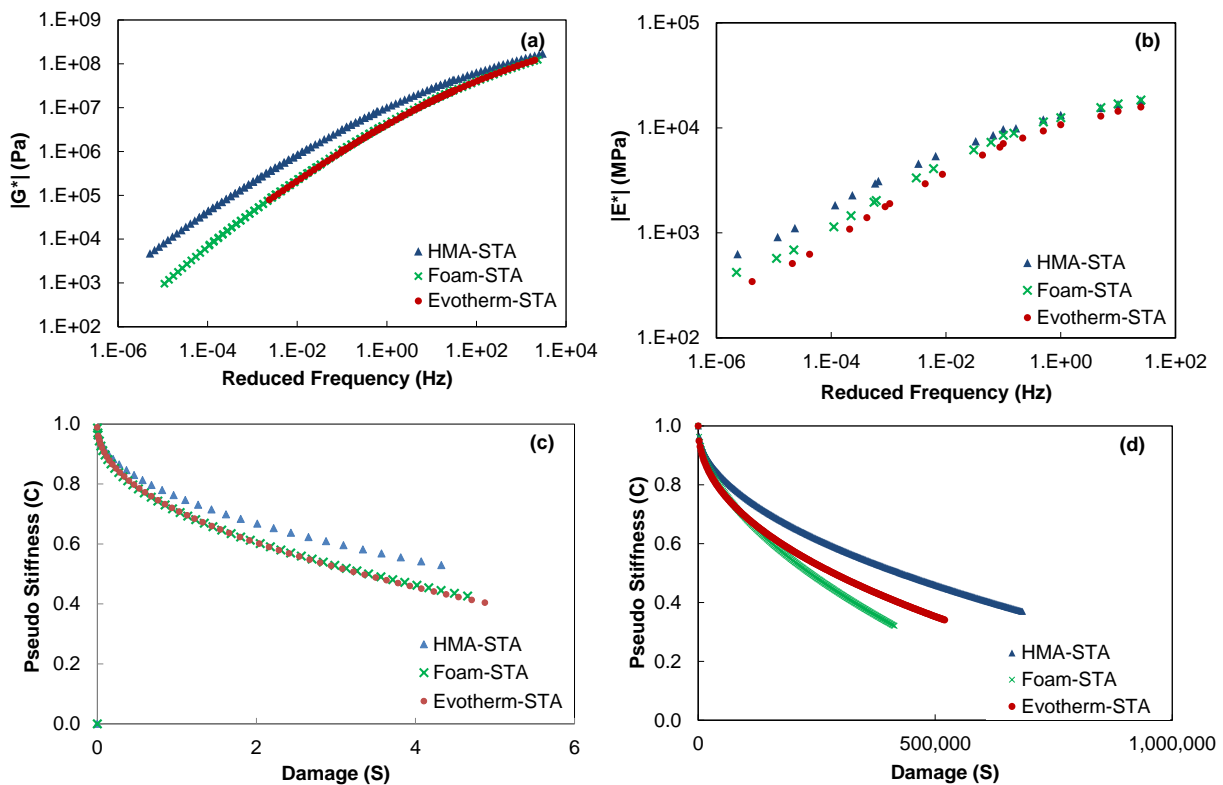


Figure 3-1. STA master curves for (a) binders (b) mixtures, damage characteristic curves at a reference temperature of 19°C for (c) binders (d) mixtures.

Figure 3-2 presents the dynamic modulus and VECD damage characteristic curves for the binders and mixtures following LTA1. For LTA1, which corresponds to approximately four years of aging in the field (Zapata and Houston 2008) trends in the dynamic modulus values are similar to those observed after short-term aging. The WMA mixtures and corresponding binders have similar dynamic modulus values and are softer than the HMA mixture and binder. The VECD damage characteristic curves are also similar. However, the binder damage characteristic curves indicate less difference between the HMA and WMA binders than do the mixture results, indicating the WMA technologies' effects on aggregate-binder interaction may be significant.

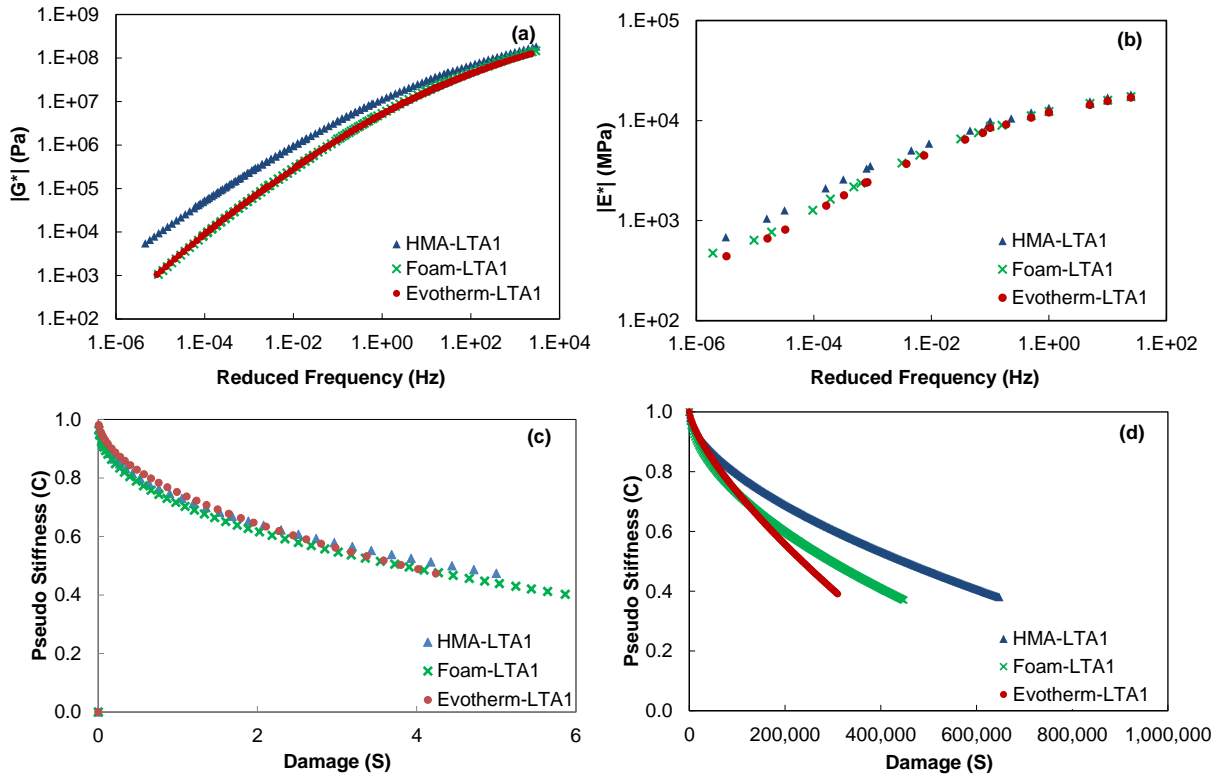


Figure 3-2. LTA1 master curves for (a) binders (b) mixtures, damage characteristic curves at a reference temperature of 19°C for (c) binders (d) mixtures.

Figure 3-3 presents the dynamic modulus and damage characteristic curves at LTA3, which corresponds to approximately 18 years of aging in the field (Zapata and Houston 2008). The results still indicate that the HMA binder is stiffer and, hence, more aged than the WMA binders as a consequence of increased production temperatures. The C versus S curves of the WMA and HMA binders and mixtures have a similar pattern, indicating important role of binder on mixture behavior.

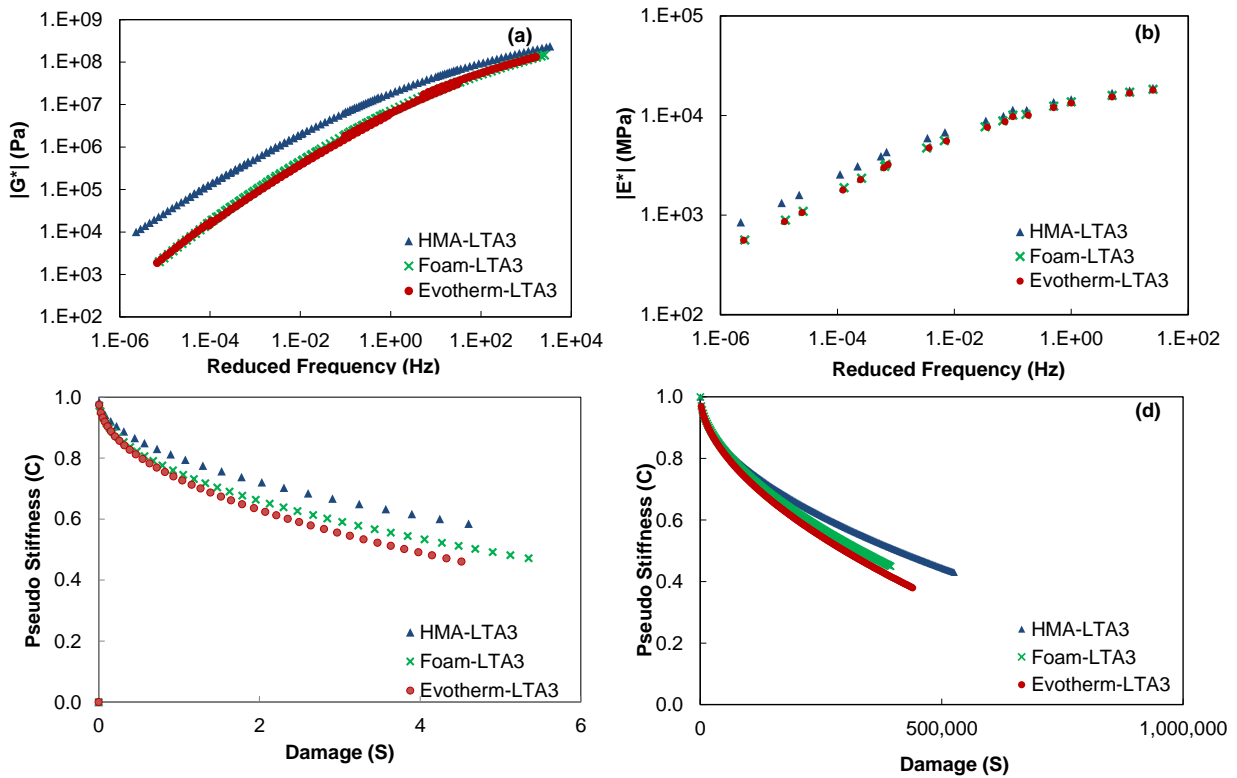


Figure 3-3. LTA3 master curves for (a) binders (b) mixtures, damage characteristic curves at a reference temperature of 19°C for (c) binders (d) mixtures.

In addition to observing trends in the dynamic moduli and fatigue damage characteristic curves, trends in the cross-over modulus ($|G_c^*|$) with age level were analyzed. The cross-over modulus is the value of the dynamic shear modulus at the cross-over frequency (i.e., the frequency when the phase angle is equal to 45°). Farrar et al. (2013) demonstrated that binder oxygen uptake is linearly correlated with the inverse of the log $|G_c^*|$. Thus, trends in the inverse of log $|G_c^*|$ serve as an adequate ‘aging index property’ to study the extent of oxidation using rheological measurements. Figure 3-4 presents the trends in the aging index property for the HMA and WMA binders considered in this study. It shows that at all aging levels, the aging index property of the HMA binder is higher than that of the WMA binders. Figure 3-4 also indicates that although the aging index property follows expected trends, relative changes in

magnitude are quite small. Also noteworthy is that the HMA aging index increases much less with long-term aging than for the WMA binders, particularly at LTA3, indicating a higher long-term aging rate in the WMA binders compared to the HMA binder. This phenomenon can possibly be explained by asphalt oxidation kinetics. Asphalts typically oxidize in two stages: first according to a nonlinear fast-rate period and later according to a linear constant-rate period (Jin et al. 2011). For HMA, most of the fast-rate oxidation occurs during production. However, for WMA, this may not be the case, and fast-rate oxidation may extend to the pavement's early service life. Consequently, the aging characteristics of HMA and WMA may be very different early in a pavement's service life, but after extensive long-term aging, the differences may become less significant.

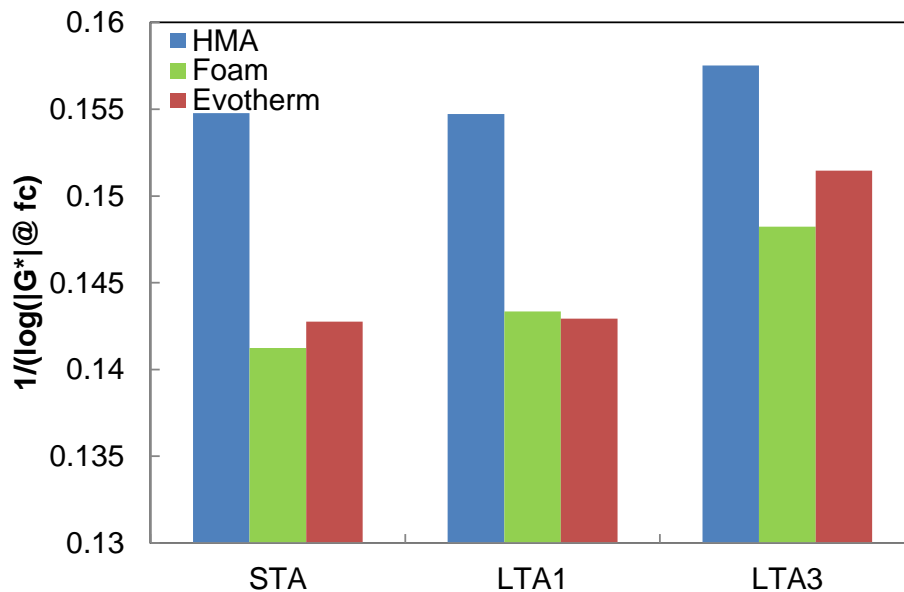


Figure 3-4. Trends in aging index property.

Use of the binder cross-over modulus as an aging index property was validated through comparison to trends in mixture dynamic modulus ratio, taken to be ratio between $|E^*|$ after long-term aging and the $|E^*|$ after short-term aging. $|E^*|$ ratios at 10Hz loading frequency for all

temperatures of testing for both LTA1 and LTA3 aging levels are presented in Figure 3-5. Results show several interesting trends. It can be seen that the $|E^*|$ ratio is highly dependent on the temperature (and thus, rate of loading). At low temperatures (or analogously high loading frequencies), aging level has little effect on $|E^*|$ as evident by low $|E^*|$ ratios. However, at high temperatures (and/or low loading rates), aging ratios become significant. At the LTA3 aging level, the WMA $|E^*|$ ratios at 20°C, 40°C, and 60°C are higher than those for HMA, indicating a higher extent of oxidation following short-term aging. Generally, the trends in Figure 3-5, specifically at higher temperatures where the effect of aging on mixture dynamic modulus is found to be significant, are in good agreement with trends in Figure 3-4, indicating promise for the use of the crossover modulus as an aging index property.

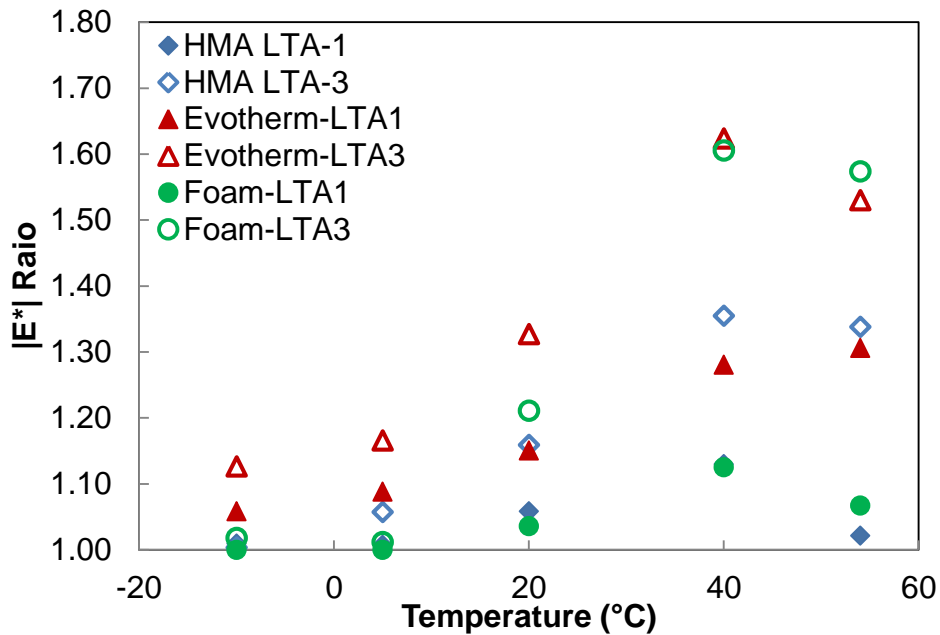


Figure 3-5. $|E^*|$ ratio ($|E^*|$ after long-term aging / $|E^*|$ after short-term aging) values at 10 Hz loading frequency.

3.5.2 Fatigue failure definition

In addition to the damage characteristic curves that are used to define fatigue resistance, the damage and material integrity (i.e., C value) at failure is also important in defining fatigue resistance. In this study, the fatigue life of asphalt mixture specimens tested in cyclic direct tension was determined by trends in phase angle. It has been demonstrated that the phase angle increases until the point of damage localization and, hence, the onset of macrocracking, and then decreases during the remainder of the test.

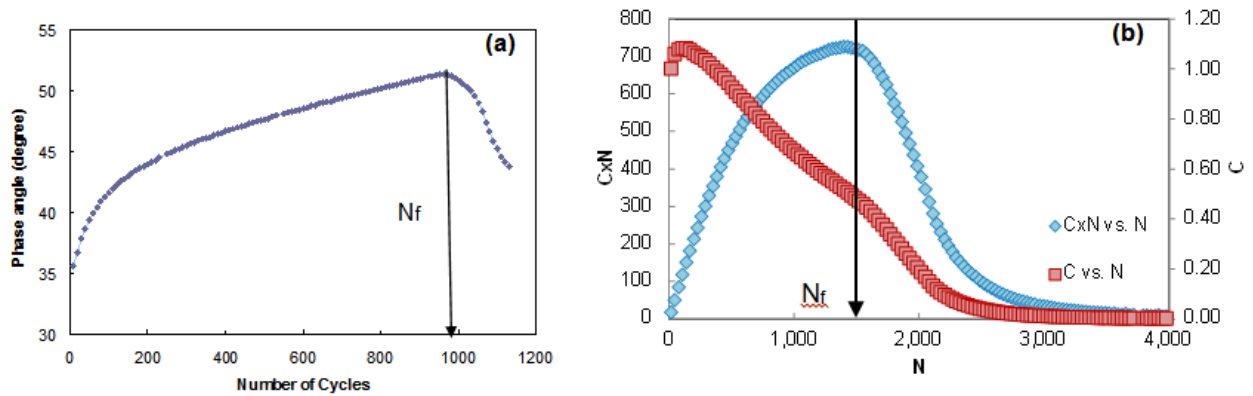


Figure 3-6. Fatigue failure definitions for (a) asphalt mixtures and (b) asphalt binders.

Figure 3-6 (a) illustrates this phenomenon. For the asphalt binders, the trends in phase angle are less clear. Thus, in the case of the asphalt binders, the peak in C times N (where N is the number of loading cycles) versus N is used to define failure, which is similar to the stiffness times N approach proposed by (Rowe 1993). Similar to the phase angle failure definition, the peak in C times N corresponds to a marked change in the rate of loss in material integrity, as shown in Figure 3-6 (b), and is therefore considered a logical failure definition.

Figure 3-7 (a) and (b) present the results of C value at failure (C_f) for the HMA and WMA mixtures and binders tested at all levels of aging using the aforementioned definitions of fatigue failure, respectively. Similar trends are observed for C_f for both the binders and mixtures,

indicating the ability of the LAS test to capture the binder's contribution to mixture fatigue and the important role that asphalt binder plays in determining mixture fatigue resistance. The C_f value generally increases as the aging level increases, which is intuitive, because an increase in C_f implies damage localization at a high material integrity level and, hence, increased brittleness, which is expected as the oxidation level increases. In addition, the binder C_f values are higher than those for the mixtures are and appear to be somewhat more sensitive to material type in general. However, there is some discrepancy in material ranking between the binder and mixture results at LTA3.

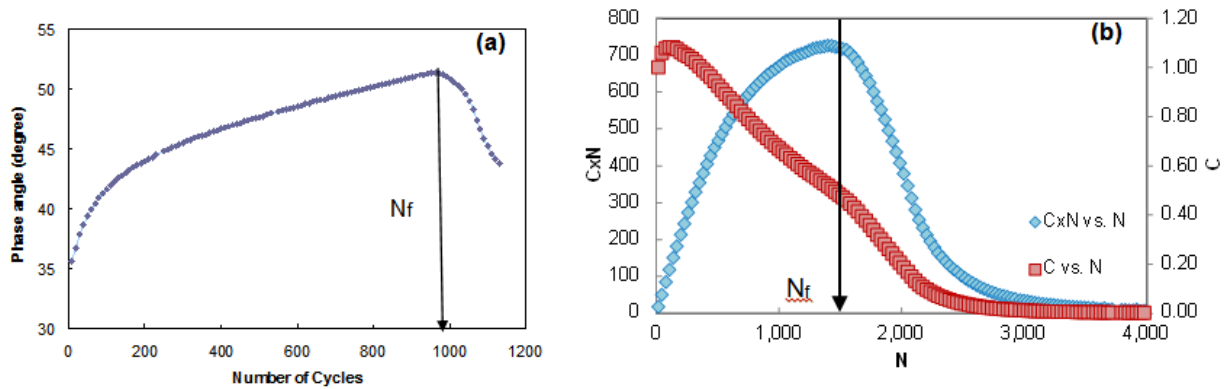


Figure 3-7. Fatigue failure definitions for (a) asphalt mixtures and (b) asphalt binders.

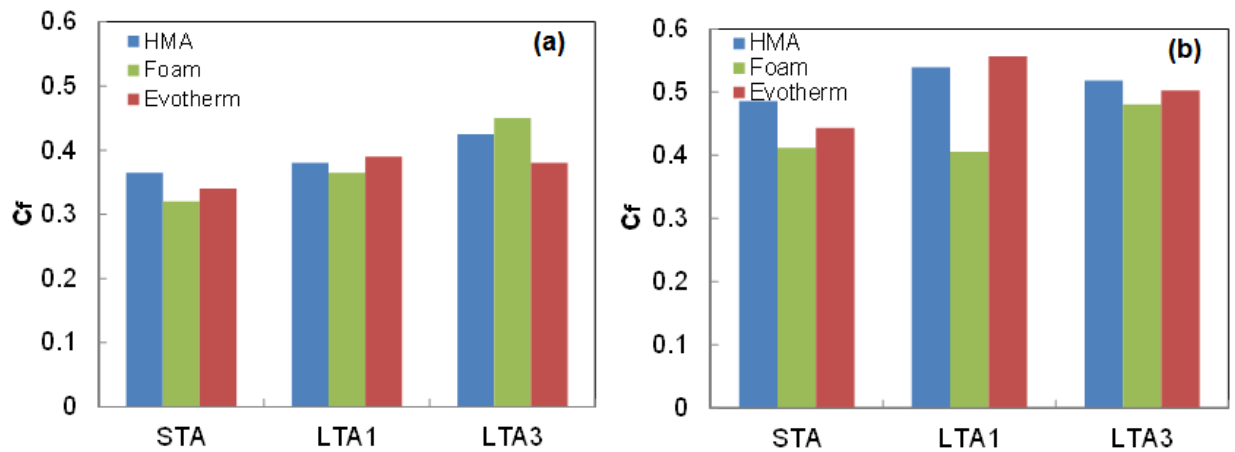


Figure 3-8. C at failure values for (a) mixtures and (d) binders.

3.5.3 Fatigue performance analysis

The fatigue performance of pavements is a function of the material's ability to resist damage and a function of the strain that the material experiences. Thus, it is important to consider both the loading that a given material will undergo in a given pavement structure as well as the material's damage resistance characteristics to predict how an asphalt mixture will perform in the field. In this study, the fatigue performance of the asphalt mixtures was evaluated by combining the VECD model and the pavement responses determined from the structural analysis of the pavement. The structural analysis consists of applying a layered viscoelastic analysis (LVEA) model developed at North Carolina State University to determine the strain kernel at the bottom of an asphalt pavement layer. The pavement structural model used in this study has a 4-inch thick asphalt layer over subgrade with an elastic modulus of 70 MPa. The temperature gradient of the asphalt layer is determined by first dividing the asphalt layer into three sublayers. The average temperature of each of the three sublayers is determined from the data obtained from the Enhanced Integrated Climatic Model (EICM) for April 2004 in Raleigh, North Carolina. This temperature gradient results in the dynamic modulus gradient along the depth of the asphalt layer in the calculation of the strain kernel. A single moving wheel load is simulated using a contact pressure of 758 kPa, contact area of 0.3 m x 0.18 m, and velocity of 26.8 m/sec for a rectangular wheel load. The single wheel moving load is applied repeatedly to the pavement until the strain response of a steady-state condition is obtained. The pavement response in the steady-state condition is used as a repeated constant input loading history for the S-VECD model. This strain kernel is then input to the VECD model, and the fatigue life is determined by applying the asphalt mixture's C_f as the failure criterion. This procedure is

accomplished using an effective cyclic modulus, $|S^*|$, defined in Equation (3.8) (Underwood 2011).

$$|S^*| = \frac{\max\left(\int_0^t E(t-\tau) \frac{d(\varepsilon_0 f(t))}{d\tau} d\tau\right)}{\varepsilon_0} \quad (3.8)$$

Where ε_0 is the peak strain from the pavement response simulation, and $f(t)$ is a function that describes the time dependence of the strain for a single loading cycle. If a power law model (Equation (3.8)) is fitted to the data, the number of cycles to failure can then be derived analytically, as presented in Equation (3.9) (Underwood 2011).

$$C = 1 - C_{11}(S)^{C_{12}} \quad (3.9)$$

$$N_f = \frac{(2^\alpha) S_f^{\alpha - \alpha C_{12} + 1}}{(\alpha - \alpha C_{12} + 1)(C_{11} C_{12})^\alpha [\varepsilon_0 |S^*|]^{2\alpha} (t_p) K_1} \quad (3.10)$$

Where S_f is the damage at failure.

Figure 3-9 presents the results of the fatigue performance evaluation. Figure 3-9 (a), (b), and (c) show the strain kernels for the HMA, foamed WMA, and Evotherm WMA mixtures, respectively. It can be seen that, as expected, as the aging level increases, the strain levels in the pavement decrease as a result of an increase in the asphalt concrete stiffness. Also, it can be seen from Figure 3-8 that the strain level in the HMA pavement is lower than that of the WMA mixtures due to the lower stiffness values of the WMA mixtures compared to the HMA. These results highlight the importance of considering the pavement structural responses in predicting fatigue performance, as the results could be misleading if the fatigue performance of the WMA and HMA mixtures was evaluated at the same strain amplitude. Figure 3-9 (d) presents the fatigue life prediction results of the pavement structural analysis combined with the S-VECD

model results. Because fatigue is the accumulation of damage over time, these results suggest that the HMA mixtures perform better than the WMA mixtures due to the superior performance of the HMA during the first two levels of aging. That is, Figure 3-8 shows that at STA and LTA1, the HMA shows superior fatigue performance compared to the WMA. However, at LTA3, the differences in fatigue performance between the WMA and HMA become negligible, indicating that the effects of reduced short-term aging in WMA compared to HMA diminish with increasing long-term aging for this pavement structure.

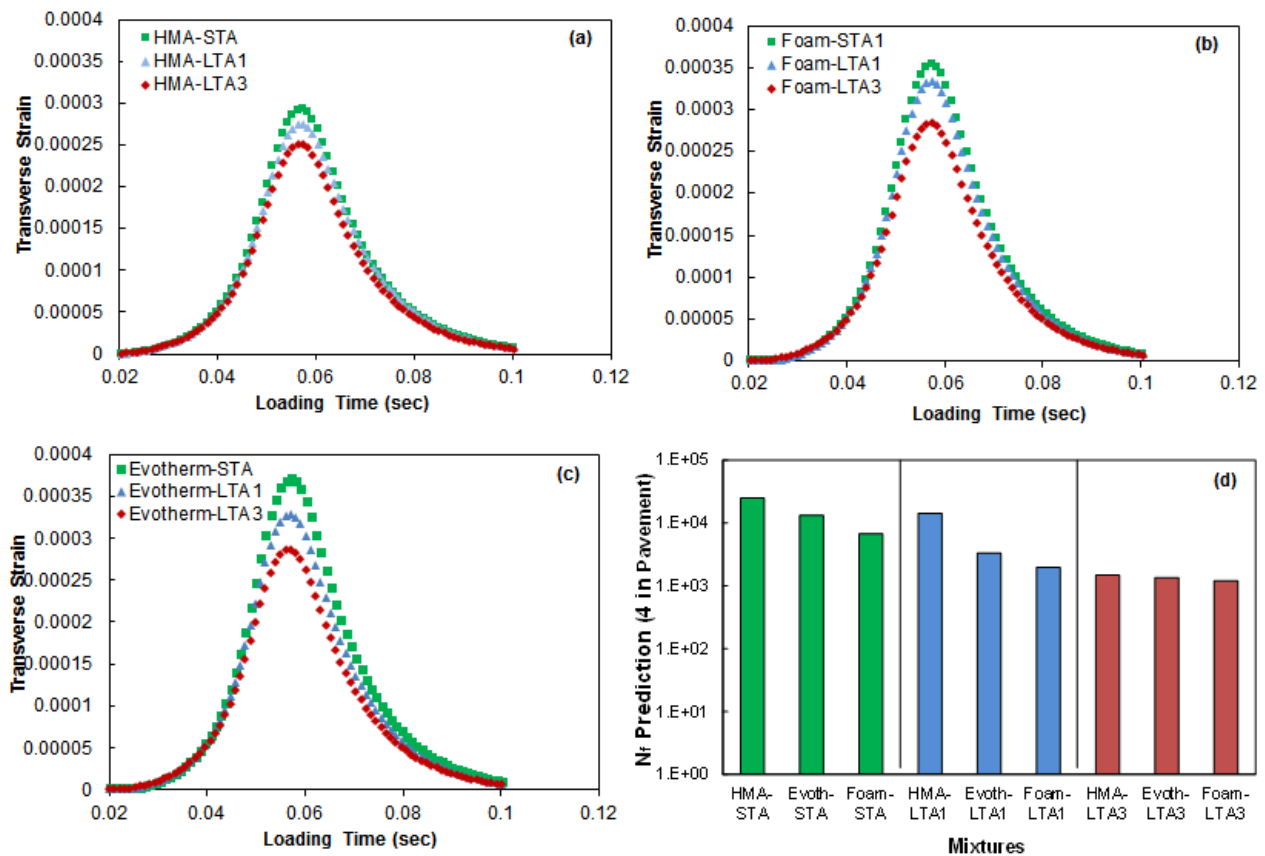


Figure 3-9. Fatigue performance analysis results for asphalt mixtures: (a) HMA, (b) Foam WMA, (c) Evotherm WMA, and (d) Fatigue life comparison of the mixtures.

A similar approach was taken to evaluate asphalt binder fatigue performance using the pavement response strain kernels. However, it is not straightforward to convert the strain kernel

results in into equivalent asphalt binder strain levels. That is, it is difficult to determine the strain within the binder phase of an asphalt mixture. Some studies have been conducted to estimate the ratio between binder strain and mixture strain. Kose et al. (2000) performed a finite element analysis of HMA cross-sectional images to study strain distributions within asphalt concrete and concluded that the strain in the binder phase of asphalt concrete is 9 to 90 times that of the bulk mixture strain. Underwood concluded that “a good rule of thumb” is that the strain in the binder phase of a mixture is 122.5 times that of the bulk mixture strain (Underwood 2011). Assuming that damage originates in the binder phase of the mix, and in order to gain a reasonable estimate of the appropriate strain to evaluate the fatigue resistance of the binders, the ratio between the binder and mix strains was adjusted to give a 1:1 relationship between the binder and mixture fatigue life based on the S-VECD results of the binder testing. It was found that this trend occurred when the strain in the binder was assumed to be 80 times that of the bulk mixture (corresponding to a binder strain amplitude on the order of 2% to 3%), which is within the range proposed in the literature. Figure 3-10 presents the correlation between binder and mixture fatigue life using a binder-to-mixture strain ratio of 80. Although there is a fair amount of scatter around the line of equality (LOE), the results demonstrate reasonable agreement (R^2 of 0.84) between the mixture and binder fatigue life predictions. Also, trends with aging in Figure 3-10 are consistent with Figure 3-9 (d), demonstrating that as aging progresses, the relative difference in performance of HMA and WMA diminishes. These results suggest promise that the LAS test coupled with S-VECD analysis can capture the asphalt binder’s contribution to mixture fatigue. However, it should be noted that this is only a single data set and thus, findings should be validated in future work.

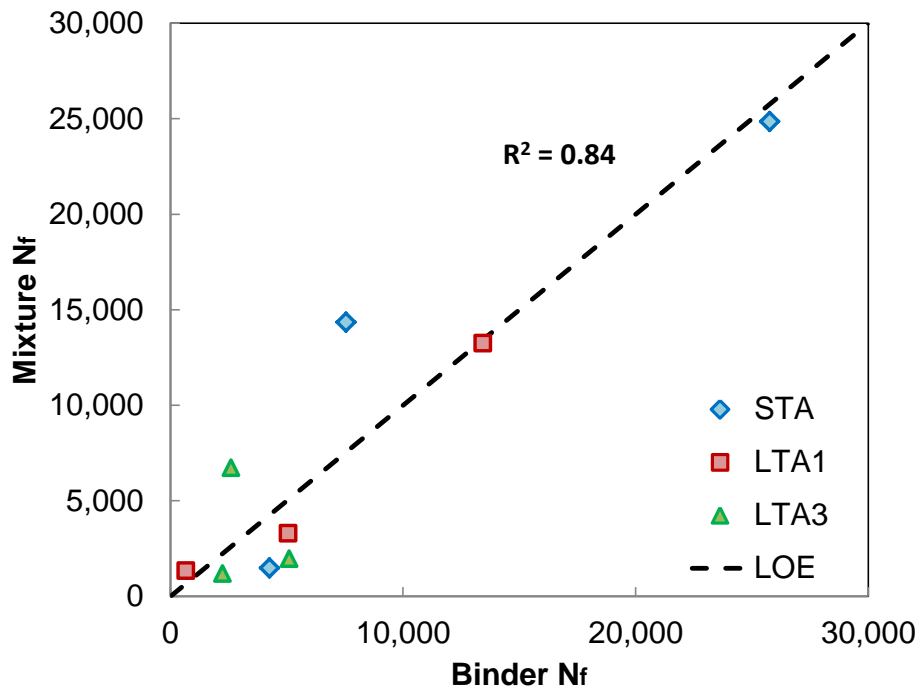


Figure 3-10. Comparison between mixture and binder fatigue life.

3.6 Conclusions

The following conclusions can be drawn from the results and analysis presented:

- The HMA mixtures and binders have higher modulus values than the WMA mixtures and binders, even following long-term aging, which indicates that the effects of reduced short-term aging in WMA lead to differences in long-term aging. However, as the level of long-term aging progresses, the effect of reduced short-term aging diminishes somewhat.
- Based on a combination of pavement structural responses and S-VECD analysis, it is demonstrated that HMA used in this study shows superior fatigue performance compared to corresponding foamed and Evotherm WMA mixtures at STA and LTA1. However, at LTA3, the differences in the fatigue performance of WMA and HMA mixtures are

negligible. It is noted that this finding is limited to the mixtures used in this study and should not be generalized to all HMA and corresponding WMA mixtures.

- The results of this study generally demonstrate good agreement between the asphalt binder and mixture results, highlighting the importance of asphalt binder in determining the performance of asphalt mixtures and also demonstrating the ability of the LAS test coupled with S-VECD analysis to capture the binder's contribution to asphalt mixture fatigue.

CHAPTER 4 TEMPERATURE EFFECTS IN LINEAR AMPLITUDE TESTING AND ANALYSIS³

4.1 Introduction

Fatigue in asphalt pavements is caused by the accumulation of damage under repeated traffic loading. Fatigue cracks generally initiate and propagate within the binder phase of asphalt concrete. Therefore, specification of properties related to asphalt binder fatigue resistance can serve as a screening tool to select binders that are not inherently susceptible to fatigue under given environmental and traffic loading. Pavements are subjected to seasonal and daily fluctuations in temperature. Asphalt binder exhibits temperature dependent viscoelastic behavior. Consequently, asphalt binder fatigue resistance varies with temperature (Soenen and Eckmann 2000, Anderson et al. 2001, Martono 2008, Bodin et al. 2010, Al-Khateeb and Ghuzlan 2014). Therefore, consideration of temperature effects in developing specifications to address fatigue resistance of asphalt binder is critically important.

Current Superpave Performance Grading (PG) specifications to address asphalt binder fatigue resistance place a maximum limit on the parameter $|G^*| \cdot \sin \delta$ at the intermediate climatic PG to evaluate fatigue performance (AASHTO MPI-93 IA Edition). The parameter $|G^*| \cdot \sin \delta$ is determined by applying cyclic loading in the Dynamic Shear Rheometer (DSR) for very few cycles at small strain amplitude (1%), assumed to be within the linear viscoelastic range of the material. The specification was developed under the assumption that a lower dissipated energy implies lower propensity for cracking (Bahia et al. 2001). A major drawback of the current

³ This chapter has been published as: Safaei, F., and Castorena, C.(2016). “Temperature Effects in Linear Amplitude Sweep Testing and Analysis” *Journal of Transportation Research Record*, DOI: 10.3141/2574-10

specification is that it is based on linear viscoelastic properties and not inherent cracking resistance. Consequently, it has been proven that $|G^*| \cdot \sin \delta$ does not reflect true material fatigue resistance (Bahia et al. 2001). In addition, the current “intermediate temperature” specification defined as the average of the high and low PG temperatures + 4°C lacks theoretical or practical basis (AASHTO TP 101). Thus, there is a need to develop an improved asphalt binder specification that better reflects fatigue resistance. Furthermore, an improved definition of “intermediate” temperature is needed to better reflect critical climatic conditions associated with a high propensity for cracking.

The Linear Amplitude Sweep (LAS) test (AASHTO TP 101) has been proposed as a practical replacement to the current specification (AASHTO TP 101). The LAS test consists of cyclic loading in the DSR, utilizing the standard 8mm parallel plate geometry. The LAS test includes an oscillatory strain amplitudes sweep to induce fatigue damage at an accelerated rate. The LAS test also includes a frequency sweep to obtain a fingerprint of the material’s undamaged material response, which can be run directly before the amplitude sweep on the same specimen. Total testing time is 30 minutes. Simplified Viscoelastic Continuum Damage (S-VECD) modeling can be applied to LAS test results to enable prediction of fatigue life at any strain amplitude of interest. Recently, the analysis protocol has been enhanced to include a failure criterion to improve predictability (Wang et al. 2015). However, specification for the selection of LAS test temperature and modeling of temperature effects within the S-VECD framework remain to be resolved. Currently, AASHTO TP 101 specifies test temperature selection consistently with the current PG specifications for intermediate temperature, which lacks relation to climatic conditions and/or material characteristics under which fatigue is most

critical. Therefore, this study seeks to improve upon the current specification for selection of LAS test temperature and to integrate temperature effects into the S-VECD model.

4.2 Objectives

The objectives of this study are to:

1. Develop improved specifications for selection of LAS test temperature based on climatic Performance Grade (PG)
2. Enable fatigue life prediction at varying temperatures using the S-VECD model

4.3 Developing Improved Specification for Selection of LAS Test Temperature

It is important to consider two factors in developing specifications for the selection of LAS test temperatures: (1) climatic conditions and (2) material characteristics under which the binder is most susceptible to fatigue cracking. It is generally assumed that fatigue damage in asphalt pavements is most critical at intermediate temperatures corresponding to springtime when the poor drainage in the pavement causes the loss of underlying support, leading to high deformation in the asphalt concrete under traffic loading (Huang 1993). However, fatigue presumably occurs throughout the year and thus, consideration of the most frequent temperatures a pavement experiences in a given climate is also an important consideration. In addition, test temperature can affect the failure mechanism of the asphalt binder during LAS testing. Hintz and Bahia Hintz and Bahia (2013) observed cohesive radial cracks propagating from the sample periphery towards the specimen in LAS tests. However their study only included testing of asphalt binder over a limited range of temperatures and did not take the confounding effects of

edge flow in to account. Soenen and Eckmann (Soenen and Eckmann 2000, Soenen et al. 2004) reported that when binders are subjected to cyclic loading in the DSR at too high of temperatures, edge flow occurs but at sufficiently low temperature, fatigue cracks developed. Anderson et al. (2001) made similar observations and defined a transition between true fatigue and instability flow based on the modulus of the binder by observing the fatigue life trends with temperature. Safaei and Hintz (2014) evaluated the effect of temperature on asphalt binders cyclically loaded at constant strain amplitude in the DSR. They recommended that test temperatures be selected such that linear dynamic shear moduli corresponding to the test temperature and frequency are within the range of 10 and 60 MPa to avoid confounding effects of flow or adhesion loss. The LAS test aims to characterize cohesive cracking resistance and thus, it is imperative that test temperatures be selected such that specimens fail by cohesive cracking.

4.4 Incorporation of Temperature Effects into S-VECD Modeling of LAS

Test Results

4.4.1 Simplified Viscoelastic Continuum Damage Modeling

Simplified Viscoelastic Continuum Damage (S-VECD) modeling of LAS test results relies on the relationship between material integrity (C) and an internal state variable representing damage (S) derived based on Schapery's work potential theory (Schapery 1984). Material integrity is quantified using pseudostiffness, C , which is calculated using Equation (4.1).

$$C(S) = \frac{\tau_p}{\gamma_p^R \cdot DMR} \quad (4.1)$$

where τ_p is the peak stress in the cycle of interest, $DMR = \text{dynamic modulus ratio} = |G^*|_{\text{fingerprint}} / |G^*|_{LVE}$, where $|G^*|_{\text{fingerprint}}$ is determined based on the initial $|G^*|$ in the amplitude sweep and $|G^*|_{LVE}$ is the corresponding linear viscoelastic $|G^*|$ determined from the frequency sweep, and γ_p^R is peak pseudostrain in the cycle of interest. Effectively, pseudostrain is equivalent to the linear viscoelastic stress response to the loading history of interest divided by an arbitrary reference modulus, often selected to be one as is the case here. Peak pseudostrain in a given cycle can be calculated using Equation (4.2).

$$\gamma_p^R = \frac{1}{G_R} \cdot (\gamma_p \cdot |G^*|_{LVE}) \quad (4.2)$$

where G_R is an arbitrary modulus, selected to be one and $|G^*|_{LVE}$ is the linear viscoelastic dynamic shear modulus at the fatigue testing temperature and loading frequency. Based on Equations (1) and (2), it can be observed that C equals one if the specimen behaves linear viscoelastically. As damage ensues, the measured stress responses deviate from that of linear viscoelastic behavior and consequently, the value of C will be less than one. Damage, S , is derived using Scahpery's work potential theory and calculated using Equation (4.3):

$$S(t) = \sum_{i=1}^N \left[\frac{DMR}{2} (\gamma_p^R)^2 (C_{i-1} - C_i) \right]^{\frac{\alpha}{1+\alpha}} \cdot [t_i - t_{i-1}]^{\frac{1}{1+\alpha}} \quad (4.3)$$

where t is time, and i refers to the cycle number. The parameter α is a material dependent constant. For the work herein, α is defined as $1/m + 1$ where m is the steady-state slope of the dynamic shear modulus master curve in log space (Underwood 2011). The power of the S-

VECD model is that the relationship between C and S is loading history independent, which allows for back-calculating response to any loading history of interest using limited test results.

Temperature effects have been incorporated into the S-VECD model for asphalt mixtures through use of time-temperature superposition (Chehab et al. 2002, Daniel and Kim 2002, Underwood et al. 2006, Hintz et al. 2011). Chehab et al. (2002) demonstrated that when reduced time and frequency are used in place of actual time and frequency, the relationship between C and S is temperature independent (Underwood et al. 2006, Hintz et al. 2011). Reduced time and frequency are calculated using linear viscoelastic time temperature shift factors and thus, the framework allows for predicting fatigue response at any temperature of interest using fatigue test results at a single test temperature coupled with linear viscoelastic time-temperature shift factors.

To incorporate time-temperature superposition temperature into the asphalt binder S-VECD model, damage is calculated using reduced time (ζ) as shown in Equation (4.4).

$$S(t) = \sum_{i=1}^N \left[\frac{DMR}{2} (\gamma_p^R)^2 (C_{i-1} - C_i) \right]^{1+\alpha} \cdot [\xi_i - \xi_{i-1}]^{1+\alpha} \quad (4.4)$$

4.4.2 Performance Prediction

To enable performance prediction, a clear definition of fatigue failure is needed. In addition, a failure criterion which can predict when the fatigue failure will occur under loading conditions other than those used in model characterization testing is needed.

4.4.2.1 Failure Definition

Failure in LAS tests is defined based on the peak in stored pseudostrain energy (W_s^R) (Wang et al. 2015). Stored pseudostrain energy (PSE) is defined in Equation (4.5).

$$W_s^R = \frac{1}{2} C \cdot (\gamma_p^R)^2 \quad (4.5)$$

Stored PSE represents the PSE that is stored with each loading cycle applied. An increasing W_s^R indicates that the material retains the ability to store additional energy as the loading amplitude (and hence energy input) increases in the LAS test. However, a decrease in W_s^R indicates that the material is losing the ability to store PSE as the loading input increases, indicating that failure has occurred. The peak in W_s^R corresponds to a transition to rapid loss in material integrity as shown in Figure 4-1 (a) and thus, represents an appropriate means for defining failure in LAS test results.

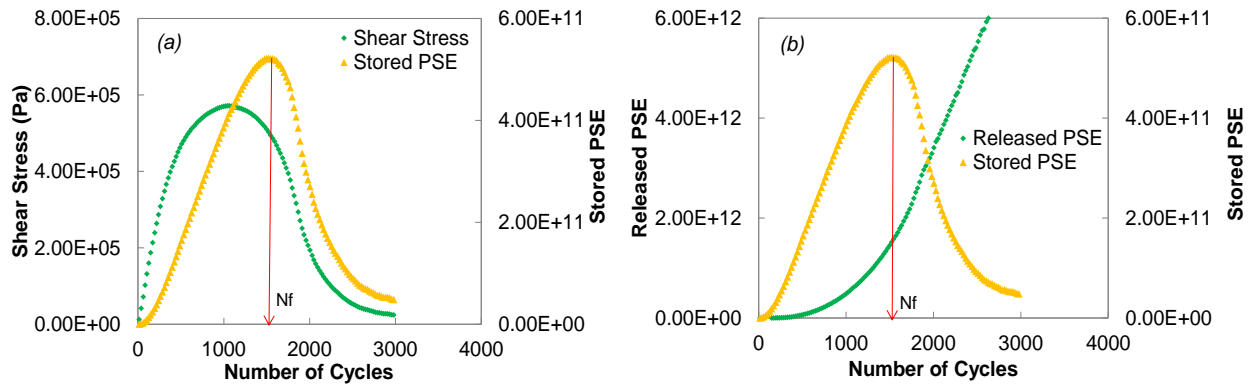


Figure 4-1. Depiction of (a) failure definition (b) calculation of released PSE.

4.4.2.2 Failure Criterion

A unified failure criterion is necessary to enable performance prediction of when failure will occur under conditions other than those used in testing. For example, a binder might fail at a material integrity (C) value of 0.3 under LAS loading history but may fail at a material integrity of 0.5 under constant loading at strain amplitude of 3%. Wang et al. (2015) developed the so-called G^R -based failure criterion for asphalt binders subjected to cycling loading in the DSR to enable prediction of failure under any loading history of interest using LAS test results. G^R is

defined as the average rate of PSE release up to the point of failure. Released PSE represents the difference between the total PSE and stored PSE and is calculated using Equation (4.6).

$$W_r^R = \frac{1}{2}(1-C)(\gamma_p^R)^2 \quad (4.6)$$

Correspondingly, G^R is defined in Equation (4.7).

$$G^R = \frac{\overline{W_r^R}}{N_f} = \frac{A}{N_f^2} \quad (4.7)$$

where A is the area under W_r^R curve until failure as illustrated in Figure 4-1 (b).

The relationship between fatigue life (N_f) and G^R comprises the failure criterion. This relationship has been shown to be loading history independent for asphalt binders and thus, effective in capturing loading history dependence on the material integrity at failure (Wang et al. 2015). The effect of temperature on the failure criterion has not been evaluated for LAS asphalt binder test results. However, Sabouri and Kim (2014) demonstrated that the relationship between N_f and G^R is independent of loading history and temperature for asphalt mixtures and thus, there is promise to extend the approach to capture the effects of temperature on binder failure.

4.4.2.3 Fatigue Life Prediction

Wang et al. (2015) integrated the S-VECD model and G^R failure criterion for prediction of fatigue life at any strain amplitude of interest using LAS test results. To incorporate the S-VECD model into fatigue life predictions, a power law model is fit to the damage characteristic curve $C(S)$ versus S according to Equation (4.8).

$$C = 1 - C_1(S)^{C_2} \quad (4.8)$$

where C_1 and C_2 are experimentally determined coefficients. Similarly, a power law model is fit to G^R versus N_f using Equation (4.9).

$$G^R = a (N_f)^b \quad (4.9)$$

The G^R failure criteria and damage characteristic curve models can then be used to derive a relationship between N_f and strain amplitude (γ), shown in Equation (4.10).

$$N_f = \left[\frac{A}{a} \cdot (\gamma)^{2+2\alpha\left(\frac{C_2}{k}\right)} \right]^{\frac{1}{b+1-\frac{C_2}{k}}} \quad (4.10)$$

where

$$k = 1 - \alpha \cdot C_2 + \alpha \quad (4.11)$$

$$A = \frac{1}{2} \cdot C_1 \cdot (|G^*|_{LVE})^2 \cdot B^{-C_2/k} \cdot \frac{1}{C_2/k + 1} \quad (4.12)$$

$$B = \frac{f_R \cdot 2^\alpha}{k \cdot (C_1 \cdot C_2)^\alpha (|G^*|_{LVE})^{2\alpha}} \quad (4.13)$$

where f_R is the reduced frequency and $|G^*|_{LVE}$ is the linear viscoelastic dynamic shear modulus corresponding to the conditions of interest. If temperature effects can successfully be incorporated into the S-VECD model and G^R failure criterion, Equation (4.12) can be used to predict fatigue life at any temperature and strain amplitude of interest using LAS results at a single temperature coupled with linear viscoelastic characterization at other temperatures of interest. Linear viscoelastic shift factors must be determined for the specific binder of interest using temperature – frequency sweep testing.

4.5 Experimental Plan

A set of asphalt binder experiments including linear viscoelastic and fatigue characterization were conducted on four binders with differing PGs. Results were used for two purposes (1) to observe trends in failure mechanisms and measured fatigue lives with temperature (and moduli) and (2) evaluate applicability of time-temperature superposition to LAS test results within the S-VECD model framework. In addition, climatic data covering a broad range of geographical regions was analyzed to identify the most frequent temperatures corresponding to peak traffic hours during both the spring season and annually. Since fatigue accumulates from repeated traffic loading, consideration of the most frequent temperatures is important in developing specifications for the selection of test temperature. Results were related to corresponding climatic PGs in order to develop an improved means of selecting test temperatures to reflect critical temperatures with respect to fatigue resistance.

4.5.1 Materials and Test Methods

The four binders evaluated in this study with corresponding experiments conducted are detailed in Table 4-1. Note that the PG 64-28 binder is a polymer modified asphalt while the other three binders are unmodified. All binders were aged in the standard Rolling Thin Film Oven (RTFO) + Pressure Aging Vessel (PAV) prior to testing. All tests were conducted in a TA AR-G2 DSR with the 8 mm parallel plate set-up. To determine the linear viscoelastic properties of each binder, frequency sweep tests were performed using 1% strain amplitude at temperatures of 35°C, 20°C, and 5°C and loaded at frequencies ranging from 0.1 to 30 Hz. Results were used to form dynamic shear modulus master curves and correspondingly, determine linear viscoelastic dynamic shear moduli and time-temperature shift factors corresponding to all fatigue tests.

Fatigue characterization of the asphalt binders was conducted using the LAS test. To support the LAS results, Time Sweep (TS) tests were performed in displacement controlled mode at 10 Hz loading frequency. Time sweep tests consist of repeated cyclic loading in the DSR at constant strain or stress amplitude. Predictions of TS results from S-VECD modeling of LAS test data were used to evaluate model capabilities. Standard LAS tests were conducted at 5, 10, 15, 20, 25, and 35°C to allow for comprehensive assessment of the effect of temperature on fatigue resistance. In addition to standard LAS (AASHTO TP 101), several additional LAS-type tests were conducted as deriving the failure criterion requires multiple data points with varying N_f (Wang et al. 2015). In the standard LAS, strain amplitudes are linearly increased from 0.1 to 30% over the period of 300 sec, corresponding to a constant strain amplitude rate (CSR) of increase of approximately 30%/300 sec or 0.001 s⁻¹. The additional LAS-type tests were conducted by varying the CSR but maintaining same strain amplitude range of 0.1 to 30%.

To evaluate the effect failure mechanisms in each fatigue test, samples were frozen following testing to preserve specimens and prevent healing. Following freezing, DSR spindles were carefully detached using the procedure proposed by Hintz and Bahia (2013) to allow for visual analysis of failure morphology. Bulging of the specimen outwards from the DSR plates and analysis of the failure morphology were used to identify failure mechanisms.

Table 4-1. Experimental Plan.

Binder	Test Temperature (°C)					
	LAS 0.1 1/S	LAS 0.05 1/S	LAS 0.01 1/S	TS 3%	TS 4%	Frequency Sweep
PG 70-22	5,10,15,20,25,30	20	20	5,10,15,20,25,30	25	5,20,35
PG 64-28	5,10,15,20,25,30	20	20	5,10,15,20,25,30	15	5,20,35
PG 64-22	5,10,15,20,25,30	20	20	5,10,15,20,25,30	20	5,20,35
PG 58-28	5,10,15,20,25,30	20	20	5,10,15,20,25,30	20	5,20,35

4.5.2 Pavement Temperature Analysis

Analysis of temporal variations in pavement temperature was conducted to identify temperatures, which reflect critical conditions to evaluate fatigue resistance of asphalt binders for a representative set of locations in the United States with climatic PGs corresponding to those of the binders evaluated (Table 4-1). For each PG under consideration, five locations in varying geographic regions were selected for analysis with the exception of PG 70-22, which was found to be rare, and thus, only two locations were considered. Selection of locations was conducted using LTPPBind software. Since spring is considered the most critical season for fatigue resistance, analysis of both spring and annual trends were considered. Spring was selected to be the period of March to May, consistent with the U.S. meteorological definition. Fatigue accumulates over repeated traffic loading. Therefore, it is assumed that the most frequent temperatures in a given pavement reflect critical conditions. Frequency distributions of pavement temperature for each location analyzed indicated that pavement temperatures are normally distributed and thus, average annual pavement temperatures and average spring pavement temperatures were considered critical temperatures to consider. In addition, consideration of peak traffic periods is important. Thus, average temperatures corresponding to 8 AM and 5 PM, assumed to correspond to rush hours, were considered and compared to 24 hour averages. In addition, since trucks are the primary cause of fatigue cracking, peak truck traffic periods were considered. The default values for hourly truck traffic distributions in Pavement ME suggest the hours from 10 AM to 4 PM correspond to the highest period of truck traffic. Since 10 AM is generally cooler than 4 PM, average 10 AM temperatures annually and in spring were also considered. The Enhanced Integrated Climatic Model (EICM) (Safaei and Castorena 2016) was used to estimate annual variations in pavement temperature. The EICM is a one-dimensional

model, which allows for predicting temporal and depth variations in pavement temperature. While it is recognized that fatigue is often assumed to initiate from the bottom of the pavement, depths corresponding to the bottom of an asphalt layer will vary with pavement structure and thus, for practical considerations a depth of 25 mm was considered herein. Results of EICM analyses were compared to corresponding climatic PGs and trends in binder fatigue characterization results in order to develop improved specifications for selection of LAS test temperature.

4.6 Results

4.6.1 Effect of Temperature on LAS Failure Mechanism and Relation to Binder Modulus

Three failure mechanisms were observed in LAS tests as depicted in Figure 4-2 depending on the test temperature and corresponding linear viscoelastic dynamic shear modulus. Under high moduli test conditions (i.e., low temperature), adhesion loss rather than cohesive failure occurred frequently. At low moduli test conditions (i.e., high temperature), bulging of specimens indicate flow rather than fracture failure. At intermediate moduli (i.e., intermediate temperature), failure occurred by cohesive cracking where little radial deformation of specimens was observed and failure morphology indicated the formation of radial cracks.

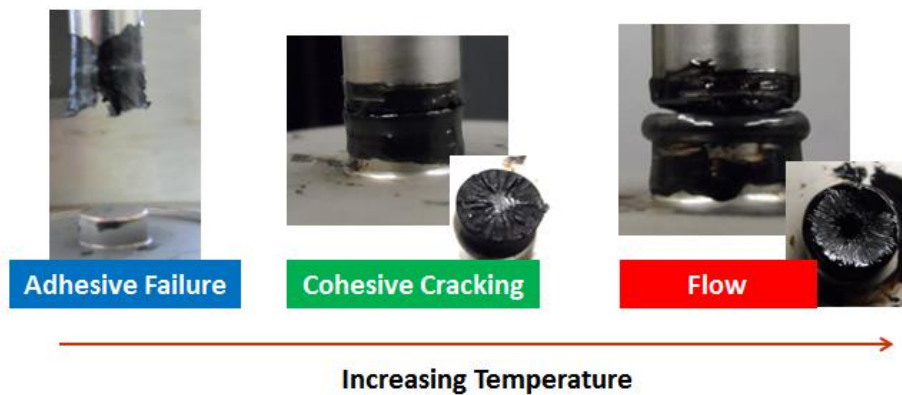


Figure 4-2. LAS failure mechanisms.

The LAS targets cohesive cracking. In order to determine test conditions, which will produce cohesive cracking, failure mechanisms were correlated to corresponding linear viscoelastic dynamic shear moduli. Results are shown in Table 4-2 where linear viscoelastic moduli at 10 Hz frequency and varying temperatures are presented and corresponding LAS test failure mechanisms are indicated by color coding. Results suggest that the cohesive fatigue cracking of asphalt binder will occur during LAS tests if the test temperature is selected such that the linear viscoelastic dynamic shear modulus at 10 Hz loading frequency is between 12 and 60 MPa. In another study which considered three additional binders, Safaei and Hintz (2014) reported that cohesive cracking occurs when the linear viscoelastic dynamic shear modulus is between 10 and 60 MPa, which is more or less consistent with findings herein. Thus, in developing specifications for the selection of test temperature, care should be given to ensure dynamic shear moduli values are within the range of 12 to 60 MPa.

Table 4-2. Relationship between $|G^*|_{LVE}$, Test Temperature, and Failure Mechanism.

Temperature (°C)	5	10	15	20	25	30
	$ G^* _{LVE}$ (MPa)					
PG70-22	150.05	96.62	58.97	34.31	19.20	10.43
PG64-22	115.80	74.02	41.40	23.17	12.45	8.03
PG64-28	64.02	39.05	22.85	12.91	7.10	3.82
PG58-28	76.47	45.64	25.98	14.21	7.54	3.93

= cohesive fracture,
 = cohesive fracture with moderate flow,
 = adhesion loss,
 = instability flow

4.6.2 Application of Time-Temperature Superposition to S-VECD Damage Curves

LAS C versus S “damage characteristic curves” with and without the application of time-temperature superposition are presented in Figure 4-3. Note that only data corresponding to tests where cohesive fracture failure was observed are included in S-VECD analyses. To apply time

temperature superposition to damage characteristic curves, linear viscoelastic time-temperature shift factors were determined from frequency sweep results for each temperature of LAS testing using a reference temperature of 20°C. Time-temperature shift factors were used to calculate reduced time in place of actual time in determining S and plotted against C . Results indicate significant temperature dependence of damage characteristic curves for all binders evaluated in this study based on results before application of time temperature superposition. However, results indicate time-temperature superposition is applicable within the S-VECD framework as damage characteristic curves obtained from differing test temperatures collapse to a single curve after applying time-temperature superposition. These results suggest the S-VECD model can be used to efficiently characterize fatigue damage through LAS testing at a single temperature coupled with linear viscoelastic time-temperature shift factors.

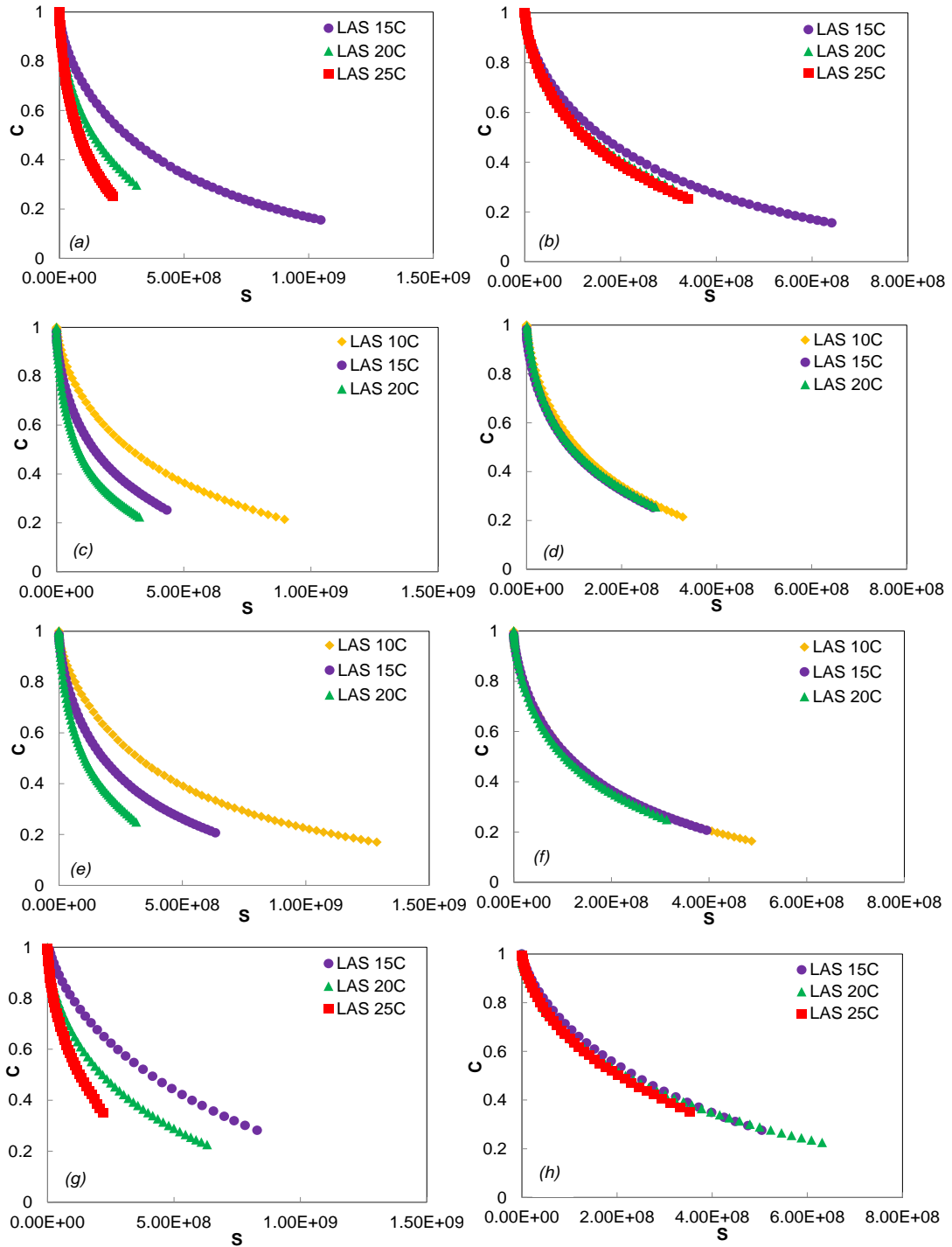


Figure 4-3. Comparison of LAS damage characteristic curves before application of time-temperature superposition (TTS) for (a) PG64-22 (c) PG64-28 (e) PG58-28 (g) PG70-22 and after application of TTS for (b) PG64-22 (d) PG64-28 (f) PG58-28 (h) PG70-22.

4.6.3 Failure Criteria

The effect of temperature on the G^R versus N_f failure criteria was evaluated as shown in Figure 4-4. Only results where cohesive cracking was the dominant failure mechanism are plotted. Plots include data from LAS and TS tests with varying loading history and temperatures (with no adjustment of data from differing temperatures). A unique relationship exists between G^R and N_f that is independent of temperature, loading frequency, and loading history (TS or LAS), suggesting the failure criterion is suitability for use in performance prediction.

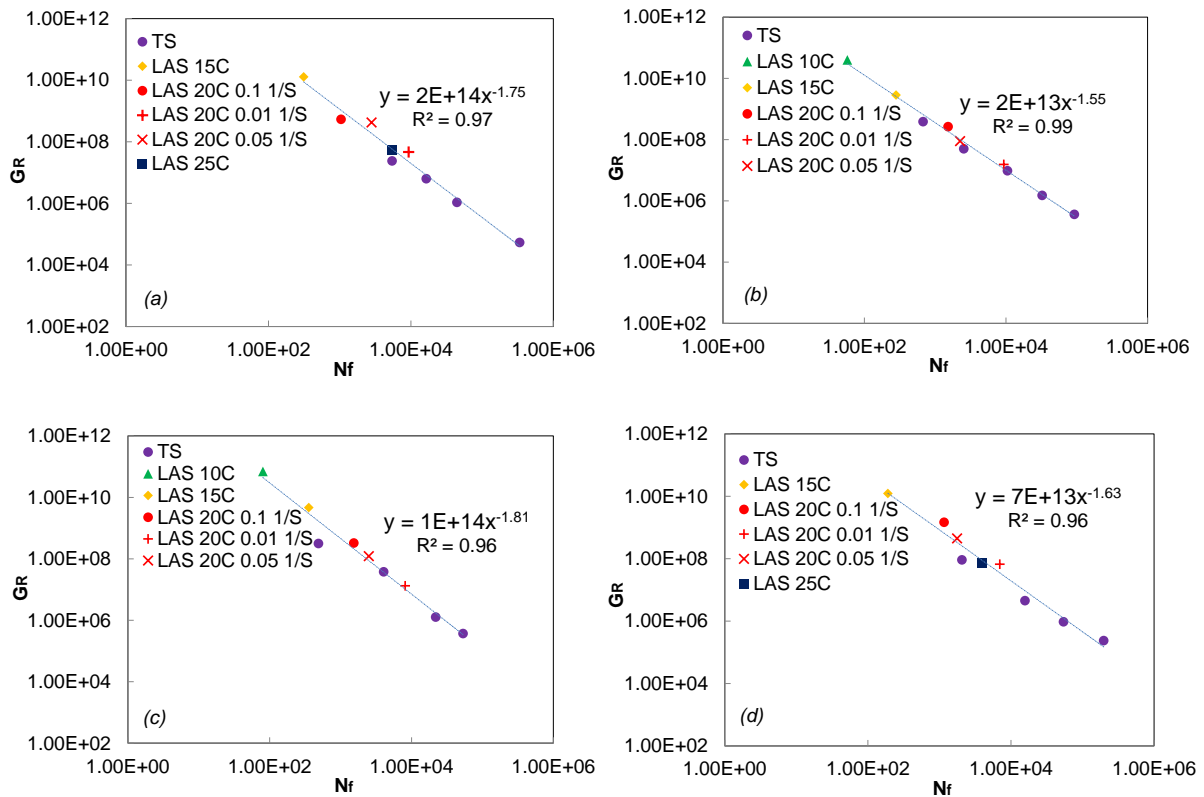


Figure 4-4. G^R vs. N_f for (a) PG64-22 (b) PG64-28 (c) PG58-28 (d) PG70-22.

4.6.4 Model Validation

In order to assess the ability of LAS test results to predict fatigue life at any strain amplitude and temperature of interest, the C versus S curves derived from the LAS tests conducted with differing loading histories and temperatures were fitted with one curve (Equation (4.8)) using a reference temperature of 20°C. Also, LAS test results were used to fit the G^R failure criterion (Equation (4.9)). (Note that time sweep tests were excluded from fitting). Failure criteria and damage characteristic curve model parameters were incorporated into Equation (4.10) and used to predict fatigue life measured from TS tests at varying strain amplitudes and temperatures, (corresponding to conditions where cohesive cracking is the dominant failure mechanism). Figure 4-5 shows the comparison between predicted and measured fatigue lives. Results indicate relatively good agreement between measured and predicted fatigue lives. At conditions corresponding to high fatigue lives (i.e., low strain and high temperature), the LAS tends to under predict fatigue life somewhat. However, rankings of predicted fatigue lives amongst differing materials and test conditions remain in good agreement to measured trends in time sweep tests, indicating the LAS can still be used to rank material fatigue performance as a practical specification test. It is speculated that under prediction is the result of material nonlinearity associated with the high strain amplitudes included in the LAS test which are neglected in analyses for simplicity. Separating nonlinearity and damage is very challenging and would require much more extensive testing than the quick LAS test. Thus, while it is recommended that future research quantifies the effects of nonlinearity on LAS test results, given the relatively good agreement between LAS predicted fatigue lives to measured, it is recommended that the current LAS protocol still be utilized for practical, efficient fatigue characterization of asphalt binders.

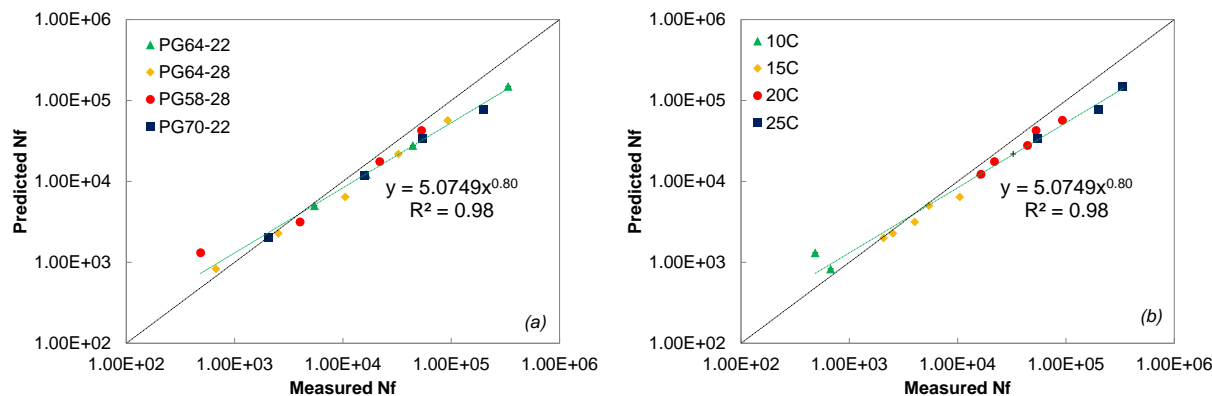


Figure 4-5. Comparison between measured and LAS predicted fatigue lives with (a) delineation by binder type and (b) delineation by test temperature.

4.6.5 Pavement Temperature Analysis

Results of EICM analysis are presented in Figure 4-6. Note that results presented for each PG are averaged from the different locations considered. Error bars represent the standard error arising from differences between averages from differing geographic locations with the same PG. Thus, it is observed that average temperatures do not vary appreciably with geographic region, given the climatic PG is the same. Results presented include average temperatures corresponding to spring and annual hourly pavement temperature data (i.e., 24 hour averages). Additionally, average spring and annual averages for peak traffic hours of 8 AM and 5 PM are presented. In addition, average spring and annual averages for 10 AM are reported, which correspond to a period of peak truck traffic. It can be seen that 24 hour and 8 AM average spring and annual temperatures are generally quite similar and represent most critical temperatures presented (i.e., lowest). Average annual and spring pavement temperatures corresponding to 10 AM and 5 PM are generally higher. Thus, based on the results reported, the average spring temperature is utilized in developing specifications for LAS test temperature. Spring corresponds

to the most critical conditions for pavement deflection due to loss of underlying support associated with high moisture contents.

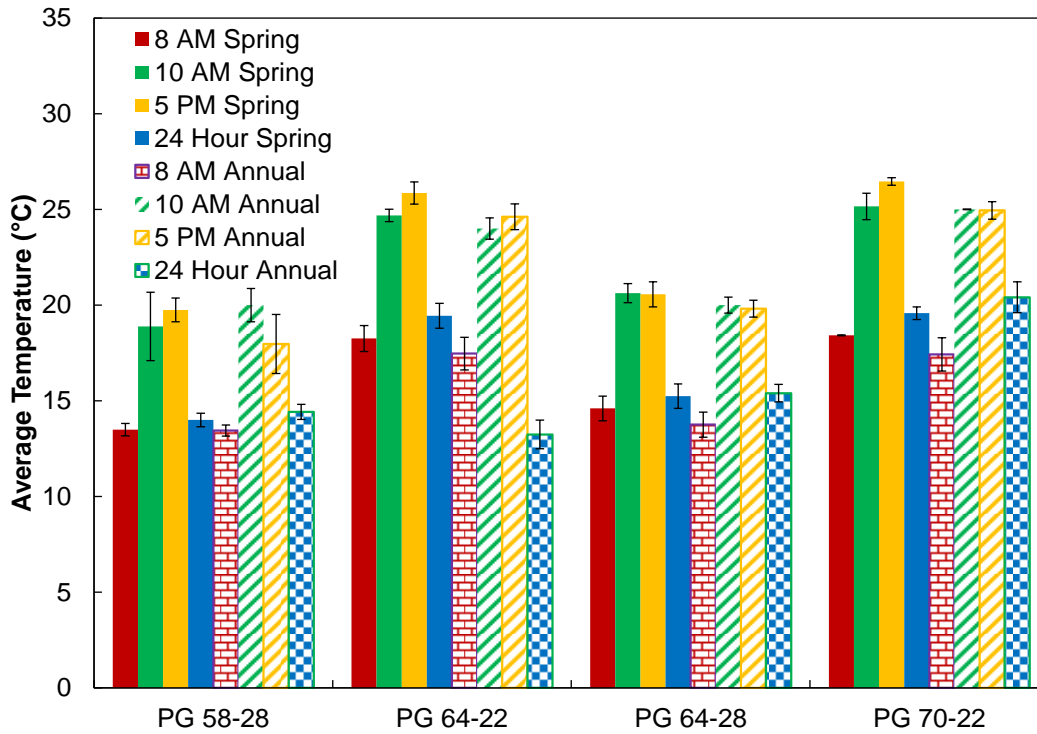


Figure 4-6. Average of mean temperatures of representative locations for all the tested binders for 24 and peak hours of spring and annual.

Average pavement temperatures during spring were related to climatic PGs. It was found that the average is very similar to the average climatic PG – 4°C as shown in Table 4-3. Linear viscoelastic dynamic shear moduli corresponding to the average climatic PG – 4°C for the binders studied are also included in Table 4-3. Results demonstrate that the specification of the average PG – 4°C will lead to failure by cohesive cracking as all corresponding linear viscoelastic dynamic shear moduli are within the range of 12 and 60 MPa.

Table 4-3. Comparison between Average Spring Pavement Temperature and Climatic PG.

Performance Grade	Average Temperature: Spring (°C)	Average PG – 4 (°C)	$ G^* _{LVE}$ @ Ave. PG – 4 and 10Hz (MPa)
PG 58-28	13	14	29
PG 64-22	18	17	33
PG 64-28	16	14	26
PG 70-22	19	20	34

4.7 Conclusions

This study sought to develop recommendations for selection of LAS test temperature based on climatic Performance Grades (PGs) and to enable fatigue life prediction at varying temperatures using the S-VECD model. Developing recommendations for the selection of test temperature involved two components: investigation of climatic data for a wide-range of PGs and investigation of the effect of linear viscoelastic dynamic shear modulus on the observed failure mechanism in the LAS test. Temperature effects were incorporated into the S-VECD model using the principle of time-temperature superposition. Based on the results presented, it is concluded that:

- Time-temperature superposition applies to LAS test results within the S-VECD model framework when the linear complex modulus falls within the range of 12 and 60MPa.
- The G^R failure criterion is independent of temperature and loading history.
- The combined S-VECD model and G^R failure criterion can be used to predict fatigue life at any strain amplitude and temperature of interest using LAS test results at a single temperature coupled with linear viscoelastic time-temperature shift factors.
- LAS test temperature should be selected as the average climatic PG – 4°C to reflect critical climate and material conditions.

- Results presented in this study are solely based on asphalt binder performance. Future work should validate findings of this study by comparison binder predictions of fatigue life at the recommended test temperature with mixture and field performance.”

CHAPTER 5 MATERIAL NONLINEARITY IN ASPHALT BINDER FATIGUE TESTING AND ANALYSIS⁴

5.1 Introduction

Asphalt is a byproduct of petroleum refining, which has complex temperature and rate dependent viscoelastic behavior. The viscoelastic nature of asphalt binder gives rise to a variety of pavement distresses, which depend on climate and traffic conditions. Fatigue cracking is a primary form of pavement distress. The current Superpave Performance Grading (PG) specification evaluates fatigue performance of asphalt binders using the parameter $|G^*| \cdot \sin \delta$. This parameter is measured at a small strain level within linear viscoelastic (LVE) range over very few cycles and thus, is not indicative of actual fatigue damage resistance (Anderson et al. 1994, Bahia et al. 1999, Soenen and Eckmann 2000). Furthermore, fatigue damage accumulation is a function of traffic and climatic conditions, which cannot be captured using a single point measurement. Therefore, there is a need for an improved test method to characterize fatigue resistance of asphalt binder coupled with a model to predict fatigue performance under varying thermal and structural conditions.

The Time Sweep (TS) test was proposed by Bahia et al. (2001) to better characterize the fatigue damage resistance of asphalt binders. The TS test consists of repeated cyclic loading in the Dynamic Shear Rheometer (DSR) at a predefined, constant stress or strain amplitude until failure. Different stress or strain amplitudes are used to simulate different pavement structural

⁴ This chapter has been prepared for submission as: Safaei, F., and Castorena, C. "Material Nonlinearity in Asphalt Binder Fatigue Testing and Analysis" to the *Journal of Material and Design*.

conditions (e.g., higher strain amplitude to simulate weaker pavement structures). The stress or strain amplitudes are typically selected such that failure occurs in a reasonable amount of time, which generally corresponds to 2 percent to 7 percent strain amplitude when strain-controlled tests are conducted (Johnson 2010, Safaei et al. 2016). In the TS test, selection of an appropriate loading amplitude requires prior knowledge of the material's damage resistance, which makes the use of the TS test difficult within purchase specifications. The Linear Amplitude Sweep (LAS) test (AASHTO TP 101) has been proposed as an alternative to the TS test for use in asphalt binder specifications (Johnson 2010). In the LAS test, the binder is subjected to oscillatory loading at 10 Hz frequency with the strain amplitude increasing linearly from 0.1 percent to 30 percent over five minutes to expedite damage.

Under dynamic loading within the linear viscoelastic (LVE) regime, asphalt binder dynamic shear modulus is proportional to strain amplitude. However, when the strain amplitude exceeds the LVE limit, asphalt binder behavior tends to deviate from linear viscoelasticity, resulting in a softer and more viscous response (Anderson et al. 1994, Bahia et al. 1999, Bahia et al. 2001, Airey et al. 2004, Kim and Little 2004, Delgadillo 2008). Fatigue damage manifests as cracks, which lead to a reduction in the area over which loads are distributed, and thus, contributes to apparent softening. The majority of the past efforts to characterize asphalt binder fatigue using the DSR attribute all material integrity loss to fatigue damage for the sake of simplicity, which presumably leads to an overestimation of damage. However, Underwood (2016) recently proposed that the effects of nonlinearity should be considered when interpreting asphalt binder fatigue test results. This study seeks to evaluate the implications of nonlinearity in fatigue testing and analysis of asphalt binders.

The Strategic Highway Research Program (SHRP) study proposed that the LVE limit is defined as the strain amplitude where the dynamic shear modulus, $|G^*|$, decreases to 95 percent of its LVE value (Petersen et al. 1994). The LVE limit has been found to vary as a function of asphalt binder type, temperature, and loading frequency. Airey et al. (2004) found that the linear viscoelastic peak-to-peak strain amplitude limit for asphalt mixtures is on the order of 0.01 percent strain with the binder LVE limit on the order of 1 percent strain amplitude. These results indicate that nonlinearity likely is present in both TS and LAS tests.

The literature also suggests that asphalt binders experience strains within the nonlinear regime in pavements under traffic loading. For stiffer pavement structures, the binder may be subjected to stresses and strains within the linear viscoelastic region. However, for weak pavement structures, the binders may experience higher stresses or strains that are likely to be within the nonlinear region. Several studies have investigated the range of stresses and strains that asphalt binder experiences within an asphalt mixture (Drakos et al. 2001, Masad et al. 2001, Kose 2002, Kose and Bahia 2002). Because of the difference in the stiffness of asphalt binder and aggregate, most of the bulk strain is concentrated within the binder domain. Kose (2002) performed Finite Element Method (FEM) modeling to investigate the strain distribution within an asphalt concrete mixture and concluded that the local strain in the binder ranges from 8 and 510 times the bulk strain level in the mixture. Masad et al. (2001) found that the binder phase could experience shear strains as high as 90 times the bulk mixture strain under uniaxial loading based on FEM modeling. Several studies have indicated that the typical strain levels within asphalt concrete in a pavement are within the range of 70 to 200 micro-strain (Monismith et al. 1970, Thompson and Carpenter 2009, Prowell et al. 2010), which indicates that the strain within binder phase in a pavement may exceed 10 percent strain. Therefore, evaluating the implications

of nonlinearity on fatigue are not only important to asphalt binder fatigue testing and analysis but to the prediction of pavement performance.

Simplified Viscoelastic Continuum Damage (S-VECD) model has been used extensively for predicting the fatigue performance of asphalt mixture (Lee and Kim 1998, Daniel and Kim 2002, Kutay et al. 2008, Underwood et al. 2010, Sabouri and Kim 2014, Norouzi and Kim 2015). The continuum damage modeling approach ignores complicated microscale behavior and quantifies the damage evolution based on the effective stiffness reduction, which comprises the net effect of the growth of microdefects. The S-VECD model allows a constitutive relationship with damage to be derived based on a path-independent damage characteristic curve, which can be obtained using relatively limited uniaxial tests of asphalt concrete mixtures. The S-VECD modeling has been recently extended to both TS and LAS binder test results in an effort to enable the prediction of fatigue life under any loading and temperature history of interest using limited test results (Johnson 2010, Underwood and Kim 2015, Safaei et al. 2016).

Nonlinear viscoelasticity (NLVE) can be incorporated into S-VECD modeling if the nonlinear dynamic shear modulus ($G^*/_{NLVE}$) as a function of strain amplitude is known (Underwood 2016). However, characterizing the $G^*/_{NLVE}$ is challenging. Direct assessment of $G^*/_{NLVE}$ cannot be found via the temperature and frequency sweep experiments typically used for LVE characterization because these tests smear the effects of damage and NLVE together. Therefore, several researchers have proposed experimental procedures to differentiate nonlinear and damage effects using the DSR, which include: (1) the Repeated Stress Sweep (RSS) test (Underwood and Kim 2015) and (2) the Incremental Stress or Strain Sweep test (Branco 2008).

The RSS test consists of subjecting a binder to repetitive stress sweeps at constant frequency. The difference in measured moduli values at varying strain amplitudes between

consecutive stress sweeps is used to isolate damage from nonlinearity (Underwood and Kim 2015). Using the RSS test, Underwood and Kim (2015) were able to develop and verify strain level dependent NLVE models for describing the behavior of asphalt binder and mastic under cyclic loading.

The Incremental Stress or Strain Sweep test consists of applying repeated cyclic loading at constant frequency with systematically increasing either the stress or the strain amplitude (Branco 2008). The majority of DSRs, including the one used in this study, are torque-controlled by instrumentation. Torque-controlled DSRs require a feedback loop to conduct strain-controlled tests. Therefore, it can take the DSR several cycles to reach the target strain amplitude when incrementing the strain amplitude in incremental strain sweep tests. Therefore, only incremental stress sweep (ISS) testing was conducted in this study. In ISS tests, the strain amplitude response with increasing number of loading cycles at constant stress amplitude is used to infer if damage is accumulating in the specimen. If the strain amplitude response does not change as the number of loading cycles applied to the specimen increases, it is assumed that damage is not present. If the strain amplitude increases with increasing loading repetitions, it is inferred that damage is accumulating.

In this study, both the RSS and ISS procedures are evaluated for characterizing the $/G^*/_{NLVE}$ of asphalt binder at varying strain amplitudes. In addition, a new means of separating nonlinearity and damage in LAS tests using S-VECD modeling is proposed. Lastly, the implications of NLVE on fatigue life predictions are assessed.

5.2 Objective

The primary objectives of this study are to:

- Evaluate existing test methods for characterizing the nonlinear viscoelasticity of asphalt binders.
- Develop an approach to separate nonlinearity from damage in LAS test results.
- Evaluate the significance of nonlinearity on asphalt binder fatigue life predictions.

5.3 Materials and Methods

5.3.1 Materials

Four asphalt binders were evaluated in this study with differing Performance Grades (PG): PG 58-28, PG 64-22, PG 70-22 and PG 64-28. The PG 64-22, PG 58-28, and PG 70-22 asphalt binders are unmodified binders whereas the PG 64-28 is polymer modified. All binders were aged prior to testing using the standard Rolling Thin Film Oven (RTFO) and Pressure Aging Vessel (PAV).

5.3.2 Experimental Methods

5.3.2.1 Linear Viscoelastic Temperature – Frequency Sweep Test

Temperature – frequency sweep tests were performed to measure the LVE response of asphalt binders using 1 percent strain amplitude. Test temperatures included 35°C, 20°C, and 5°C with loading frequencies ranging from 0.1 to 30 Hz. Temperature – frequency sweep test results were used to form the LVE dynamic shear modulus (JG^*/LVE) master curves.

5.3.2.2 Linear Amplitude Sweep Test

Standard LAS tests (AASHTO TP 101) were performed, consisting of dynamic loading at 10 Hz frequency with strain amplitudes linearly increasing from 0.1 to 30% over a period of

300 seconds. The standard LAS test corresponds to a constant strain amplitude increase rate (CSR) of approximately 30%/300 sec or 0.001 s^{-1} . Additional LAS-type tests were conducted using a CSR value of 0.00008 s^{-1} to validate that the findings of nonlinear moduli determined from analysis of LAS test results are unique and generally applicable to other test results, which induce nonlinearity.

5.3.2.3 Time Sweep Test

TS tests were conducted using constant strain amplitude loading at 10 Hz frequency. Strain amplitudes were selected such that failure occurred within three hours of initial loading, resulting in the use of strain amplitudes ranging from 3 percent to 4 percent strain.

5.3.2.4 Repeated Stress Sweep Test

RSS tests were conducted in an effort to determine $|G^*/_{NLVE}$ values at varying strain amplitudes. The RSS test is a dynamic loading procedure performed at a fixed temperature and frequency, with incrementally increasing stress amplitude (Underwood and Kim 2015). The stress levels are predetermined and a fixed number of load cycles are applied before each increment in stress amplitude. The RSS test consists of a series of blocks and groups. Each block consists of a stress sweep and each group consists of a series of repeated blocks. The maximum stress amplitude increases from one group to the next. The concept of blocks and groups is illustrated in Figure 5-1 (a).

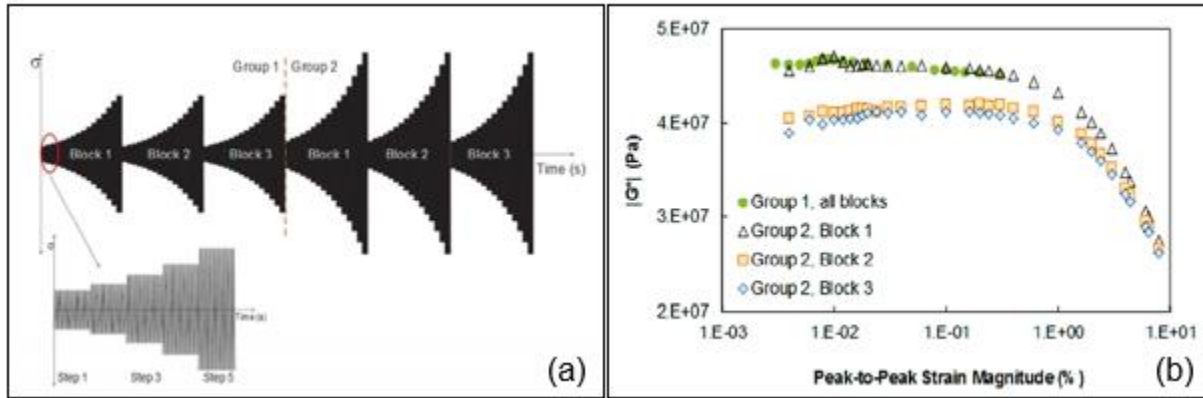


Figure 5-1.(a) RSS loading history schematic, and (b) example RSS results (Underwood and Kim 2015).

An example of RSS test results reported by Underwood and Kim (2015) is presented in Figure 5-1 (b). The stress amplitudes in Group 1 were selected such that damage is negligible, which is confirmed by the agreement between results of repeated blocks. By increasing the maximum stress amplitude in Group 2, damage occurs as evident by the differences in measured $|G^*|$ values between Blocks 1 and 2. However, it can be seen that minimal damage accumulates between Blocks 2 and 3 of Group 2. Based on this observation, Underwood and Kim (2015) introduced a correction factor, CF , to isolate separate damage from results in order to calculate the true $|G^*|_{NLVE}$ as defined in Equation (5.1).

$$CF = \frac{|G^*|_{RSS}}{|G^*|_{NLVE}} \quad (5.1)$$

where $|G^*|_{RSS}$ is the $|G^*|$ measured in the RSS test (with nonlinearity and damage smeared) and $|G^*|_{NLVE}$ is the nonlinear viscoelastic $|G^*|$.

The CF value is assumed to be constant within a block and change only from one block to another. In the case of Group 1 in Figure 5-1 (b), the CF is equal to one because there is no damage. In order to be able to differentiate between the effects of damage and nonlinearity on

the modulus reduction, the stress levels in Group 2, Blocks 2 and 3 in Figure 5-1 (b) are used since they coincide with each other. Because there is no difference between the measured $/G^*/$ values in Blocks 2 and 3, it is assumed that no damage accumulates within Block 2. Therefore, damage can be separated from nonlinearity by calculating the CF as the ratio between the modulus of Group 2, Block 2 and Group 1, Block 1, (where no damage is observed). The CF value is then applied to all other data in the block of interest to determine $/G^*/_{NLVE}$ as a function of strain level.

In this study, RSS tests were performed using a constant loading frequency with minimal rest periods between the loading blocks to avoid the influence of healing. Two groups were utilized. In the first group, the stress levels were selected such that the maximum strain amplitude was limited to approximately 1 percent, which resulted in stresses ranging from 80 to 135 kPa. In the second group, the stress levels were selected such that minimum amount of damage is observed between Group 2 Block 2 and Group 1, resulting in a maximum strain of approximately 5 percent. Two repetitions of Group 1 and four repetitions of Group 2 were applied to specimens. Testing at higher stress levels was aborted due to difficulties encountered in implementing the procedure to determine $/G^*/_{NLVE}$ at strain amplitudes exceeding roughly 5 percent which is discussed later.

5.3.2.5 Incremental Stress Sweep Test

ISS tests were also evaluated for NLVE characterization. In the ISS test, dynamic loading is applied at constant loading frequency and stress amplitude is systematically increased. ISS tests are depicted in Figure 5-2. Within each stress amplitude, the change in response for a specified number of loading cycles is monitored. A constant strain amplitude response, (linear or

nonlinear), with increasing number of load cycles indicates that there is no incremental damage to the test specimen. If the strain amplitude steadily changes with increasing number of load cycles at the same stress amplitude, damage is accumulating. To define the onset of damage, the slope of the strain amplitude response versus the number of load cycles is plotted and fit with a linear trend line. Once the change in the strain amplitude response between the start and end of a stress block exceeds 5 percent, it is assumed that damage is accumulating. Thus, Branco (2008) proposed that the test can be used to determine $/G^*/_{NLVE}$ as a function of strain amplitude up to the point where damage begins accumulating. The load increments and number of load cycles at each stress level are chosen to be high enough to allow for the evaluation of transient change in the response, (assumed to be related to damage), and low enough to avoid causing damage due to excessively long loading (i.e., cause fatigue at low amplitudes). In ISS tests herein, the initial stress amplitude was small enough to ensure that it falls within the LVE regime. At each stress level, 500 cycles at a constant frequency of 10 Hz were applied. The stress amplitude range considered spanned from 0.8 to 900 kPa for the binders tested. The stress increments were selected such that the strain response increases by approximately 1 percent between stress levels.

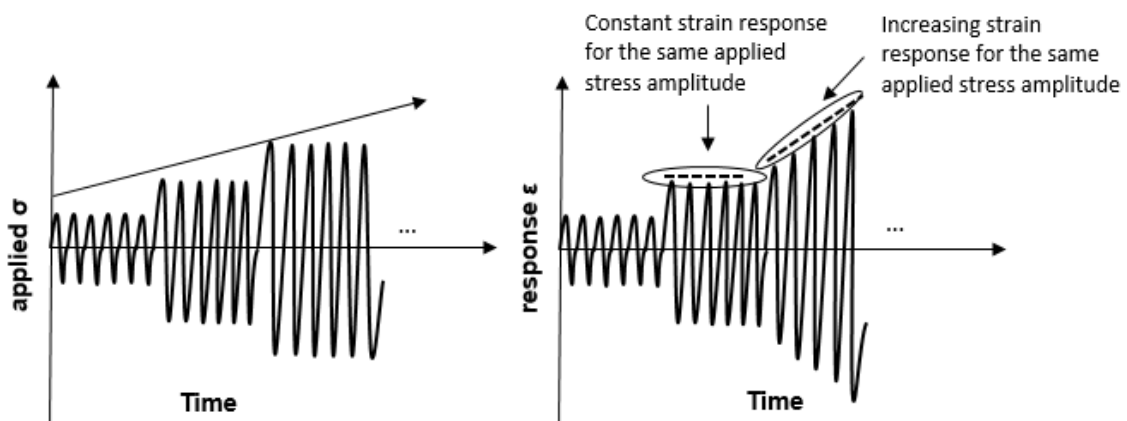


Figure 5-2. Illustration of ISS test: (a) applied stress (b) strain responses (Branco 2008).

5.4 Experimental Plan

The experimental plan is detailed in Table 5-1. Testing was performed on the PG 64-28, PG 64-22, PG 58-28 and PG 70-22 binders. Fatigue test temperatures were selected such that the LVE dynamic moduli were between 12 and 60 MPa at the test frequency per the recommendations of Safaei and Castorena (2016) who demonstrated that testing within this modulus range ensures that failure will occur by cohesive cracking.

Table 5-1. Experimental Plan.

Binder	Test Temperature (°C)					
	LAS 0.001 1/S	LAS 0.00008 1/S	TS	RSS	ISS	Frequency Sweep
PG 64-28	10,15,20	10,15,20	15,20	15,20	15,20	5,20,35
PG 64-22	15,20,25	15,20,25	15,20,25	15,20,25	15,20,25	5,20,35
PG 70-22	10,15,20	10,15,20	10,15,20	10,15,20	10,15,20	5,20,35
PG 58-28	10,15,20	10,15,20	10,15,20	10,15,20	10,15,20	5,20,35

5.5 S-VECD Modeling

5.5.1 Linear Viscoelastic Modeling

LVE properties are required as input to the S-VECD model. Temperature – frequency sweep data were used to build LVE dynamic shear modulus and phase angle mastercurves using time-temperature shift factors and the Christensen-Anderson-Marasteanu (CAM) model (Christensen and Anderson 1992), given in Equations (5.2) and (5.3).

$$|G^*|_{LVE}(\omega_R) = |G^*|_g \left[1 + \left(\frac{\omega_c}{\omega_R} \right)^v \right]^{-\frac{m}{v}} \quad (5.2)$$

$$\delta_{LVE}(\omega_R) = \frac{90 \cdot m}{\left[1 + \frac{\omega_R}{\omega_c}\right]^v} \quad (5.3)$$

where ω_R is reduced frequency; $|G^*|_g = |G^*|_{LVE}$ as $f \rightarrow \infty$: glassy dynamic modulus, equal to 1 GPa for asphalt binder; ω_c is the cross-over frequency (reduced frequency where $\delta = 45^\circ$); and m and v are shape parameters, dimensionless. The time-temperature shift factors were modeled according to Equation (5.4).

$$\log a_T = \alpha_1 T^2 + \alpha_2 T + \alpha_3 \quad (5.4)$$

where a_T is the shift factor at temperature T and, α_1 , α_2 and α_3 are best-fit coefficients.

5.5.2 Simplified Viscoelastic Continuum Damage Modeling

S-VECD modeling is based on Schapery's work potential theory which utilizes an internal state variable to quantify damage as a result of microstructural changes leading to a reduction in effective stiffness (Schapery 1984). This internal state variable representing damage is derived from the damage evolution law given in Equation (5.5):

$$\frac{dS}{dt} = \left(-\frac{\partial W^R}{\partial S} \right)^\alpha \quad (5.5)$$

where W^R is the pseudostrain energy density defined in Equation (5.5) and α is a material dependent constant.

For the work herein, α is defined as $1/m + 1$ where m is the steady-state slope of the dynamic shear modulus master curve in log space (Underwood 2011).

$$W^R = \frac{1}{2} C^*(S) (\gamma^R)^2 \quad (5.6)$$

where γ^R is pseudostrain and $C^*(S)$ is the pseudostiffness of the material. To isolate damage effects from viscoelasticity, pseudostrain is used in place of physical strain in S-VECD analyses. Effectively, pseudostrain is equal to the predicted undamaged stress response of the material to the loading history of interest divided by an arbitrary reference modulus, often selected to be one as is the case herein. In the case of cyclic loading applied in the DSR, peak pseudostrain in each loading cycle is calculated using Equation (5.7) when assuming LVE behavior.

$$\gamma_{pLVE}^R (cyclei) = \frac{1}{G_R} \cdot (\gamma_{p(cyclei)} \cdot |G^*|_{LVE}) \quad (5.7)$$

where G_R is an arbitrary modulus, selected to be one, $\gamma_{p(cyclei)}$ is the peak strain, $\gamma_{pLVE(cyclei)}^R$ is the peak LVE pseudostrain in cycle i and $|G^*|_{LVE}$ is the linear viscoelastic dynamic shear modulus at the fatigue testing temperature and frequency.

Pseudostiffness (C^*), defined in Equation (5.8), is used to quantify material integrity.

$$C^*(S) = \frac{\tau_p}{\gamma_p^R \cdot DMR} \quad (5.8)$$

where τ_p is the peak stress in the loading cycle of interest and DMR is the dynamic modulus ratio which is a parameter used to account for specimen to specimen variability equal to $|G^*|_{Initial}/|G^*|_{Undamaged}$ where $|G^*|_{Initial}$ is the measured dynamic shear modulus of specimen measured at the onset of fatigue loading.

The premise behind the use of $C^*(S)$ to quantify material integrity is that the value of $C^*(S)$ is one when the material is undamaged. As damage starts to grow, the stress response (τ_p) will decrease from that of the undamaged material response (γ_p^R), and consequently $C^*(S)$ will decrease. However, the stress response may also decrease if material nonlinearity is present and hence, lead to inaccurate calculation of $C^*(S)$.

To include material nonlinearity in S-VECD analysis, $|G^*/_{NLVE}$, (which is a function of strain amplitude), is used in place of $|G^*/_{LVE}$ as shown in Equation (5.9) (Underwood 2016). All other components of the S-VECD analysis remain unchanged. Note that NLVE may also affect phase angle values but phase angle is not used to quantify damage evolution in S-VECD modeling.

$$\gamma_{pNLVE}^R(\text{cycle } i) = \frac{1}{G_R} \cdot (\gamma_{p(\text{cycle } i)} \cdot |G^*|_{NLVE(\gamma)}) \quad (5.9)$$

The internal state variable representing damage, S , used within the S-VECD framework is given in Equation (5.10).

$$S(t) = \sum_{i=1}^N \left[\frac{DMR}{2} (\gamma_P^R)^2 (C^*_{i-1} - C^*_i) \right]^{1+\alpha} [t_{Ri} - t_{Ri-1}]^{\frac{1}{1+\alpha}} \quad (5.10)$$

$$t_{Ri} = \frac{t_i}{a_T} \quad (5.11)$$

where t_R is the reduced time, t is the time, a_T is the linear viscoelastic time-temperature shift factor and i refers to the cycle number.

The crux of the S-VECD model is the relationship between $C^*(S)$ and S , termed the *damage characteristic curve*. If the damage characteristic curve is independent of loading history and temperature, it enables prediction of the damage response at any given loading history of interest using limited test results.

5.6 Fatigue Life Prediction

Fatigue life prediction requires the use of a failure definition and failure criteria. Failure definitions for TS and LAS tests have been identified that are material-dependent and correspond

to marked changes in the rate of fatigue failure (Wang et al. 2015). The peak in the C^* times N (i.e., number of loading cycles) versus N curve defines failure in time sweep tests (Wang et al. 2015). The peak in the stored pseudo strain energy versus N curve defines failure in LAS tests (Wang et al. 2015). Stored pseudo strain energy (W_s^R) is calculated using Equation (5.12):

$$W_s^R = \frac{1}{2} \tau_p \cdot \gamma_p^R / DMR = \frac{1}{2} C^* \cdot (\gamma_p^R)^2 \quad (5.12)$$

A unified failure criterion is necessary to enable performance prediction of when failure will occur under conditions other than those used in testing. The failure criteria used herein consists of the relationship between G^R , defined as the average pseudostrain energy (PSE) release rate up to the point of failure, and fatigue life (Wang et al. 2015). Released PSE represents the difference between the total PSE and stored PSE and is calculated using Equation (5.13):

$$W_r^R = \frac{1}{2} (1 - C^*) (\gamma_p^R)^2 \quad (5.13)$$

Correspondingly, G^R is defined in Equation (5.14):

$$G^R = \frac{\overline{W_r^R}}{N_f} = \frac{A}{N_f^2} \quad (5.14)$$

where A is the area under W_r^R curve until failure. The relationship between fatigue life (N_f) and G^R comprises the failure criterion. The power law model given in Equation (5.15) is used to represent the relationship between G^R versus N_f .

$$G^R = a (N_f)^b \quad (5.15)$$

Fatigue life prediction also requires that a model be used to represent the damage characteristic curve. In this study, Equation (5.16) is used to represent damage characteristic curves.

$$C^*(S) = 1 - C_1(S)^{C_2} \quad (5.16)$$

where C_1 and C_2 are optimized coefficients.

The G^R failure criteria and damage characteristic curve models can then be used to derive a relationship between N_f and strain amplitude (γ_p), shown in Equation (5.17) to allow for the prediction of fatigue life under any strain amplitude of interest.

$$N_f = \left[\frac{A}{a} \cdot (\gamma_p)^{2+2\alpha\left(\frac{C_2}{k}\right)} \right]^{\frac{1}{b+1-\frac{C_2}{k}}} \quad (5.17)$$

where

$$k = 1 - \alpha \cdot C_2 + \alpha \quad (5.18)$$

$$A = \frac{1}{2} \cdot C_1 \cdot (|G^*|)^2 \cdot B^{-C_2/k} \cdot \frac{1}{C_2/k + 1} \quad (5.19)$$

$$B = \frac{f_R \cdot 2^\alpha}{k \cdot (C_1 \cdot C_2)^\alpha (|G^*|)^{2\alpha}} \quad (5.20)$$

where f_R is the reduced frequency and $|G^*|$ is the dynamic shear modulus (LVE or NLVE), corresponding to the conditions of interest.

5.7 Results

5.7.1 Repeated Stress Sweep (RSS) Test

The RSS test results of the PG 58-28 binder at 20°C are shown in Figure 5-3. The stress range in Group 1 was selected such that there is no damage as evident by the agreement between the DSR values reported in both Group 1 Block 1 (G1 B1) and Group 1 Block 2 (G1 B2). In Group 2, the range of stress amplitudes was expanded so that the NLVE behavior could be

captured at higher strain amplitudes. It can be seen that damage accumulates between Group 2 Block 1 (G2 B1) and Group 2 Block 2 (G2 B2) by observing the drop in apparent dynamic shear modulus between the two blocks. However, the response is more or less the same for Block 2 (G2 B2), Block 3 (G2 B3) and Block 4 (G2 B4), indicating that minimal damage accumulates after the first block in Group 2, allowing for the isolation of damage and NLVE.

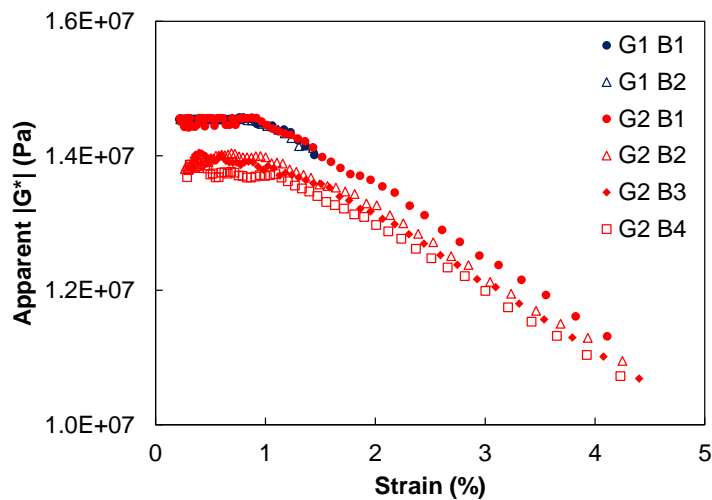


Figure 5-3. RSS test results for PG 58-28 at 20°C.

To allow isolation of nonlinearity from damage, it is required that the $|G^*|$ values stabilize upon repetition of blocks. However, a problem was faced at higher strain ranges than those presented because damage never stopped accumulating between repeated blocks. Therefore, RSS testing can only be used to determine $|G^*|_{NLVE}$ at relatively low strain amplitudes (approximately up to 5 percent) where damage accumulates at a relatively slow rate which is sufficient for characterization over the typical ranges of strain amplitudes used in TS testing but not LAS testing. This finding agrees with strain amplitude ranges proposed for RSS testing by Underwood and Kim (2015). The $|G^*|_{NLVE}$ results at 20°C acquired from RSS testing for the four binders tested presented in Figure 5-4.

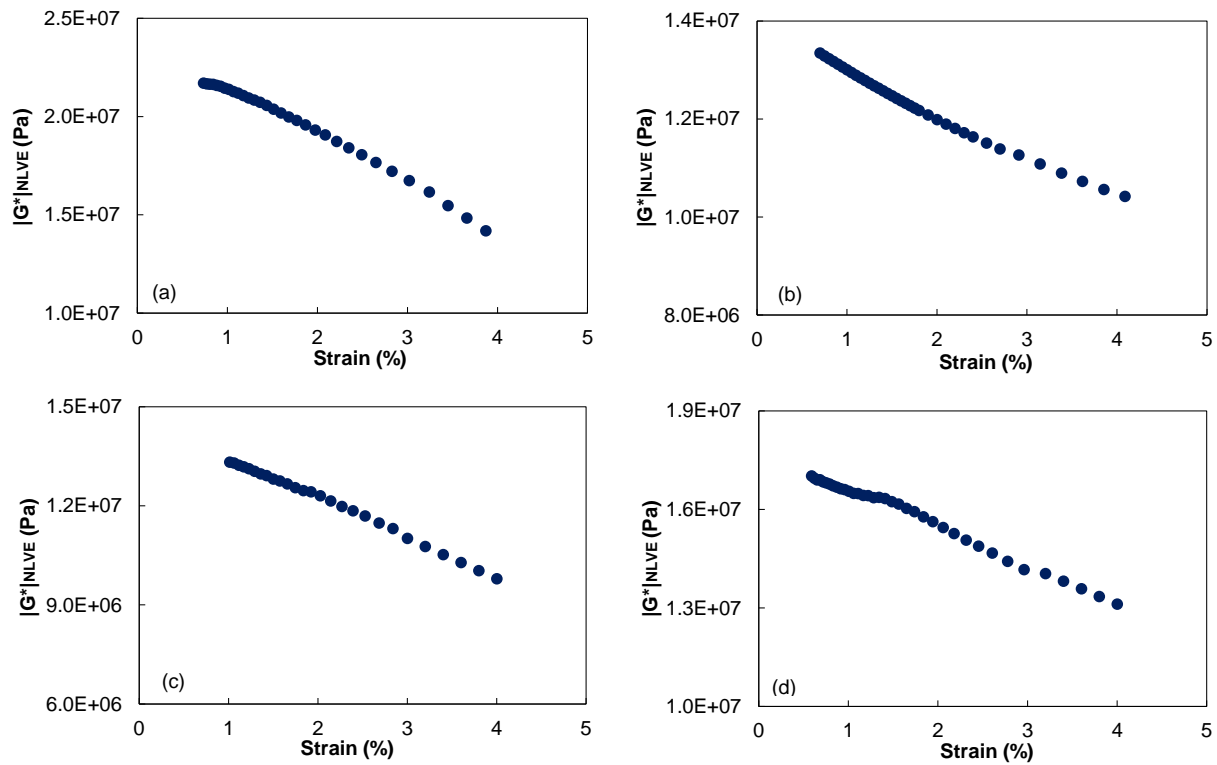


Figure 5-4. $|G^*|_{NLVE}$ relationship with strain for (a) PG 64-22 (b) PG 64-28 (c) PG 58-28 (d) PG 70-22 at 20°C.

5.7.2 Incremental Stress Sweep Test (ISS)

Figure 5-5 shows the ISS strain amplitude results of tests conducted at (a) 20°C, (b) 15°C, and (c) 10°C on the PG 58-28 binder. At 20°C, the LVE limit was found to be 1 percent strain amplitude and damage began accumulating at 5 percent strain amplitude. At 15°C, the LVE limit was also 1 percent strain amplitude but the strain level at which damage first occurred decreased to 4 percent strain amplitude due to the increase in brittleness of the binder. At 10°C, the sample failed rapidly (i.e., cohesively shattered) without exhibiting significant nonlinear behavior in the ISS test. While the ISS may help to identify the strain amplitude where damage starts accumulating in LAS tests, it cannot differentiate damage and nonlinearity once damage starts accumulating.

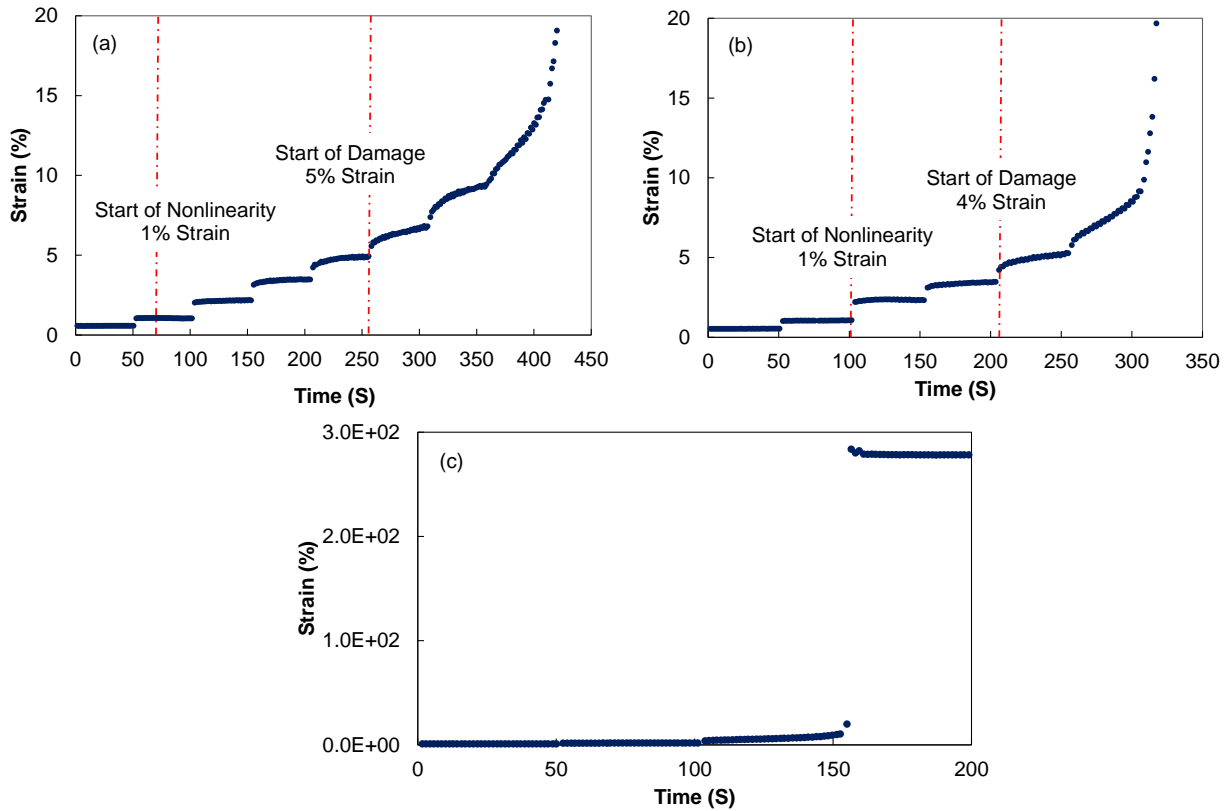


Figure 5-5. ISS strain response at (a) 20°C, (b) 15°C, and (c) 10°C.

From the results presented in Figure 5-4 and Figure 5-5, it can be concluded that TS tests are typically conducted at strain amplitudes within the NLVE regime. The results acquired in via RSS and ISS testing indicate that the $|G^*|$ decreases approximately 15 percent from its $|G^*|_{LVE}$ value at typical TS strain amplitudes (~3 percent) because of material nonlinearity.

It should be noted that TS tests with strain amplitudes within LVE region were tried to avoid the confounding effects of nonlinearity. However, the low strain amplitude did not induce any fatigue damage even after 10 hours of cyclic loading application. Therefore, the consideration of nonlinearity in TS analysis is inevitable.

The $|G^*|_{NLVE}$ results acquired from RSS and ISS testing were compared. The $|G^*|_{NLVE}$ values obtained from ISS and RSS tests for the PG 70-22 at 20°C binder can be compared in

Figure 5-6. Results demonstrate that the ISS method leads to lower $|G^*|_{NLVE}$ calculated values than the RSS test. These results indicate that the basic assumption used to interpret ISS test results that damage is not accumulating if the measured $|G^*|$ does not change with increasing cycle number is not necessarily valid. Therefore, in the study herein, RSS test was selected for determining the $|G^*|_{NLVE}$ for use in S-VECD analysis of TS test results.

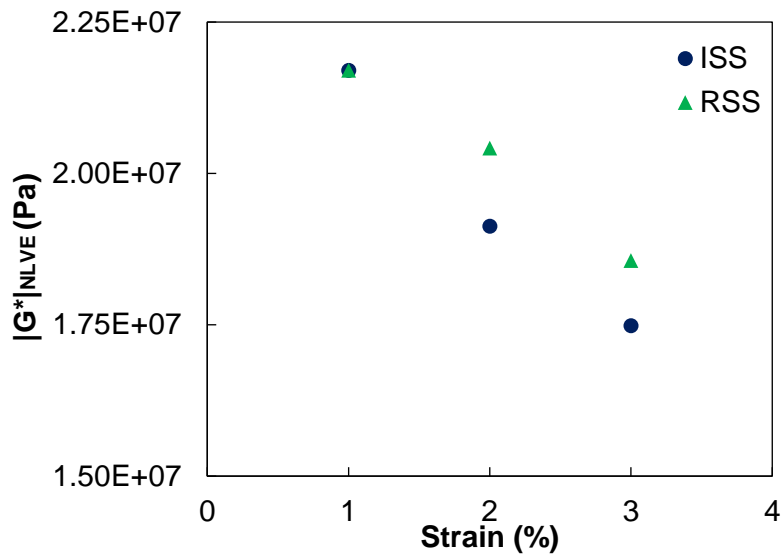


Figure 5-6. Comparison of $|G^*|_{NLVE}$ values determined using ISS and RSS method for PG 70-22 at 20°C.

5.7.3 TS S-VECD Damage Characteristic Curves

To evaluate the applicability of the NLVE S-VECD model to the asphalt binders tested under TS test, damage curves were constructed at the reference temperature of 20°C. RSS test results were used to determine $|G^*|_{NLVE}$ values corresponding to the TS strain amplitudes and temperatures.

These results were used to calculate nonlinear pseudostrain within the S-VECD framework.

Figure 5-7 demonstrates that the damage characteristic curves are unique to the binder, irrespective of temperature and strain amplitude. These results demonstrate the applicability of S-VECD modeling to TS test results. Results suggest that $C^*(S)$ is unique for each material

regardless of strain amplitude therefore is independent of material nonlinearity. It should be noted that the extent of nonlinearity was found to be both temperature and strain amplitude dependent. Thus, while only two strain amplitudes of TS testing were conducted at a single temperature, testing at an additional temperature allows for further evaluating the robustness of the NLVE S-VECD framework.

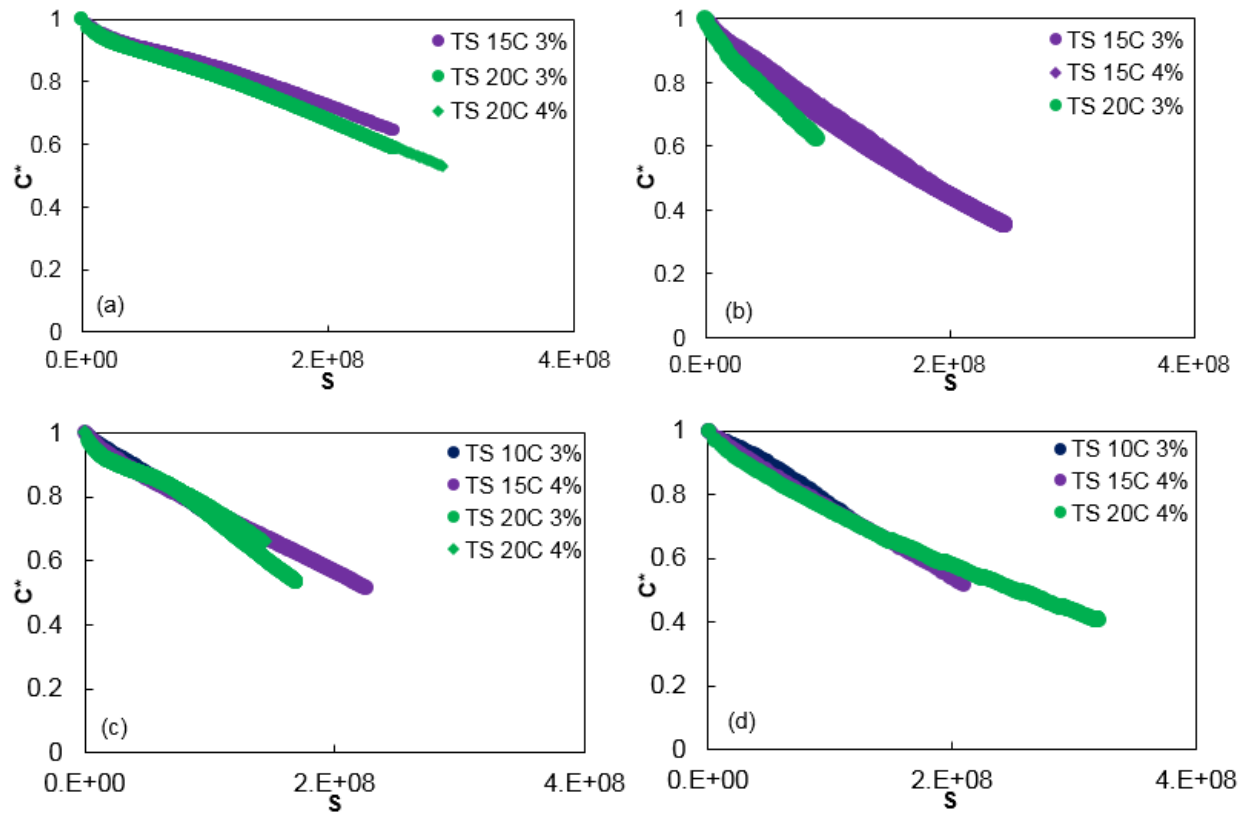


Figure 5-7. S-VECD damage characteristic curves for TS at the reference temperature of 20°C for (a) PG 64-22 (b) PG 64-28 (c) PG 58-28 (d) PG 70-22.

The comparison between S-VECD damage characteristic curves obtained using LVE and NLVE pseudostrain are shown in Figure 5-8. The results presented demonstrate that the LVE curves fall below the NLVE curves, which demonstrates the importance of considering NLVE when performing S-VECD analysis.

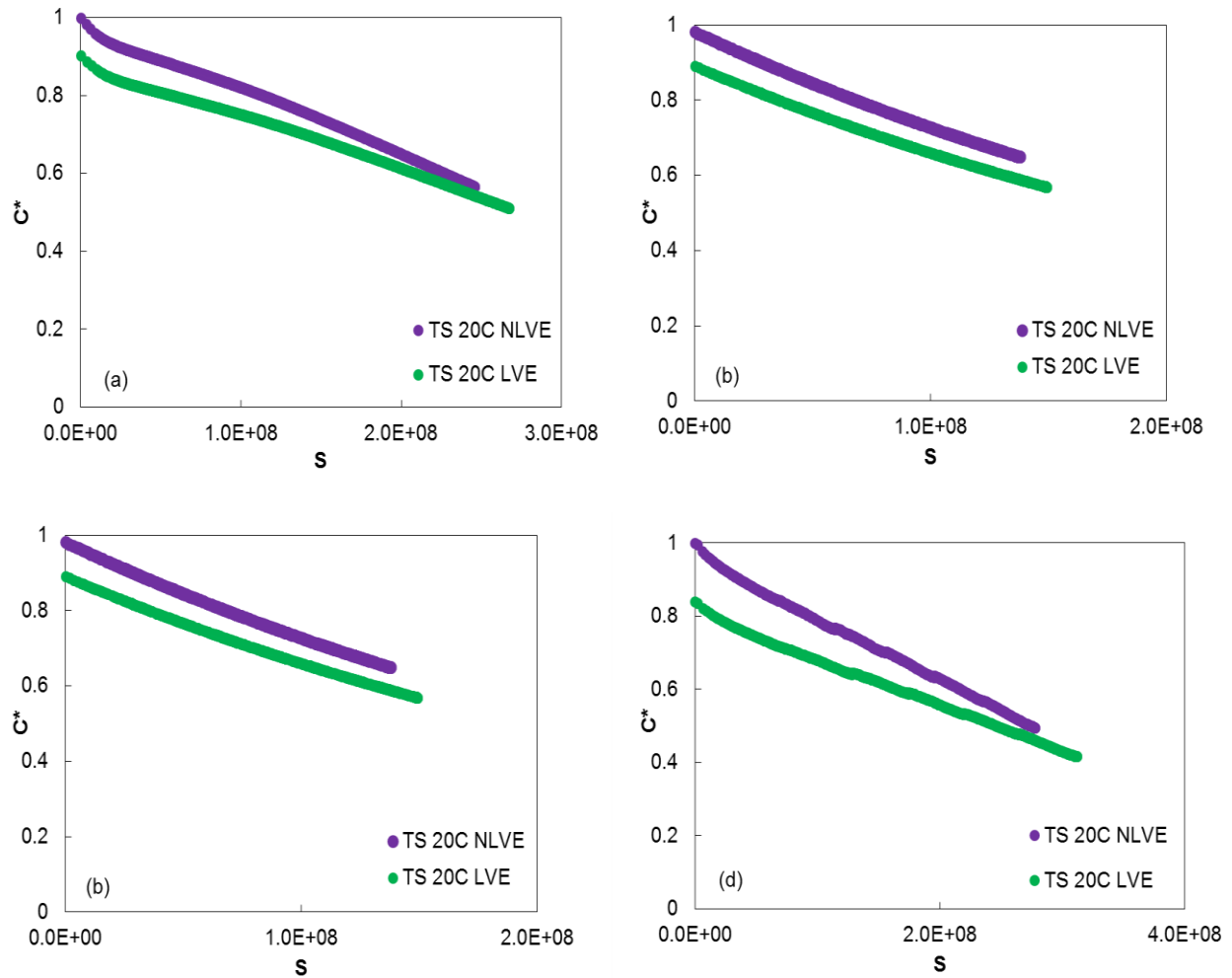


Figure 5-8. LVE vs. NLVE TS damage curves for (a) PG 64-22 (b) PG 64-28 (c) PG 58-28 (d) PG 70-22 at 20°C.

It should be noted that past efforts have reported success applying a LVE S-VECD framework to asphalt binder TS test results (Safaei et al. 2016). It is speculated that this success was the result of calculating the *DMR* using the first cycle response from the TS test, under the assumption that damage is negligible in the first cycle. Thus, the *DMR* values calculated were consistently less than one due to the presence of NLVE behavior, which indirectly compensated for the NLVE response when calculating pseudostrain. However, this approach could lead to erroneous interpretation of results if damage is present in the first cycle response.

5.7.4 Back-calculation of $|G^*/_{NLVE}$ in LAS tests using S-VECD Modeling

The results of RSS and ISS tests suggest experimental approaches can only be used to determine $|G^*/_{NLVE}$ values at relatively low strain amplitudes and thus, are not applicable to the full range of strain amplitudes used in LAS testing. In this study, an analytical method is proposed using S-VECD modeling to back-calculate $|G^*/_{NLVE}$ over the range of strain amplitudes used in LAS tests up to the point of failure. The results presented demonstrate that the C^* versus S damage characteristic curve derived from TS testing is independent of strain amplitude temperature, which suggests that the damage characteristic curve is independent of NLVE. Therefore, the results presented suggest that the damage characteristic curve corresponding to the LAS test results should be equal to the one derived from TS test results for a given material. Damage characteristic curves can be used to predict the response of an asphalt binder to any loading history of interest. Thus, the strain history of the LAS test can be input into the S-VECD model derived from TS testing and used to predict the stress response. If one accepts that the damage characteristic curve from the TS is also applicable to LAS test results, the comparison between the NLVE S-VECD model predictions of stress evolution to that measured in the LAS test can be used to back-calculate the $|G^*/_{NLVE}$ as a function of strain amplitude.

The prediction of stress response to a given strain history using the S-VECD model requires fitting a model to the damage characteristic curve. Thus, the C_1 and C_2 model coefficients in Equation (5.16) are first optimized based on RSS and TS test results. Damage (S) evolution is predicted iteratively as a function of pseudostrain history by combining Equations (5.9) and (5.10) and noting that number of loading cycles (N) is related to loading frequency (f) using Equation (5.21) to arrive at the expression given in Equation (5.22).

$$\frac{dN}{t} = f \quad (5.21)$$

$$S_{N+\Delta N} = S_N + \left(\frac{\Delta N}{f}\right)^{\frac{1}{1+\alpha}} \left[-0.5(\gamma_{p(N)} \cdot |G^*|_{NLVE(\gamma)})^2 (C^*_{N+\Delta N} - C^*_N) \right]^{\frac{\alpha}{1+\alpha}} \quad (5.22)$$

where $S_{N+\Delta N}$ and S_N are damage at cycle $(N + \Delta N)$ and cycle N , respectively. $C^*_{N+\Delta N}$ and C^*_N are the pseudostiffness at cycle $(N + \Delta N)$ and cycle N , respectively and $\gamma_{p(N)}$ is the peak strain in cycle N . To begin the prediction, it is assumed that $C^*_{N+\Delta N} - C^*_N = 0.01$ (i.e., $C^* = 0.99$) initially. After performing each calculation of S , the new $C^*(S)$ value is calculated using Equation (5.16) and used as the input to the next iteration of damage calculation. Predicted C^* evolution can be used to predict peak shear stress (τ_p) as a function of loading cycles using Equation (5.23).

$$\tau_p(N) = C^*(N) \cdot \gamma_p(N) \cdot |G^*|_{NLVE(\gamma)} \quad (5.23)$$

Because C_1 and C_2 are known a priori from the TS test, all parameters for the prediction of the stress evolution are known with the exception of $|G^*|_{NLVE}$ as a function of strain amplitude. Thus, after each iteration of damage calculation, the $|G^*|_{NLVE}$ value in Equation (5.22) and (5.23) corresponding to the strain amplitude ($\gamma_{p(N)}$) in the iteration of damage calculation can be to solved for by minimizing the difference between the measured and predicted shear stress response.

Before extending the aforementioned predictive scheme to back-calculate $|G^*|_{NLVE}$ as a function of strain amplitude from LAS test results, it was first verified to be applicable to TS testing where $|G^*|_{NLVE}$ is known a priori. Figure 5-9 shows the comparison between measured and predicted pseudostiffness for the PG 64-22 binder, demonstrating that predictive scheme is accurate when applied to TS test results (i.e., the model can be used to predict the data that it was derived from).

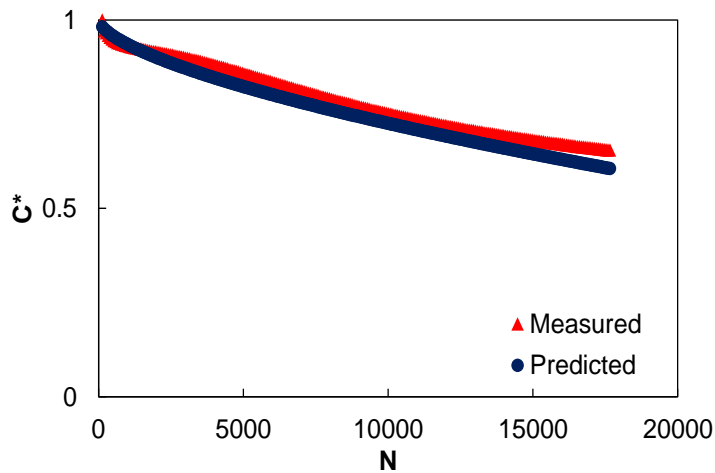


Figure 5-9. Measured vs. predicted C^* vs. N for TS test for PG 64-22 at 20°C, 4% strain.

The prediction scheme, applied to LAS test results, to back-calculate $/G^*/_{NLVE}$ as a function of strain amplitude is illustrated in Figure 5-10. Figure 5-10 (a) and shows an example of shear stress evolution using the S-VECD damage characteristic curve parameters obtained from TS test results coupled with the use of $/G^*/_{NLVE}$ for the calculation of pseudostrain. It can be seen that there is a significant over prediction of stress response because of the assumption of LVE behavior at all strain amplitudes. Figure 5-10 (b) shows the comparison between the measured and predicted stress evolution in an LAS test using the back-calculated $/G^*/_{NLVE}$ values. The corresponding back-calculated $/G^*/_{NLVE}$ values as a function of strain amplitude until the point of failure are presented in Figure 5-10 (c). It can be seen that $/G^*/_{NLVE}$ initially decreases with increasing strain amplitude but ultimately reaches an asymptotic value. The asymptotic value was generally reached around 10 percent strain amplitude for the binders tested.

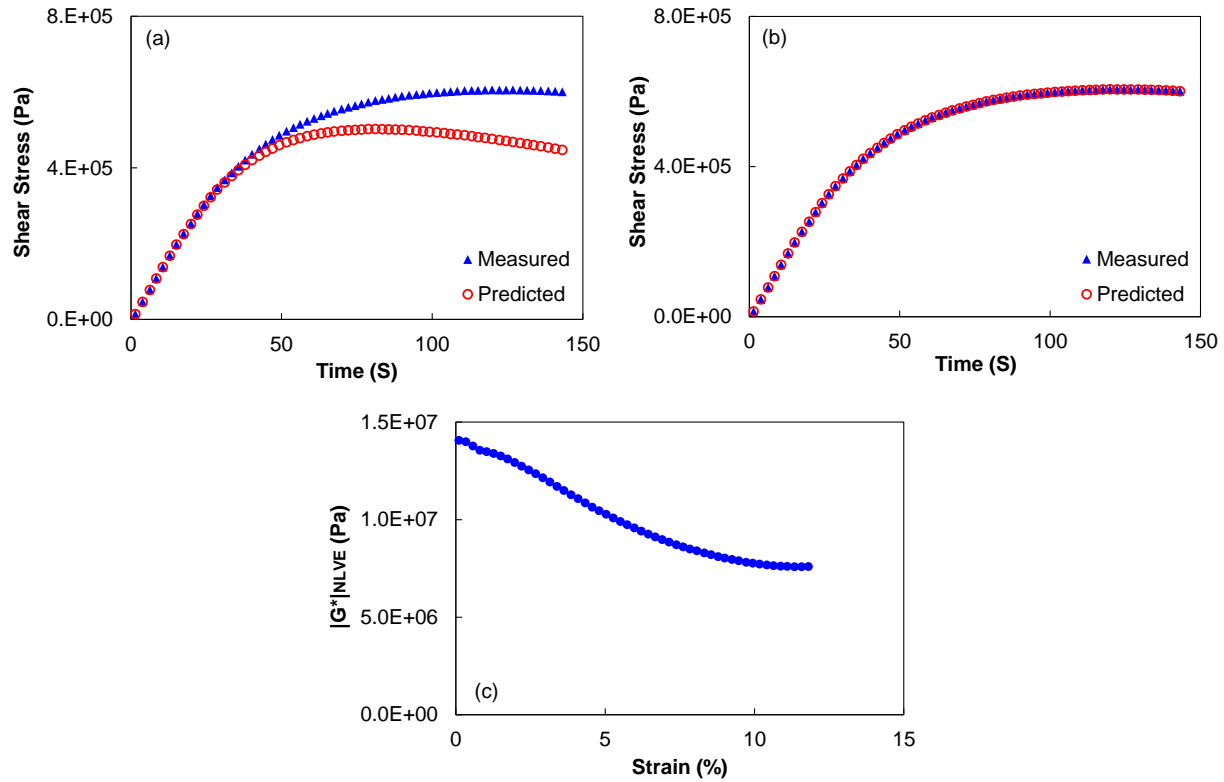


Figure 5-10. Comparison of measured and predicted shear stress for PG 64-28 at 20°C (a) before optimization (b) after optimization (c) back calculated $|G^*|_{NLVE}$ relationship with strain.

5.7.5 Comparison between $|G^*|_{NLVE}$ Values Determined from RSS Tests and Back

Calculation using S-VECD Model

The $|G^*|_{NLVE}$ values back-calculated using S-VECD modelling from LAS test results were compared to the $|G^*|_{NLVE}$ values obtained from RSS tests over the range of strain amplitudes where it was possible to elucidate at $|G^*|_{NLVE}$ in RSS tests. The comparison between back-calculated and RSS testing determined $|G^*|_{NLVE}$ values for the PG 70-22 binder is shown in Figure 5-11. It can be seen that the $|G^*|_{NLVE}$ values obtained from the RSS and back-calculation methods are in good agreement, providing good evidence that the back-calculation approach is valid.

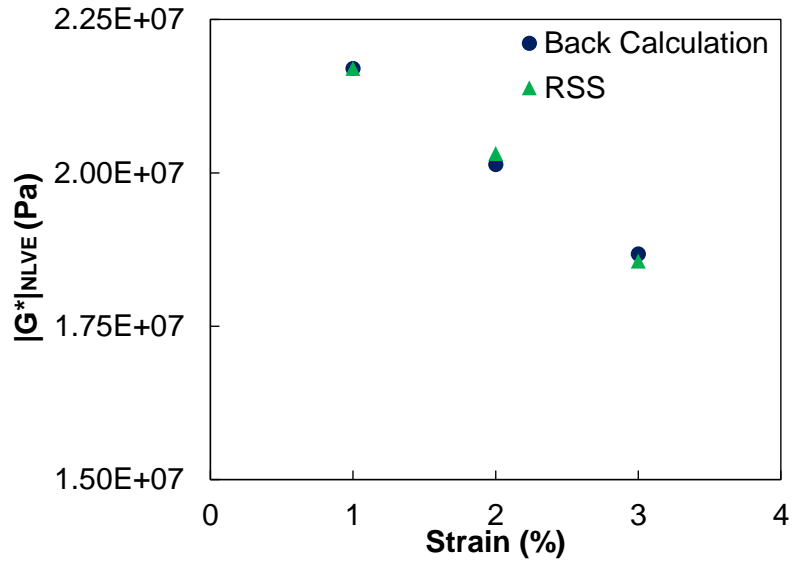


Figure 5-11. Comparison of $|G^*|_{NLVE}$ values determined using RSS and back calculation method for PG 70-22 at 20°C.

5.7.6 Implications of Nonlinearity on Failure Criteria

To evaluate the effect of considering NLVE when interpreting asphalt binder fatigue test results, the relationship between fatigue life (N_f) and G^R was determined using both linear and nonlinear S-VECD models applied to TS and LAS results (Figure 5-12). It can be seen that considering NLVE has a significant impact on the failure criteria. In addition, it can be seen that including NLVE in the analysis leads to more precise definition of the failure criteria (i.e., generally higher R^2 values and lower scatter).

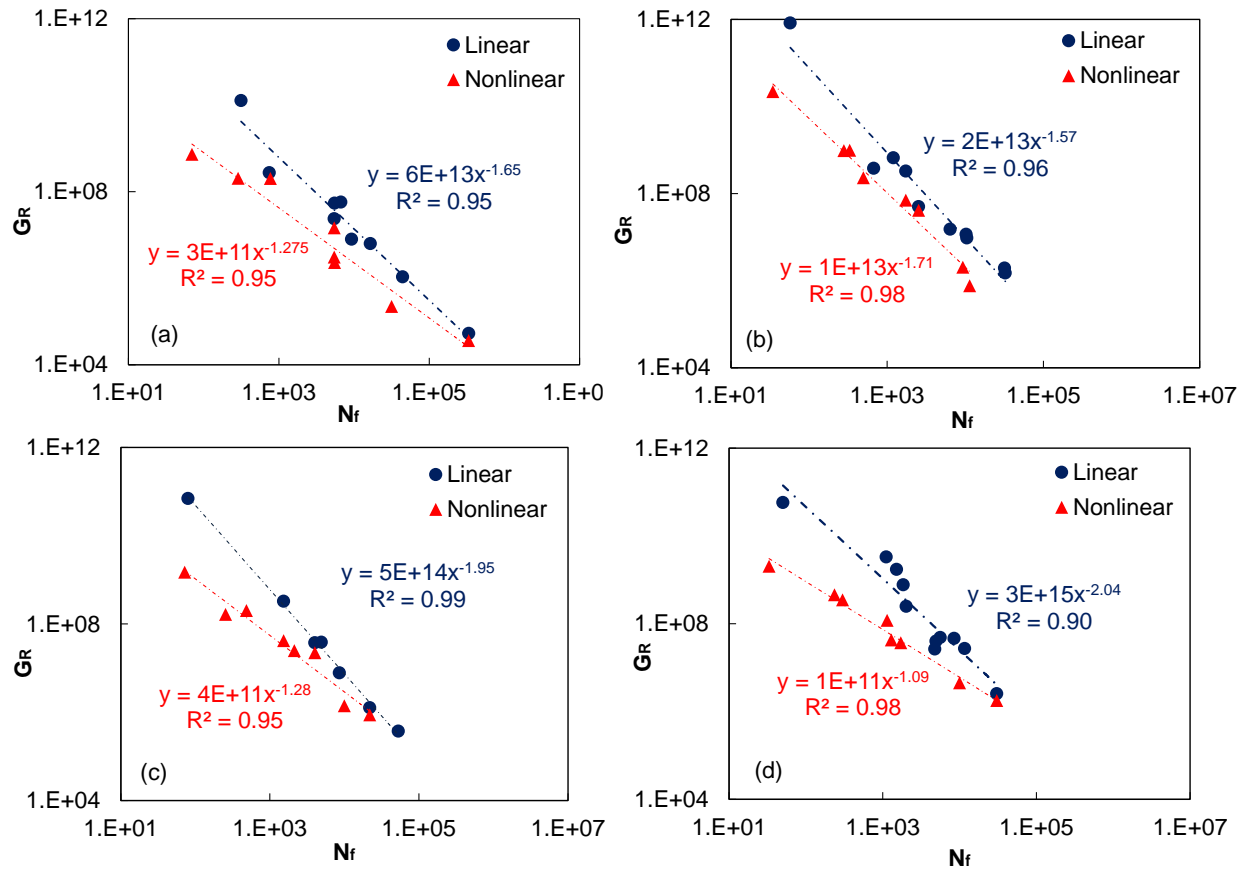


Figure 5-12. G^R vs. N_f using linear vs. nonlinear S-VECD for (a) PG 64-22 (b) PG 64-28 (c) PG 58-28 (d) PG 70-22.

5.7.7 Validation of the $|G^*/_{NLVE}$ Back-calculation using S-VECD Modeling

The LAS tests conducted using a CSR of 0.00008 s^{-1} were used to independently validate the presented approach for the back-calculation of $|G^*/_{NLVE}$ at high strain amplitudes. The standard LAS test uses a CSR of 0.001 s^{-1} . Thus, the strain amplitude is increased more rapidly in the standard LAS test than the tests conducted using a CSR of 0.00008 s^{-1} . Therefore, damage evolution will be very different in the two tests. However, $|G^*/_{NLVE}$ is a material property and thus, the relationship between $|G^*/_{NLVE}$ and strain amplitude in the two tests should not differ.

5.7.7.1 Nonlinear Shear Dynamic Modulus Relationship with Strain

The $|G^*|_{NLVE}$ values as a function of strain amplitude were back-calculated independently using LAS tests conducted using both CSR values of 0.001 s^{-1} (i.e., standard LAS test) and 0.00008 s^{-1} . Figure 5-13 shows that back-calculated $|G^*|_{NLVE}$ values for the standard LAS and LAS with CSR of 0.00008 s^{-1} . It can be seen that the $|G^*|_{NLVE}$ values derived from the two tests are generally in good agreement, validating the back calculation approach.

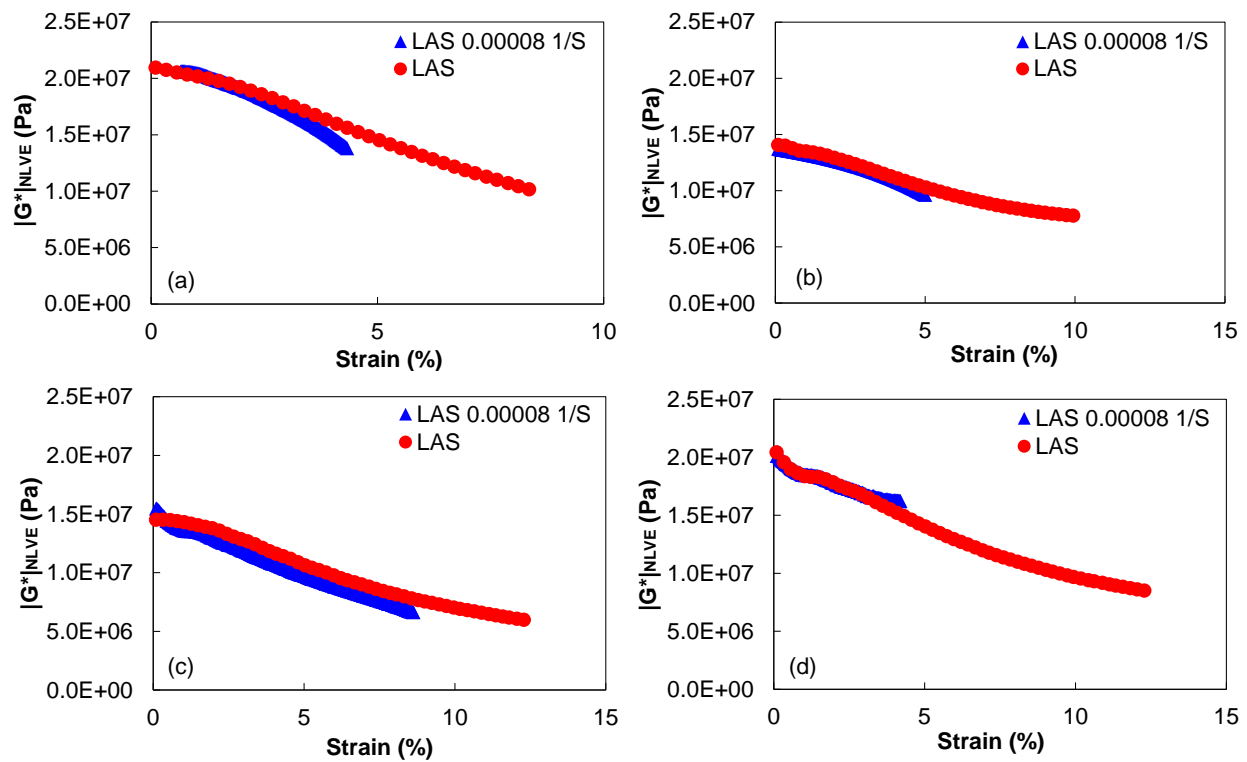


Figure 5-13. Back calculated $|G^*|_{NLVE}$ for standard LAS and LAS with 0.00008 s^{-1} CSR at 20°C for (a) PG 64-22 (b) PG 64-28 (c) PG 58-28 (d) PG 70-22.

5.7.7.2 Damage Characteristic Curves

To further validate the back-calculation approach, the back-calculated $|G^*|_{NLVE}$ values as a function of strain amplitude obtained from standard LAS were used to calculate $C^*(S)$ using the LAS test results conducted using a CSR of 0.00008 s^{-1} . If the back-calculation approach is

valid, the resulting $C^*(S)$ curve should match that obtained from the TS test results. Results are presented in Figure 5-14. It can be seen that the $C^*(S)$ curves are all in good agreement, indicating that the $/G^*/_{NLVE}$ values back-calculated from the LAS test are accurate and applicable to other loading schemes.

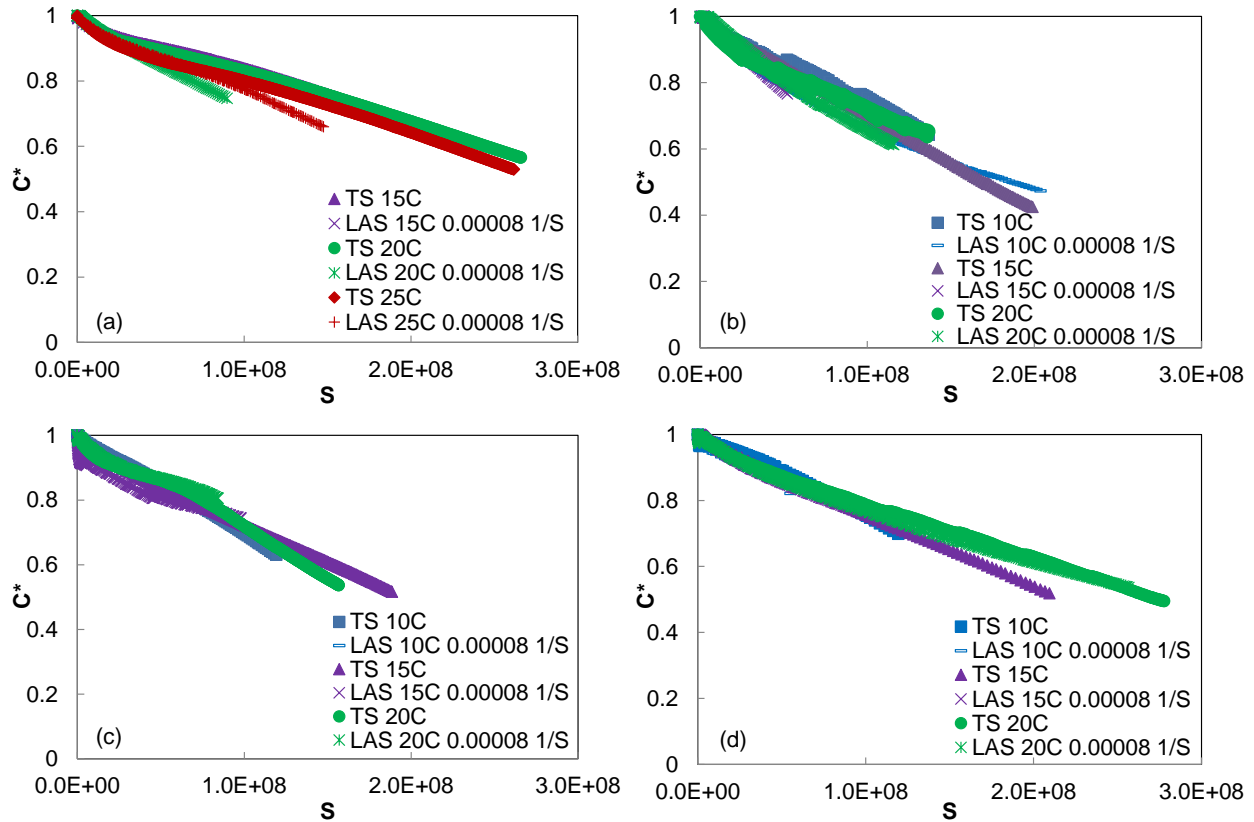


Figure 5-14. Nonlinear S-VECD damage characteristic curves for (a) PG 64-22 (b) PG 64-28 (c) PG 58-28 (d) PG 70-22.

5.7.7.3 Fatigue Life Prediction

As an additional validation metric, the $/G^*/_{NLVE}$ values back-calculated using standard LAS test results coupled with the damage characteristic curves derived from TS tests were used to predict the fatigue life in LAS tests with a CSR value of 0.00008 s^{-1} . The comparison between measured and predicted fatigue lives (N_f) is shown in Figure 5-15. Results presented in

Figure 5-15 demonstrate very good agreement between the measured and predicted fatigue lives, validating the back-calculated $/G^*/_{NLVE}$ values and damage characteristic curves can be applied for fatigue accurate performance prediction at high strain amplitude conditions.

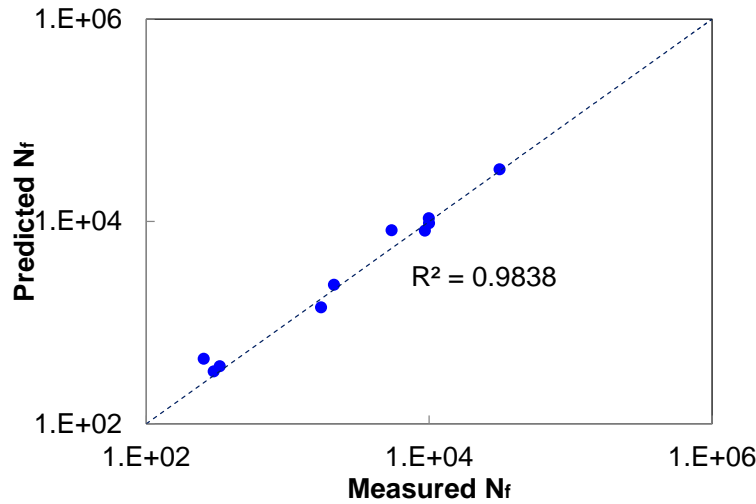


Figure 5-15. Comparison of measured and predicted fatigue lives for LAS test with CSR value of 0.00008 s⁻¹ using nonlinear S-VECD.

5.7.8 Implications of Nonlinearity on Fatigue Life Predictions

The LAS test has been proposed for efficient fatigue characterization within a binder purchase specification framework (Johnson 2010). The results presented herein indicate that a NLVE S-VECD model cannot be derived using LAS test results alone. Rather, RSS and TS tests must first be conducted to obtain the S-VECD model damage characteristic curve parameters and subsequent LAS testing can solely be used to determine $/G^*/_{NLVE}$ values at strain amplitudes where RSS testing cannot be used to elucidate damage from NLVE effects. The ability to determine $/G^*/_{NLVE}$ values at high strain amplitudes could have important implications for use in a multi-scale modeling framework to predict pavement fatigue performance because the literature suggests that the strain within the binder phase of an asphalt concrete pavement can be upwards of 10 percent (Monismith et al. 1970, Thompson and Carpenter 2009, Prowell et al.

2010). However, TS and RSS testing in their current state is impractical for routine use in purchase specifications. Therefore, the significance of considering NLVE on S-VECD fatigue life predictions was evaluated to determine if the LAS test results could potentially still be used to rank asphalt binders for use in a purchase specification using LVE-based analyses. The fatigue lives predicted from LVE and NLVE S-VECD models fit using LAS test results were compared to those measured in the TS tests. Note that the prediction is in essence a ‘loop’ in the case of the NLVE model prediction because the TS tests are used in calibrating the NLVE S-VECD model.

Figure 5-16 shows the relationships between measured and predicted fatigue lives using the LVE and NLVE S-VECD models. Fatigue life predicts using the nonlinear S-VECD model tend to be very accurate. Results indicate that when nonlinearity is neglected, the resulting S-VECD model tends to under predict fatigue life. However, the correlation between measured and predicted fatigue lives is still strong. These results suggest that if rigorous asphalt binder fatigue modeling is conducted, the nonlinear S-VECD model should be used. For example, if binder fatigue results are used within a multi-scale modeling framework to predict pavement fatigue performance, the propagation of error between length scales from the assumption of linear viscoelasticity may have a significant impact on model results. However, given the strong correlation between linear S-VECD model predictions and measured fatigue lives, it is proposed that the current LAS testing and linear S-VECD model framework may still hold merit for ranking asphalt binder fatigue performance within a purchase specification.

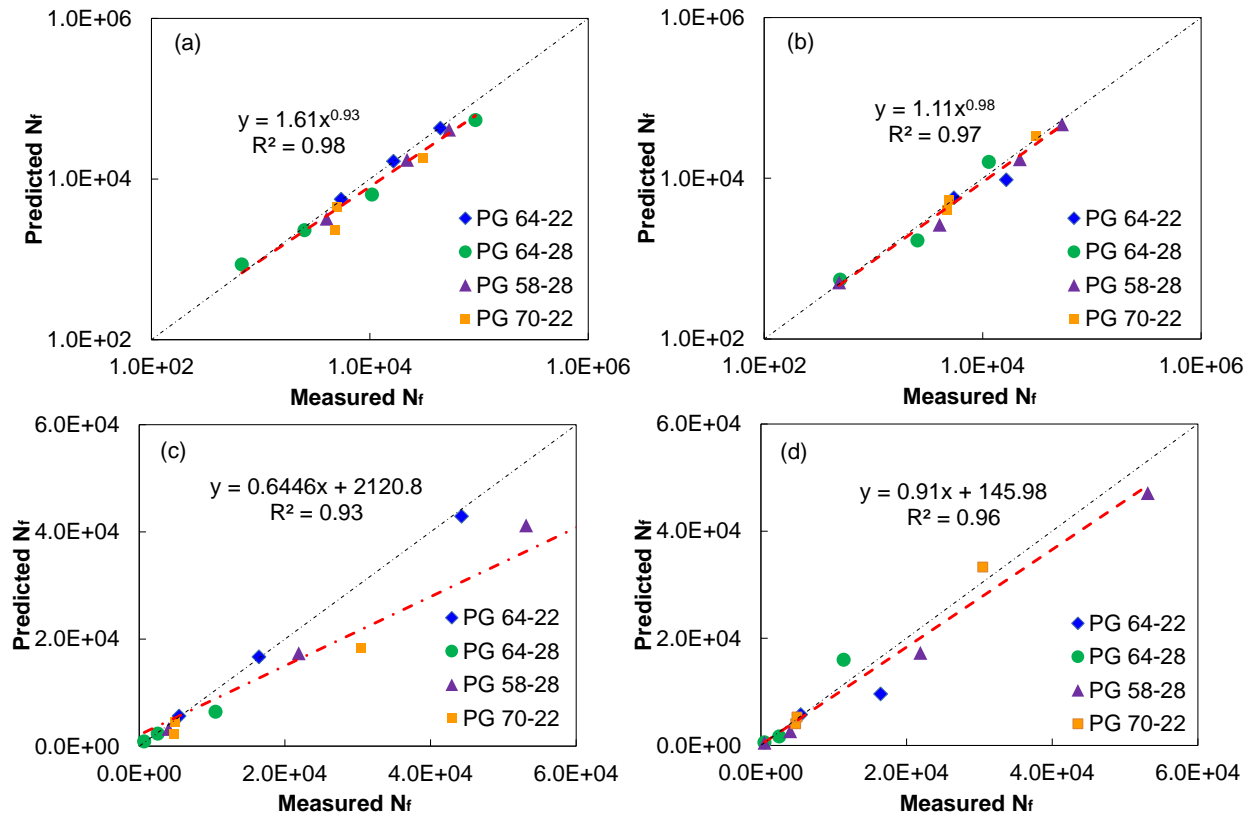


Figure 5-16. Comparison of measured and predicted fatigue lives when using LAS test results within (a) linear S-VECD log scale (b) nonlinear S-VECD log scale (c) linear S-VECD linear scale (d) nonlinear S-VECD linear scale.

5.8 Recommended Test Procedures

Based on the results presented, two levels of testing are recommended for the fatigue characterization of asphalt binder based on the desired level of accuracy and simplicity, which are presented in Table 5-2. Level 1 indicates the most sophisticated and accurate set of testing for accurate fatigue modeling, which allows for the consideration of NLVE at high strain amplitudes. Level 1 requires LVE characterization using the frequency sweep (FS) and NLVE characterization at relatively low strain amplitudes (~5% strain) using the RSS test. Two TS tests, conducted at different strain amplitudes within the strain range of RSS testing,

are required to calibrate the S-VECD model damage characteristic curve. In addition, one LAS test (using a CSR of 0.001/s) is required to determine NLVE behavior at high strain amplitudes. In addition, the TS and LAS test results are used to calibrate the failure criterion. Level 2 is recommended for practical fatigue characterization where the ranking of materials at different strain and temperature conditions is the primary object (e.g., Performance Grading). Level 2 neglects NLVE behavior and includes FS and LAS testing only. LAS tests must be conducted at three CSR values to allow calibration of the failure criterion. As shown in Figure 5-16, Level 2 testing provides reduced accuracy compared to Level 1 but still allows for appropriate ranking of materials and therefore can be used for more practical purposes.

Table 5-2. Recommended Experimental Plan.

Level	Required Tests
1	FS, RSS, TS(2 strain amplitudes), LAS(CSR = 0.001/s)
2	FS, LAS(CSR = 0.001/s, CSR = 0.0005/s, CSR = 0.00025/s)

5.9 Conclusions

The following conclusions can be drawn from this study:

1. The Repeated Stress Sweep (RSS) can be used to characterize nonlinear dynamic shear moduli up to approximately 5 percent strain amplitude. Therefore, RSS testing can be used to determine nonlinear dynamic shear moduli when conducting analyses of time sweep test results.
2. The Incremental Stress Sweep (ISS) results indicate that one can infer if fatigue damage is accumulating based on monitoring the change in strain response to a given stress

amplitude is invalid. Thus, the ISS test is not recommended for nonlinear viscoelastic characterization.

3. Nonlinear viscoelasticity should be considered in Simplified Viscoelastic Continuum (S-VECD) modeling of asphalt binders for accurate fatigue life prediction.
4. The S-VECD model, derived using RSS and TS test results, can be used to back-calculate the nonlinear dynamic shear modulus in LAS test results. The back-calculation approach allows for determining the nonlinear dynamic shear modulus at higher strain amplitudes than can be elucidated using RSS testing.
5. Nonlinear dynamic shear moduli cannot be determined using LAS testing alone, thereby making consideration of nonlinear viscoelasticity in S-VECD modeling impractical for routine specification use. The linear viscoelasticity-based S-VECD model applied to LAS test results, while less accurate, and still provides a good indication of the relative fatigue performance of binders. Therefore, two levels of testing to characterize the fatigue resistance of asphalt binder are proposed in Table 5-2, with varying levels of accuracy and practicality. For the secondary level, the LAS testing coupled with linear viscoelasticity-based S-VECD analysis is recommended and merits further consideration for incorporation into future binder fatigue specifications. The primary level includes the nonlinear S-VECD model and is recommended if rigorous modeling is conducted using asphalt binder fatigue test results (e.g., within a multi-scale model to predict pavement fatigue).

CHAPTER 6 IMPROVED INTERPRETATION OF ASPHALT BINDER PARALLEL PLATE DYNAMIC SHEAR RHEOMETER (DSR) CYCLIC FATIGUE TESTS

6.1 Introduction

The Dynamic Shear Rheometer (DSR) has been used extensively to characterize the viscoelastic properties of asphalt binder in research and in practice (Bahia et al. 1999, Airey et al. 2004, Masad et al. 2008, Wu et al. 2008). DSR testing serves as the basis for determining the high and intermediate Performance Grades (PG) of asphalt binders in the Superpave specifications (AASHTO M332, AASHTO M320). In addition, the use of the DSR has been extended for the fatigue characterization of asphalt binders using the Time Sweep (TS) test (Bahia et al. 2001, Safaei et al. 2016, Underwood 2016, Shan et al. 2017). The TS test consists of sinusoidal loading in the DSR at constant torque or displacement amplitude. It has been demonstrated that asphalt binder TS test results correlate favorably with asphalt mixture fatigue performance, providing evidence that the test is able to capture asphalt binder contribution to mixture fatigue performance (Bahia et al. 2001).

Past efforts have employed the parallel plate DSR geometry for the fatigue characterization of asphalt binders in the DSR (Bahia et al. 2001, Safaei et al. 2016, Underwood 2016, Shan et al. 2017). The parallel plate geometry consists of adhering a cylindrical asphalt binder specimen to two parallel plates as shown in Figure 6-1. The top plates rotates whereas the bottom plate remains fixed, which imposes radially inhomogeneous strain field, which results in a radial inhomogeneous stress field.

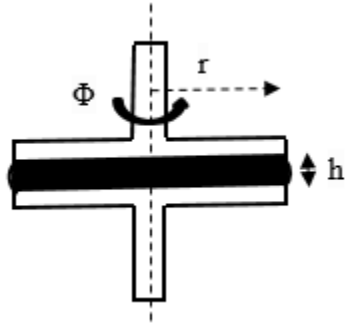


Figure 6-1. Parallel plate geometry.

Consequently, it has been demonstrated that cracking initiates at the sample periphery where the stresses are largest and propagate inward when an asphalt binder is subjected to repeated oscillatory loading in the DSR using the parallel plate geometry (Hintz and Bahia 2013, Shan et al. 2017). Figure 6-2 shows the failure surface of an asphalt binder sample after cyclic parallel plate fatigue testing in the DSR where there is evidence of radial cracks that emanate from the periphery with the center of the specimen remaining intact.



Figure 6-2. Parallel plate failure surface.

Researchers have applied Simplified Viscoelastic Continuum Damage (S-VECD) modeling to TS (Hintz et al. 2011, Safaei et al. 2016, Underwood 2016) asphalt binder test results to enable the prediction of fatigue life under any loading and temperature history of

interest using limited test results. Past efforts have monitored the apparent shear stress at the sample edge to infer fatigue damage to interpret fatigue test results and derive S-VECD model parameters. Apparent edge stress is calculated using linear mapping to the total torque, which is erroneous in the presence of material or geometric nonlinearities such as cracking. Therefore, the interpretation of DSR cyclic fatigue test results have been erroneous in past studies.

The cone and plate DSR geometry offers a means to generate a uniform stress field within an asphalt binder sample subjected to torsional shear. The cone and plate geometry is shown in Figure 6-3. In the cone and plate set-up, the upper plate is conical to impose radially homogenous strain within the sample.

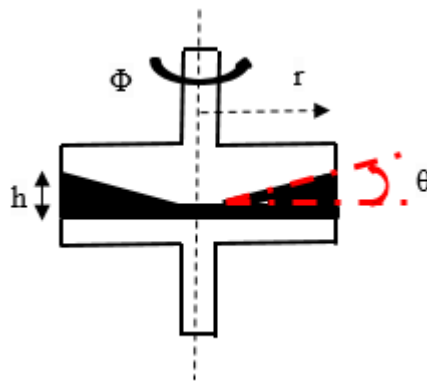


Figure 6-3. Cone and plate geometry.

However, the cone and plate geometry has several disadvantages compared to the parallel plate geometry. The sample height is fixed. Altering the sample height for a given cone would lead to a non-uniform strain field. However, the sample height can be easily adjusted in the parallel plate geometry, which allows for applying a wide range of shear strains and stresses than the cone and plate geometry (de Souza Mendes et al. 2014). In addition, the use of the cone and plate requires very small gaps between the upper and lower plates. Thus, the geometry precludes the testing of filled systems (de Souza Mendes et al. 2014), such as asphalt mastics or crumb

rubber modified asphalt binders. Lastly, the small gap used in cone and plate tests leads very small sample volumes. Consequently, the change in sample volume with temperature can affect the sample size significantly. Thus, the samples must be changed between each test temperature when performing temperature – frequency sweeps using the cone and plate geometry. A single sample can be used for multiple test temperatures in parallel plate tests, given that the loading applied to the sample does not induce any damage.

The present study seeks to improve the interpretation of parallel plate cyclic fatigue tests by accounting for the nonlinear radial gradient in stress response. To develop the methodology, the cone and plate geometry is first used to measure the cyclic fatigue response of asphalt binders in the absence of a radially inhomogeneous stress field. The results of cone and plate fatigue tests are used to calibrate the ‘true’ S-VECD model. Then, under the assumption of linear variation in the strain with respect to sample radius, the S-VECD model derived from the cone and plate tests is used to successfully predict torque evolution under oscillatory fatigue loading in the parallel plate geometry. Subsequently, a means to determine the true S-VECD model parameters, accounting for the nonlinear radially gradient in shear stress, is derived and validated using experimental results.

6.2 Objectives

The primary objective of this study is to improve the interpretation of parallel plate cyclic fatigue tests by properly considering the nonlinear radial gradient in stress response.

6.3 Theory

6.3.1 Parallel Plate Geometry

In the parallel plate geometry, the shear strain is calculated using Equation (6.1) (Macosko and Larson 1994).

$$\gamma(r) = \frac{r \cdot \theta}{h} \quad (6.1)$$

where r is the radial distance from the axis of rotation, h is the gap between the plates, and θ is the angular displacement (radians). Thus, the strain varies linearly from zero at the specimen center to a maximum value at the sample periphery.

A general derivation of the relationship between the torque (T) and the shear stress (τ) in the parallel plate geometry is given in Equation (6.2) (Macosko and Larson 1994, Shaw and Liu 2006, Hellström et al. 2014).

$$T = \int_0^R 2\pi r^2 \tau(r, t) dr \quad (6.2)$$

where $\tau(r, t)$ is the local, axisymmetric shear stress, r is the radial distance from the center of rotation, and R is the sample radius, and t is time. Generally, the apparent shear stress (τ_{app}) at the sample edge (i.e., $r = R$) is reported. The apparent shear stress is calculated by assuming linear variation in the stress with radial distance from the specimen center within Equation (6.2) which yields Equation (6.3) (Macosko and Larson 1994).

$$\tau_{app}(r) = \frac{2}{\pi \cdot R^3} \cdot T \quad (6.3)$$

Equation (6.3) is valid if the stress is proportional to the strain (i.e., within the linear viscoelastic regime). However, within the nonlinear viscoelastic regime or in the presence of damage that varies radially, the assumptions behind Equation (6.3) are violated.

6.3.2 Cone and Plate Geometry

In cone and plate geometry, the shear strain and stress are uniform throughout the sample. The strain is related to the angle of rotation and cone angle (ϕ) as shown in Equation (6.4). The cone angle dictates the gap required ensuring a uniform strain field and thus, the plate gap cannot be adjusted for a given cone.

$$\gamma = \frac{\theta}{\phi} \quad (6.4)$$

The shear stress in the cone and plate geometry is related to the torque and sample radius as shown in Equation (6.5).

$$\tau = \frac{3T}{2\pi R^3} \quad (6.5)$$

6.3.3 Linear Viscoelasticity

Linear viscoelastic (LVE) properties are required as an input to the S-VECD model. Both the cone and plate and parallel plate geometries provide reliable results within the LVE regime. Temperature – frequency sweep data can be used to build LVE dynamic shear modulus and phase angle mastercurves using time-temperature shift factors and the Christensen-Anderson-Marasteanu (CAM) model (Christensen and Anderson 1992) given in Equation (6.6).

$$|G^*|(\omega_R) = |G^*|_g \left[1 + \left(\frac{\omega_c}{\omega_R} \right)^v \right]^{-\frac{m}{v}} \quad (6.6)$$

where ω_R is reduced frequency; $|G^*|_g = |G^*|$ as $f \rightarrow \infty$: glassy dynamic modulus, equal to 1 GPa for asphalt binder; ω_c is the cross-over frequency (reduced frequency where $\delta = 45^\circ$); and m and v are shape parameters, dimensionless. The time-temperature shift factors in this study are modeled according to Equation (6.7).

$$\log a_T = \alpha_1 T^2 + \alpha_2 T + \alpha_3 \quad (6.7)$$

where a_T is the shift factor at temperature T and, α_1 , α_2 and α_3 are best-fit coefficients.

6.3.4 Nonlinear Viscoelasticity

The strain amplitudes in TS testing generally exceed the LVE regime (Underwood 2016). The use of strain amplitudes within the LVE regime is not possible because the fatigue damage will accrue at too slow of a rate to induce failure in a reasonable amount of time. The presence of nonlinearity viscoelasticity (NLVE) will lead to a nonlinear variation in stress response with radial location in parallel plate DSR tests even in the absence of damage. Therefore, the calculation of edge stress using Equation (6.3) is erroneous in the presence of NLVE.

Ng et al. (2011) derived an equation to determine the true edge stress response in parallel plate tests conducted within the NLVE regime. The derivation was conducted using Equation (6.2) using the assumption that the strain maintains a linear relationship to radially location. Ng et al. (2011) solution for determining the corrected peak edge stress (τ_{p-corr}) in sinusoidal parallel plate tests is given in Equation (6.8).

$$\tau_{p-corr}(\gamma_p, \omega) = \frac{2}{\pi R^3} \left[\frac{3}{4} T_p(\gamma_p, \omega) + \frac{\gamma_p}{4} \frac{\partial T(\gamma_p, \omega)}{\partial \gamma_p} \right] \quad (6.8)$$

where T_p is the torque amplitude measured by the DSR and γ_p is the strain amplitude. Equation (6.8) requires the partial derivative of the torque amplitude with respect to strain amplitude. Thus, the application of Equation (6.8) requires that the change in torque response with respect to strain amplitude be measured and is therefore only applicable to amplitude sweep tests. In addition, Equation (6.8) assumes that the derivative of the torque amplitude with respect to the strain amplitude is unique to the loading frequency of interest. Thus, Equation (6.8) is invalid in the presence of fatigue damage.

The use of amplitude sweeps to characterize the NLVE properties of asphalt binders is challenging because it is difficult to differentiate the effects of geometric nonlinearities (e.g., cracking) and NLVE on the measured response. Underwood and Kim (2015) proposed the use of Repeated Stress Sweep (RSS) tests to isolate the effects of NLVE from damage. The RSS test is a dynamic loading procedure performed at a fixed temperature and frequency. In the RSS tests, repeated stress sweeps are performed. The initial stress sweeps are conducted at relatively low stress levels to avoid inducing damage in the specimen. Subsequent stress sweeps are applied that extend to higher stress levels where both damage and NLVE effects are expected. The difference in measured response at varying strain amplitudes between consecutive stress sweeps is used to isolate damage from nonlinearity (Underwood and Kim 2015). Since the approach simply requires monitoring the change in response (i.e., displacement amplitude) from one block to the next, it can be used to easily isolate damage from NLVE in both parallel plate and cone and plate tests.

Herein, RSS tests are used to determine the NLVE dynamic shear moduli of asphalt binders over the range of strain amplitudes used in TS tests using both the cone and plate and parallel plate geometries. The applicability of Equation (6.8) to parallel plate tests to provide accurate measurements of NLVE dynamic shear moduli is evaluated.

6.3.5 Simplified Viscoelastic Continuum Damage Modeling

6.3.5.1 Model Framework

S-VECD modeling is based on Schapery's work potential theory which uses an internal state variable to quantify damage that results from microcracking (Schapery 1984). The internal state variable is derived from the damage evolution law given in Equation (6.9).

$$\frac{dS}{dt} = \left(-\frac{\partial W^R}{\partial S} \right)^\alpha \quad (6.9)$$

where W^R is the pseudostrain energy density defined in Equation (6.10) and α is a material dependent constant. For the work herein, α is defined as $1/m + 1$ where m is the steady-state slope of the dynamic shear modulus master curve in log space (Underwood 2011).

$$W^R = \frac{1}{2} C^*(S) (\gamma^R)^2 \quad (6.10)$$

where γ^R is pseudostrain and $C^*(S)$ is the pseudostiffness of the material. To isolate damage effects from viscoelasticity, pseudostrain is used in place of physical strain in S-VECD analyses. Effectively, pseudostrain is equivalent to the predicted undamaged stress response of the material to the loading history of interest divided by an arbitrary reference modulus. Herein, the reference modulus value is selected to be one. In the case of cyclic loading applied in the DSR, the pseudostrain amplitude in each loading cycle is calculated using Equation (6.11).

$$\gamma_{pNLVE}^R(i) = \frac{1}{G_R} \cdot (\gamma_{p(i)} \cdot |G^*|_{NLVE, \gamma_p}) \quad (6.11)$$

where G_R is an arbitrary modulus, selected to be one, $\gamma_{p(i)}^R$ is the peak pseudostrain in a given cycle i , γ_p is the strain amplitude in cycle i and $|G^*|_{NLVE, \gamma_p}$ is the nonlinear dynamic shear modulus, which is a function of γ_p .

Pseudostiffness ($C^*(S)$) is used within the S-VECD framework to quantify the material integrity and is defined in Equation (6.12).

$$C^*(S) = \frac{\tau_p}{\gamma_{pNLVE}^R \cdot DMR} \quad (6.12)$$

where τ_p is the peak stress in the loading cycle of interest and DMR is the dynamic modulus ratio which is a parameter used to account for specimen to specimen variability equal to $|G^*|_{fingerprint}/|G^*|_{LVE}$ where $|G^*|_{fingerprint}$ is the measured dynamic shear modulus of specimen using a fingerprint test conducted at low strain amplitude prior to the onset of fatigue loading.

The internal state variable representing damage, S , is derived by combining Equations (6.9) and (6.10) and is given in Equation (6.13).

$$S(t) = \sum_{i=1}^N \left[\frac{DMR}{2} (\gamma_p^R)^2 (C^*_{i-1} - C^*_i) \right]^{1+\alpha} [t_{Ri} - t_{Ri-1}]^{\frac{1}{1+\alpha}} \quad (6.13)$$

where i refers to the cycle number, and t_R is the reduced time defined in Equation (6.14).

$$t_R = \frac{t}{a_T} \quad (6.14)$$

Where t is the time and a_T is the linear viscoelastic time-temperature shift factor. The crux of the S-VECD model is that the relationship between pseudostiffness and damage is a fundamental material that is independent of loading and temperature history. Thus, the relationship between pseudostiffness and damage can be calibrated using limited testing and be used to predict the

response of the material to any loading and temperature history of interest. In this study, Equation (6.15) is used to represent damage characteristic curves for the purpose of fatigue performance prediction.

$$C^*(S) = 1 - C_1(S)^{C_2} \quad (6.15)$$

where C_1 and C_2 are optimized parameters.

6.3.6 Accounting for the Nonlinear Radial Stress Gradient in Parallel Plate Fatigue Tests

The application of the S-VECD model presented is straightforward when the strain within the specimen is uniform such as in the cone and plate geometry. The application of the S-VECD model to parallel plate tests is less direct. In past efforts, analysis has been conducted at the sample edge, using Equation (6.3) to calculate the apparent edge stress. However, the radially strain gradient in parallel plate tests will result in a higher rate of damage accumulation (i.e., cracking) with increasing radial distance from the specimen center. Damage leads to reduction in the area over which stresses are distributed, resulting in a decrease in the effective stiffness and thus, $C^*(S)$ of the binder will vary with radial location as fatigue accumulates in parallel plate tests. A radially gradient in effective stiffness will result in a nonlinear radial distribution in shear stress, making Equation (6.3) invalid.

Torque and angular displacement are the only measurements that can be made directly in the DSR. Thus, direct inference of the stress at any given radial location is not possible in the presence of damage using DSR measurements. However, the S-VECD model framework can be used to derive the torque evolution for a given strain amplitude history in the parallel plate geometry given the S-VECD model parameters in Equation (6.15). The derivation assumes that

the linear variation in strain with radially location is maintained in the presence of damage and is presented in the following section.

Equation (6.2) can be written in terms of torque amplitude (T_p) in terms of stress amplitude (τ_p) under sinusoidal loading (de Souza Mendes et al. 2014). In fatigue testing, the torque amplitude will also vary as a function of loading cycles, N , due to the growth of cracks under repeated loading, resulting in the expression given in Equation (6.16).

$$T_p(N) = 2 \cdot \pi \int_0^R \tau_p(r, N) \cdot r^2 dr \quad (6.16)$$

The peak shear stress as a function of N at a given radial location (r) is defined in Equation (6.17) under the S-VECD framework.

$$\tau_p(r, N) = C^*(S(r, N)) \cdot \gamma_{pNLVE}^R(r, N) \quad (6.17)$$

Where $S(r, N)$ is the damage at a given cycle and radial location and $\gamma_{pNLVE}^R(r, N)$ is the peak pseudostrain in a given cycle and radial location. Equations (6.9), (6.11), and (6.15) can be used to derive damage as a function of radial location and cycles for the specific case of constant strain amplitude TS loading as shown in Equation (6.18).

$$S(r, N) = \left(\frac{N \cdot (\alpha - \alpha C_{12} + 1) \cdot \left(|G^*|_{NLVE, \gamma_p(r)} \right)^{2\alpha} \cdot \gamma_p(r)^{2\alpha} (C_{11} C_{12})^\alpha}{f_R \cdot 2^\alpha} \right)^{\frac{1}{\alpha - \alpha C_{12} + 1}} \quad (6.18)$$

Where $\gamma_p(r)$ is the peak strain at radial location r , defined in Equation (6.1) and $|G^*|_{NLVE, \gamma_p(r)}$ is the nonlinear dynamic shear modulus corresponding to the peak strain at radial location r .

Combining Equations (6.15) and (6.18) yields Equation (6.19), which can be used within Equation (6.17) to solve for the peak stress history as a function of radial location and cycles.

$$C^*(S(r, N)) = 1 - C_{11} \left(\frac{N \cdot (\alpha - \alpha C_{12} + 1) \cdot \left(|G^*|_{NLVE, \gamma_p(r)} \right)^{2\alpha} \cdot \gamma_P(r)^{2\alpha} (C_{11} C_{12})^\alpha}{f_R \cdot 2^\alpha} \right)^{C_{12} / (\alpha - \alpha C_{12} + 1)} \quad (6.19)$$

Equation (6.17) can then be used within Equation (6.16) to predict torque evolution in parallel plate TS tests. In this study, Equation (6.16) was solved numerically by applying the trapezoidal rule. Thus, the torque history in parallel plate TS tests can be predicted using the S-VECD damage characteristic curve model parameters in Equation (6.15), accounting for the nonlinear variation in shear stress with radial distance from the specimen center.

The framework presented is used for two applications in this study. First, the framework is validated by applying the S-VECD damage characteristic curve model parameters derived from cone and plate TS testing where the stress field is uniform within the framework to successfully predict torque evolution in parallel plate TS tests (termed ‘forward analysis’ herein). Second, the torque history measured in parallel plate TS tests is used to solve for the S-VECD damage characteristic curve parameters in Equation (6.15) by performing a least squares optimization between measured and predicted torque evolution (termed ‘backward analysis’ herein). The results demonstrate that the S-VECD model can be accurately calibrated using parallel plate fatigue test results.

6.3.6.1 Fatigue Life Prediction

Ultimately, the goal of using the S-VECD model is to enable fatigue life prediction under a wide range of conditions using limited test results. To enable fatigue life prediction, a unified failure criterion is necessary in addition to the damage characteristic curve parameters in Equation (6.18). The failure criterion is needed for the prediction of when failure will occur under conditions other than those used in testing. The failure criteria used herein consists of the

relationship between G^R , defined as the average pseudostrain energy (PSE) release rate up to the point of failure, and fatigue life (Wang et al. 2015). Released PSE represents the difference between the total PSE and stored PSE and is calculated using Equation (6.20).

$$W_r^R = \frac{1}{2}(1 - C^*)(\gamma_{p,NLVE}^R)^2 \quad (6.20)$$

Correspondingly, G^R is defined in Equation (6.21)

$$G^R = \frac{\overline{W_r^R}}{N_f} = \frac{A}{N_f^2} \quad (6.21)$$

where A is the area under W_r^R curve until failure. The relationship between fatigue life (N_f) and G^R comprises the failure criterion. The power law model given in Equation (6.22) used to represent the relationship between G^R versus N_f .

$$G^R = a (N_f)^b \quad (6.22)$$

The G^R failure criteria and damage characteristic curve models can then be used to derive a relationship between N_f and strain amplitude (γ_p), shown in Equation (6.23) to allow for the prediction of fatigue life under any strain amplitude of interest.

$$N_f = \left[\frac{A}{a} \cdot (\gamma_p)^{2+2\alpha(\frac{C_2}{k})} \right]^{\frac{1}{b+1-\frac{C_2}{k}}} \quad (6.23)$$

where

$$k = 1 - \alpha \cdot C_2 + \alpha \quad (6.24)$$

$$A = \frac{1}{2} \cdot C_1 \cdot (|G^*|_{NLVE,\gamma_p})^2 \cdot B^{-C_2/k} \cdot \frac{1}{C_2/k + 1} \quad (6.25)$$

$$B = \frac{f_R \cdot 2^\alpha}{k \cdot (C_1 \cdot C_2)^\alpha (|G^*|_{NLVE, \gamma_p})^{2\alpha}} \quad (6.26)$$

where f_R is the reduced frequency corresponding to the conditions of interest.

6.4 Materials and Methods

Three asphalt binders were evaluated in this study with differing Performance Grades (PG): PG 58-28, PG 64-22 and PG 70-22. All binders were aged prior to testing using the standard Rolling Thin Film Oven (RTFO) and Pressure Aging Vessel (PAV). Tests were conducted in a TA AR-G2 DSR with two different geometries: parallel plate with 8-mm diameter and 2-mm gap, and cone and plate with 8-mm diameter and cone angle of 0.1 rad with a truncation gap of 150- μ m.

Temperature – frequency sweep tests for both parallel and cone and plate geometries were performed in an effort to measure the LVE response of asphalt binders using 1 percent strain amplitude. Test temperatures included 35°C, 20°C, and 5°C and loading frequencies ranging from 0.1 to 30 Hz. Results were used to form the LVE dynamic shear modulus ($|G^*|_{LVE}$) master curves. TS tests were conducted using constant strain amplitude loading at 10 Hz frequency. Strain amplitudes were selected such that failure occurred within three hours of initial loading. Repeated Stress Sweep (RSS) tests (Underwood and Kim 2015) were performed to determine $|G^*|_{NLVE}$ values for TS tests. The RSS test is a dynamic loading procedure performed at a fixed temperature and frequency, with incrementally increasing stress amplitude (Underwood and Kim 2015). In this study, two loading groups were utilized. In the first group, the stress levels were selected such that the maximum strain amplitude was limited to 1 percent, which resulted in stresses ranging from zero 65 to 180 kPa. In the second group, the stress levels

were selected such that the maximum strain amplitude was 6 percent, resulting in a maximum stress of 570 kPa. Two repetitions of Group 1 and three repetitions of Group 2 were applied to specimens. The experimental plan is detailed in Table 6-1.

Table 6-1. Experimental Plan

Binder	Test Temperature (°C)		
	TS	RSS	Frequency Sweep
PG 64-22	15,20	15,20	5,20,35
PG 70-22	15,20	15,20	5,20,35
PG 58-28	15,20	15,20	5,20,35

6.5 Results

6.5.1 Mastercurves

Dynamic shear modulus master curves obtained from parallel plate (PP) and cone and plate (CP) testing geometries are presented in Figure 6-4. Testing was conducted using 1 percent strain amplitude based on the recommendations from the literature to stay within the LVE regime (Airey et al. 2004). Because it was assumed that testing at 1 percent strain would be within the LVE regime, Equation (6.3) was used to calculate stress at the sample edge when interpreting test results. It is expected that the testing geometry will not affect the dynamic shear modulus within the LVE regime. Results of linear viscoelastic mastercurves demonstrate good agreement between parallel plate and cone and plate geometries at low and intermediate reduced frequencies. There is a deviation between the cone and plate and parallel plate mastercurves at high reduced frequencies for the PG 64-22 and PG 58-28 binders, which could indicate the presence of NLVE behavior even at 1 percent strain amplitude at a temperature of 5°C.

However, results appear to be within the LVE range at 1 percent strain amplitude for the test temperatures corresponding to fatigue testing.

NLVE behavior results in a reduction in the dynamic shear modulus. Because the strain decreases towards the specimen center in parallel plate test results, part of the specimen will remain in the LVE regime, leading to a less pronounced effect on the apparent shear stress response compared to the cone and plate, which has a homogenous strain field. Thus, the observed trends in Figure 6-4 where cone and plate dynamic shear moduli appear lower than parallel plate is consistent with expectations in the presence of NLVE behavior.

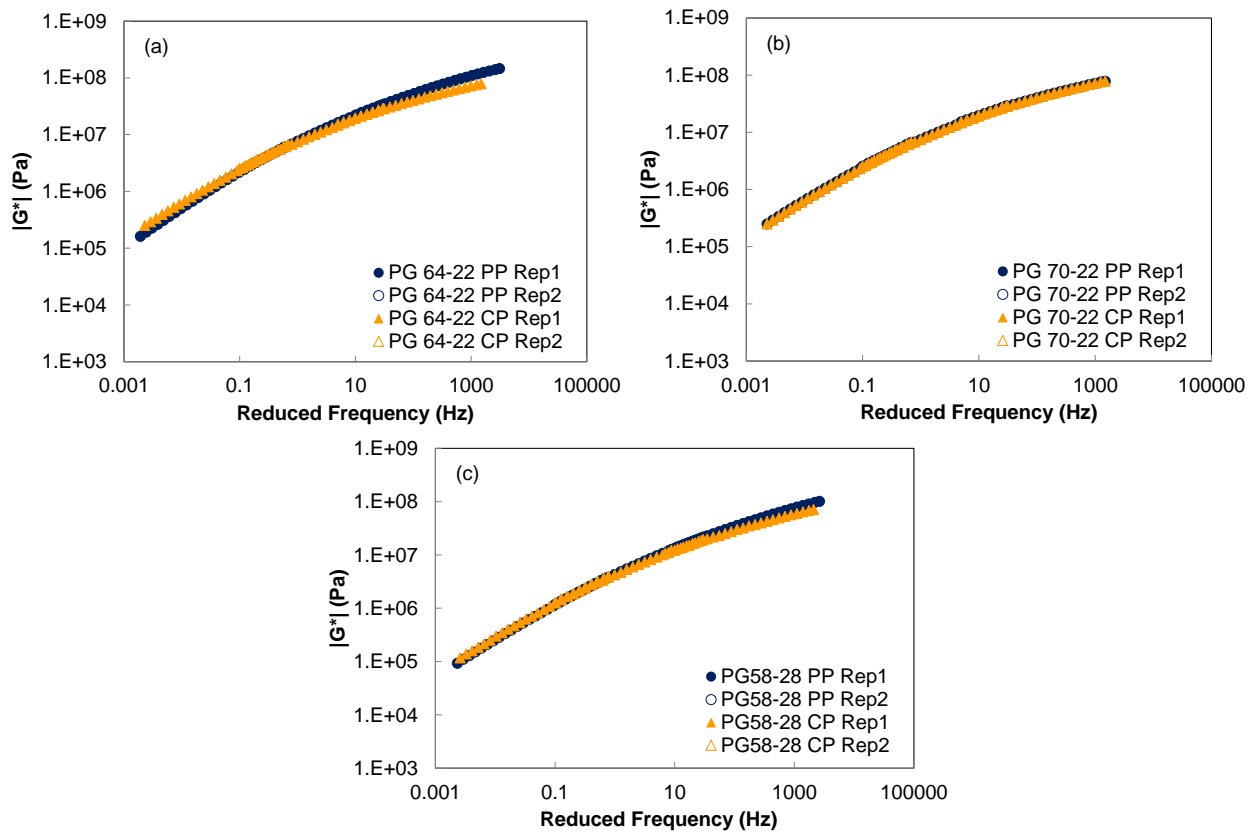


Figure 6-4. Comparison of the mastercurves at 1 percent strain amplitude for CP and PP geometries for a) PG 64-22 b) PG 70-22 c) PG 58-28.

6.5.2 RSS Test Results

Because fatigue tests are conducted at strain amplitudes within the NLVE regime, the nonlinear dynamic shear modulus, $/G^*/_{NLVE}$, as a function of strain must be determined for calculation of NLVE pseudostrain in S-VECD analysis. RSS tests were used to determine $/G^*/_{NLVE}$ using both the cone and plate and parallel plate geometries. First, damage and NLVE effects on the measured response were isolated using the procedure recommended by Underwood and Kim (2015). Subsequently, the peak edge stress in parallel plate RSS test results were calculated using Equation (6.8). The comparison between the corrected $/G^*/_{NLVE}$ results at 20°C acquired from RSS testing using the parallel plate geometry are compared to the corresponding cone and plate results in Figure 6-5. The corrected parallel plate results show good agreement to the results acquired from cone and plate testing, therefore validating the use of Equation (6.8).

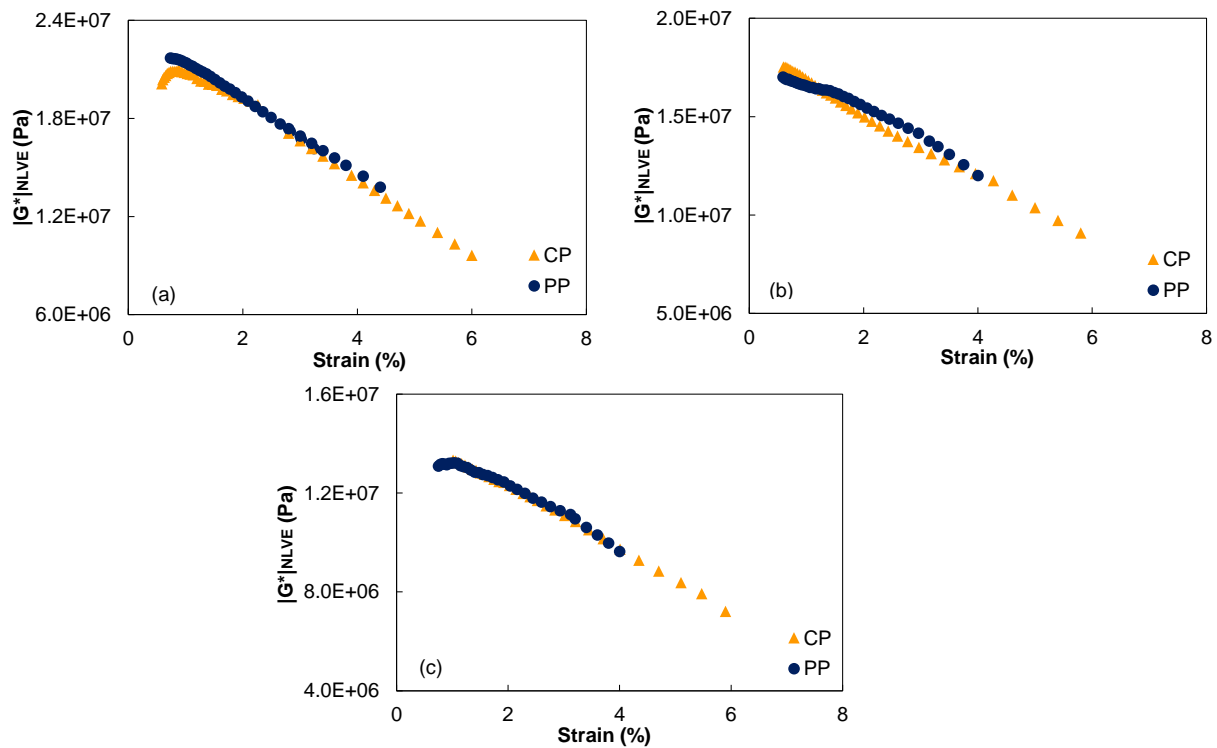


Figure 6-5. Comparison of modified parallel plate and cone and plate $|G^*|_{NLVE}$ for (a) PG 64-22 (b) PG 70-22 (c) PG 58-28 at 20°C.

6.5.3 Cone and Plate Fatigue Test Results

6.5.3.1 Failure Mechanism

In tests where asphalt binder is subjected to cyclic loading in the DSR using cone and plate geometry, there is a uniform stress state, and thus, distributed microcracks are expected to develop throughout the sample as it undergoes fatigue. A photograph of a samples following fatigue testing using the cone and plate geometry is shown in Figure 6-6. The photo was obtained by freezing the specimen following testing and then detaching the spindle using procedure proposed by Hintz and Bahia (2013). As expected, the failure surface shows evidence of damage throughout the sample in contrast to the fracture morphology shown in Figure 6-2 where there is clear evidence of cracks that initiate at the specimen edge and propagate inward.

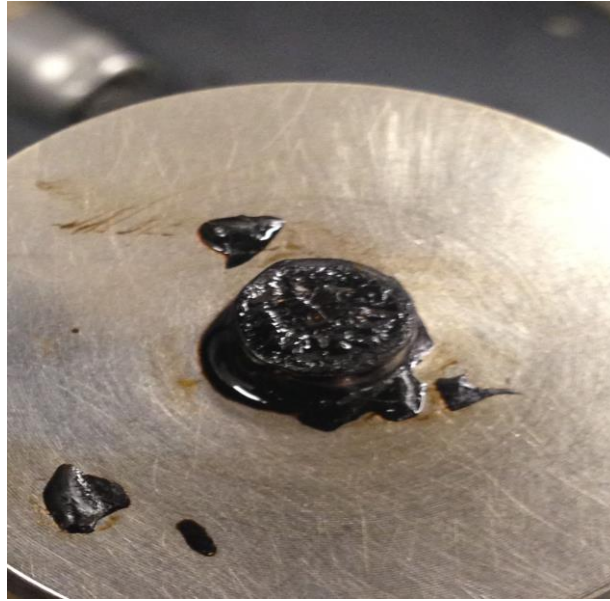


Figure 6-6. Failure surface cone and plate geometry.

6.5.3.2 Failure Definition

A clear means to define failure is an important component of fatigue characterization. The typical C^* evolution in TS test results are shown in Figure 6-7. It can be seen that the rate of change in C^* decreases as the test proceeds. Note that tests were conducted for over 10 hours to determine whether C^* would eventually show evidence of a clear failure point but a sudden drop in C^* was never observed. The observed C^* versus N evolution is similar to those in controlled on-specimen strain amplitude cyclic uniaxial tension tests conducted on asphalt mixtures. Results in Figure 6-7 show that initially and terminally, C^* versus N is linear. Therefore, a bisectional approach was used to define fatigue failure in test results as illustrated in Figure 6-7. The bisectional approach involves finding the intersection between the initial and terminal C^* versus N tangents. A similar bisectional approach was used to define fatigue failure in asphalt mixture testing by (Kim et al. (2005)).

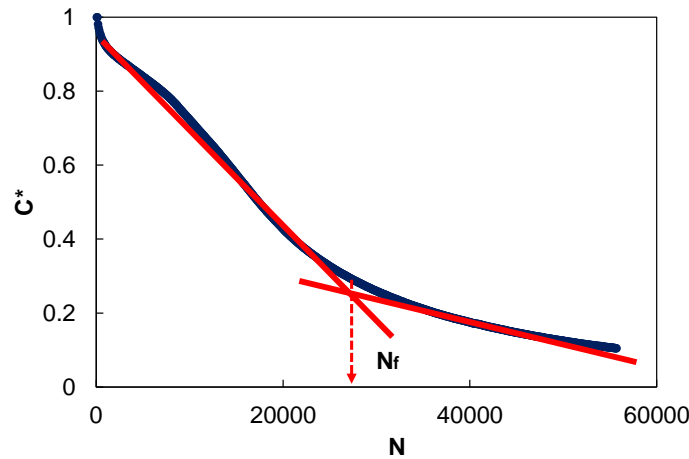


Figure 6-7. Determination of failure point for PG 64-22 TS at 20°C at 4% strain amplitude.

6.5.3.3 Applicability of S-VECD Model to Time Sweep Test Results

To evaluate the applicability of S-VECD model to the asphalt binders tested under TS test in the DSR using cone and plate geometry, damage characteristic curves were constructed using a reference temperature of 20°C for all the tested binders. RSS test results were used to determine $|G^*|_{NLVE}$ values corresponding to the TS strain amplitudes and temperatures. These results were used to calculate nonlinear pseudostrain within the S-VECD framework. The linear viscoelastic time-temperature shift factors determined from the frequency sweep tests were used to shift the TS data collected at temperatures other than 20°C to the reference temperature. Figure 6-8 demonstrates that the damage characteristic curves for a given binder are the same, irrespective of temperature and loading history, thereby verifying the applicability of S-VECD modeling to TS test results using cone and plate geometry.

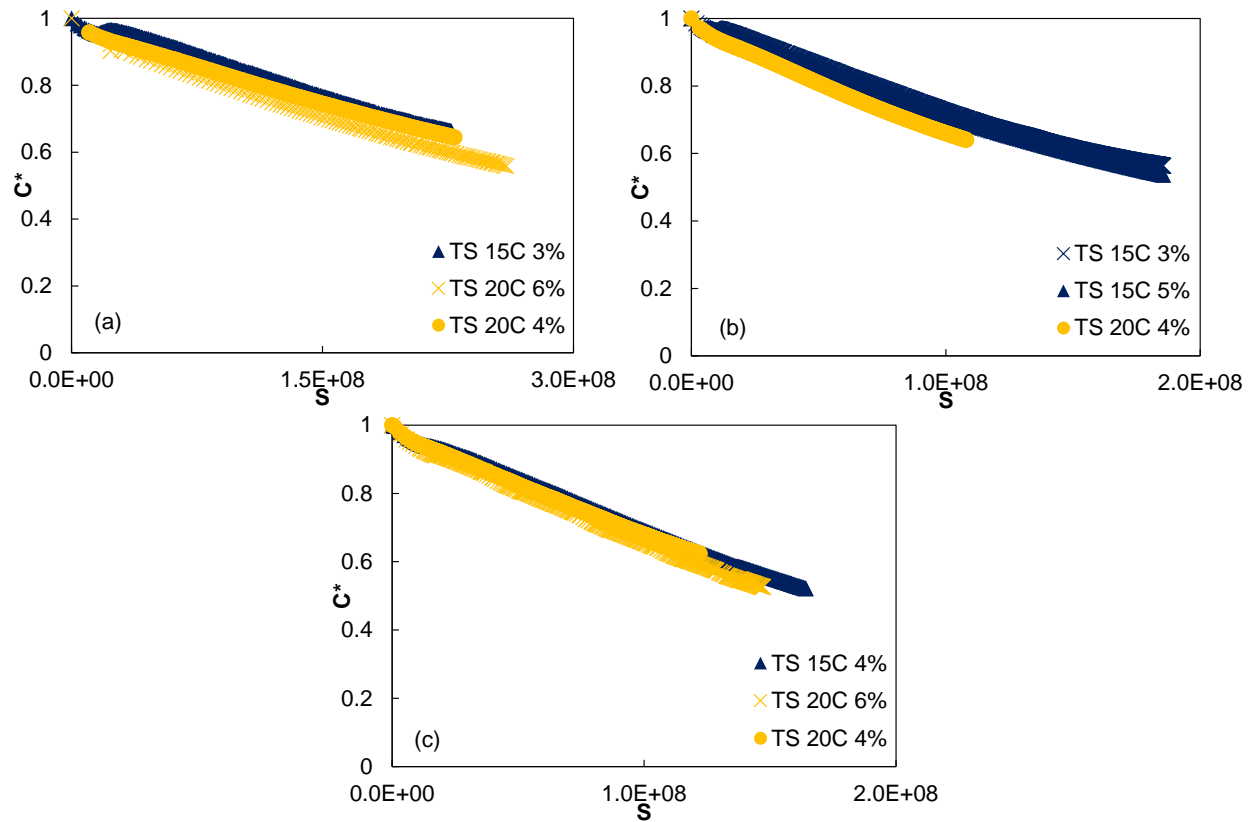


Figure 6-8. S-VECD damage characteristic curves for TS at the reference temperature of 20°C for (a) PG 64-22 (b) PG 70-22 (c) PG 58-28.

6.5.3.4 Failure Criteria

The G^R versus N_f failure criterion, derived from TS tests, is shown in Figure 6-9 for each binder tested. The results demonstrate that a unique relationship exists between G^R and N_f that is independent of loading history and temperature, validating the use of the failure criteria.

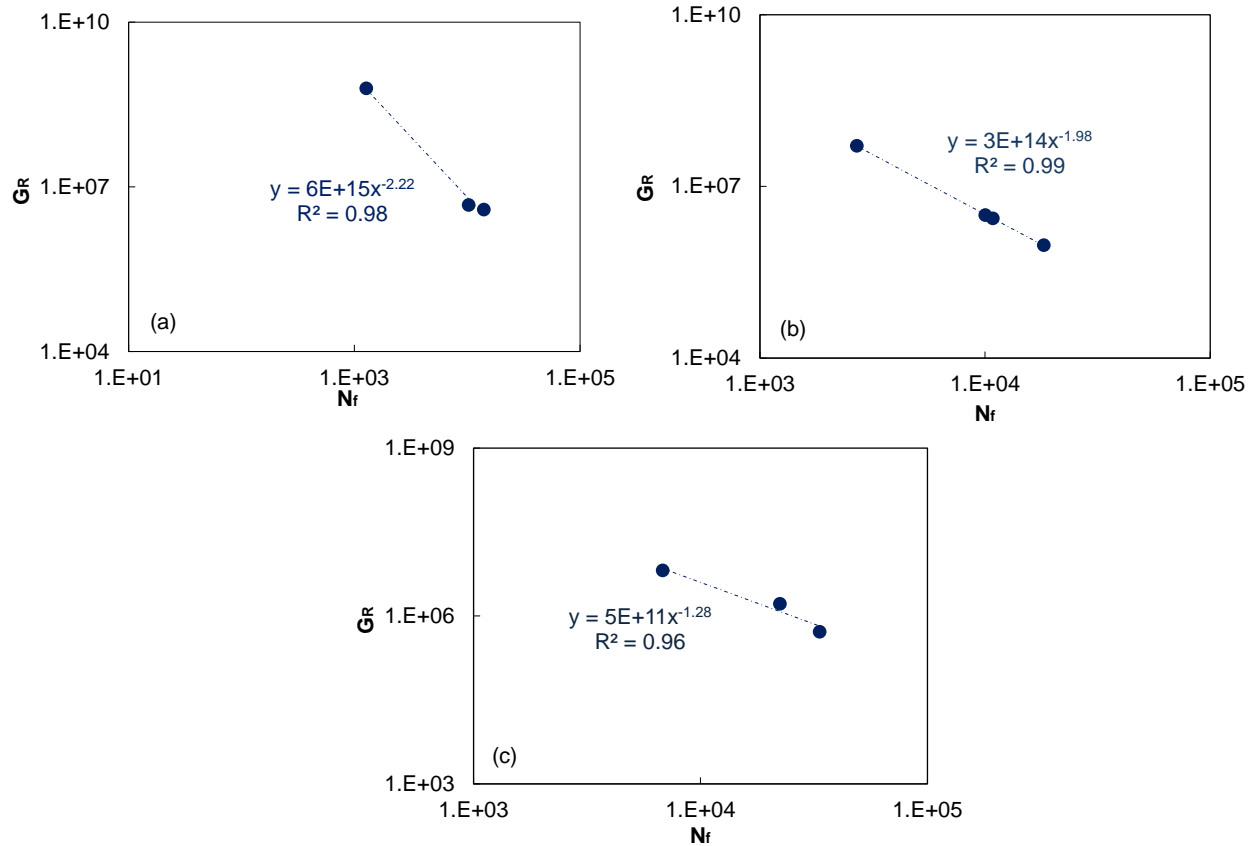


Figure 6-9. G^R vs. N_f for (a) PG 64-22 (b) PG 70-22 (c) PG 58-28.

6.5.3.5 Model Verification

The S-VECD model derived from cone and plate TS test results was verified before extending for the prediction of torque evolution in parallel plate TS tests. In order to verify the S-VECD model for performance predictions, the results from the TS tests were used to fit the damage characteristic curves and failure criterion models given in Equations (6.15) and (6.22), respectively. The ability of the S-VECD model to predict C^* evolution in the cone and plate TS tests was evaluated using Equation (6.19). Note that when Equation (6.19) is applied to cone and plate tests, there is no variation with radial distance from the specimen center, r because the strain field is uniform. In addition, optimized model coefficients were input into Equation (6.23)

in order to predict the fatigue life that corresponds to the strain amplitude and temperatures of the TS tests. The comparison between measured and predicted C^* evolution is shown for the PG 64-22 binder for a TS test conducted at 20°C and 4 percent strain amplitude is shown in Figure 6-10. The comparison between measured and predicted fatigue lives is shown in Figure 6-11. The results demonstrate good agreement between the measured and predicted C^* evolution and fatigue lives ($R^2 = 0.92$), thus providing verification that the S-VECD model coupled with cone and plate cone and plate TS tests results can be used as a tool to predict binder fatigue life.

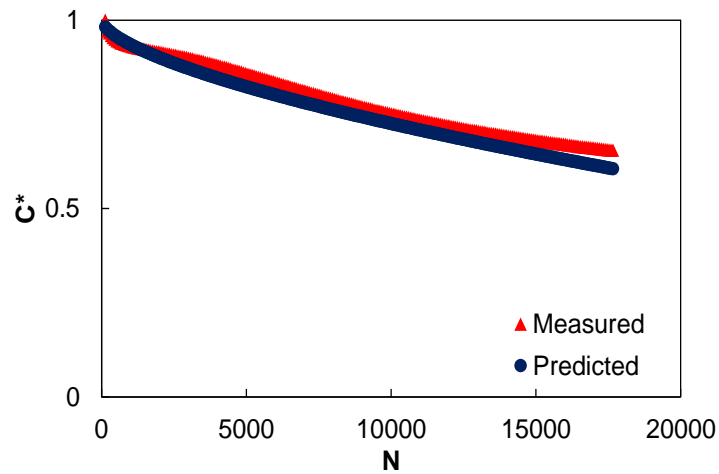


Figure 6-10. Measured vs. predicted C^* vs. N for TS test for PG 64-22 at 20°C, 4% strain.

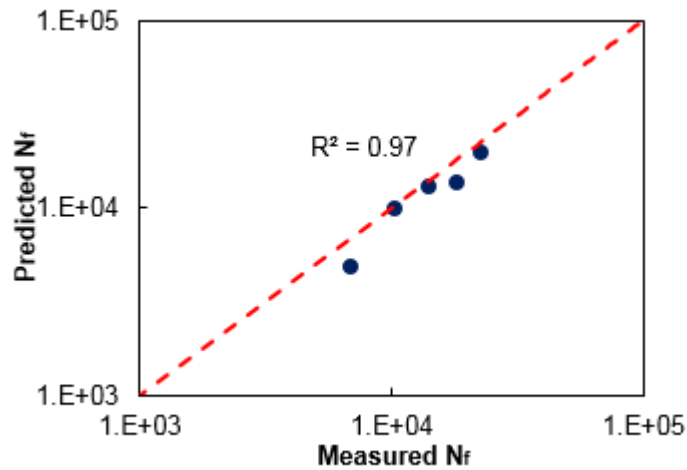


Figure 6-11. Comparison of measured and predicted fatigue lives using S-VECD model derived from the cone and plate geometry.

6.5.4 Prediction of Parallel Plate Torque Evolution S-VECD Calibrated using Cone and Plate (Forward Analysis)

After verifying the predictive capabilities of the S-VECD model derived from cone and plate test results, the framework presented in section 6.3.6 was applied to predict torque evolution in parallel plate TS tests. To apply the prediction framework, the $|G^*/NLVE$ values as a function of strain amplitude from RSS testing were used coupled with the S-VECD damage characteristic curve coefficients in Equation (6.15) calibrated using cone and plate TS test results. Example results showing the predicted evolution of shear stress as a function of radial location is presented in Figure 6-12. It can be seen that initially, that the calculation of shear stress at the sample edge using linear mapping to the total torque may not result in significant error. However, as the number of loading cycles and thus, fatigue damage increases, it can be seen that there is clearly a nonlinear relationship between the shear stress and radially location.

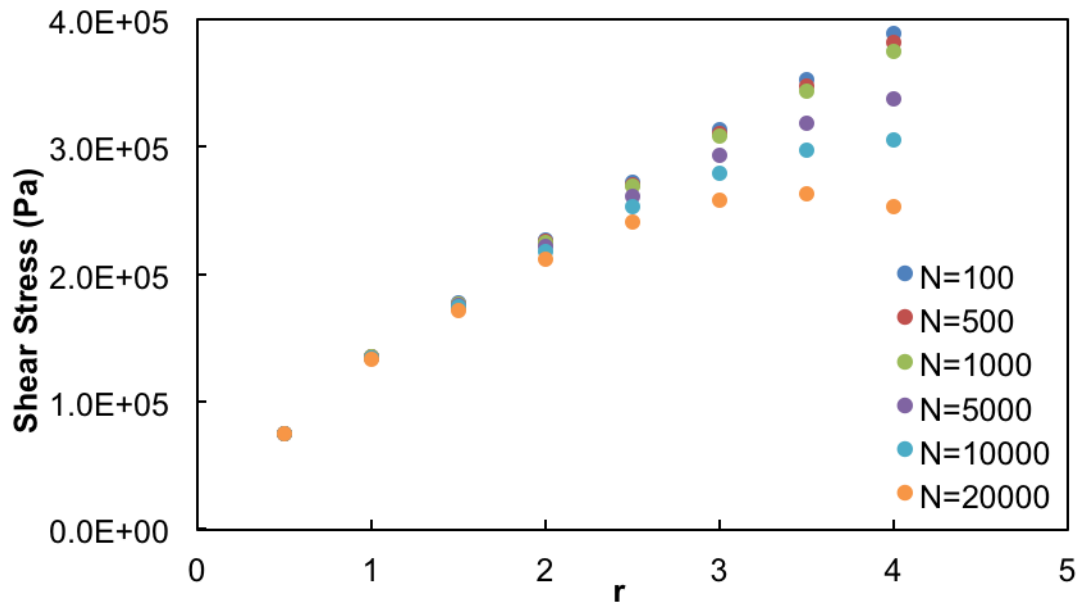


Figure 6-12. Shear stress distribution within parallel plate geometry for TS PG 58-28 at 20°C and 3% strain.

The comparison between measured torque evolution in parallel plate TS tests and the predicted torque evolution using the S-VECD model calibrated using cone and plate TS test results for each of the binders evaluated in this study is shown in Figure 6-13. Note that the torque evolution was predicted up to the failure point. The failure point is defined at the edge of the parallel plate test results based on the observed point of failure in cone and plate results using the bisectional method. Generally, the results in Figure 6-13 demonstrate that the measured and predicted torque evolution are in good agreement for the majority of the loading history with a minor deviation near the point of failure, possibly resulting from a nonlinear radial gradient in shear stress due to the presence of macrocracks. These results provide validation for the proposed framework to account for the nonlinear radial distribution in shear stress during parallel plate TS tests.

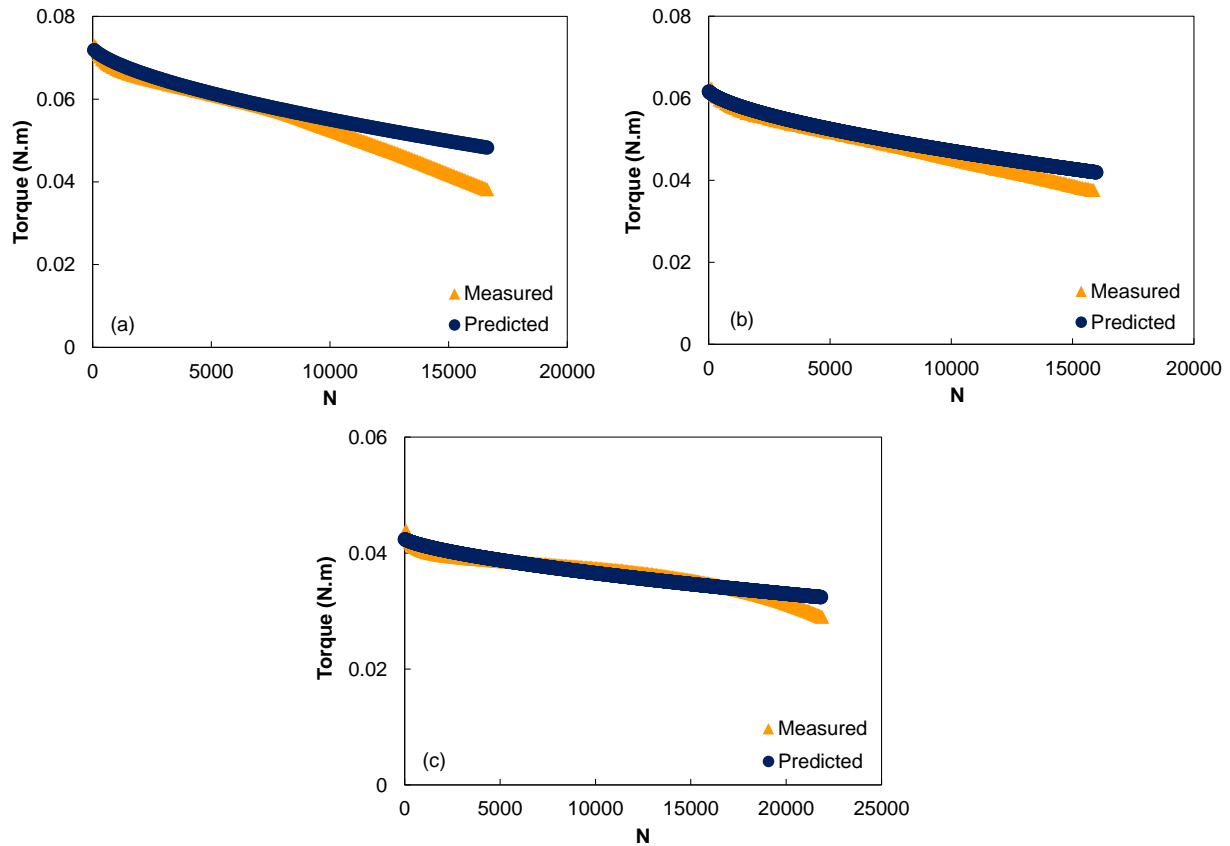


Figure 6-13. Comparison of measured and predicted torque 20°C for (a) PG 64-22 TS 4% strain (b) PG 70-22 TS 3% strain (c) PG 58-28 TS 4% strain.

6.5.5 Use of Parallel Plate Torque Evolution to Calibrate S-VECD Model (Backwards Analysis)

6.5.5.1 Calibration

After validating the S-VECD-based framework to account for the nonlinear variation in shear stress with radial location in parallel plate TS tests using the cone and plate test results, the ability to obtain S-VECD damage characteristic curve model parameters and failure criteria using parallel plate TS test results was assessed. To do so, the damage characteristic curve model parameters in Equation (6.15) were first calibrated using the torque evolution measured from

parallel plate TS tests. The comparison between damage characteristic curves obtained from cone and plate and parallel plate analysis is presented in Figure 6-14. Data is included up to the point of failure, selected using bisectional method based on predicted C^* evolution at the specimen edge for parallel plate. The good agreement between predicted and measured demonstrates that the presented framework can be used to calibrate the S-VECD model using torque evolution in parallel plate TS tests.

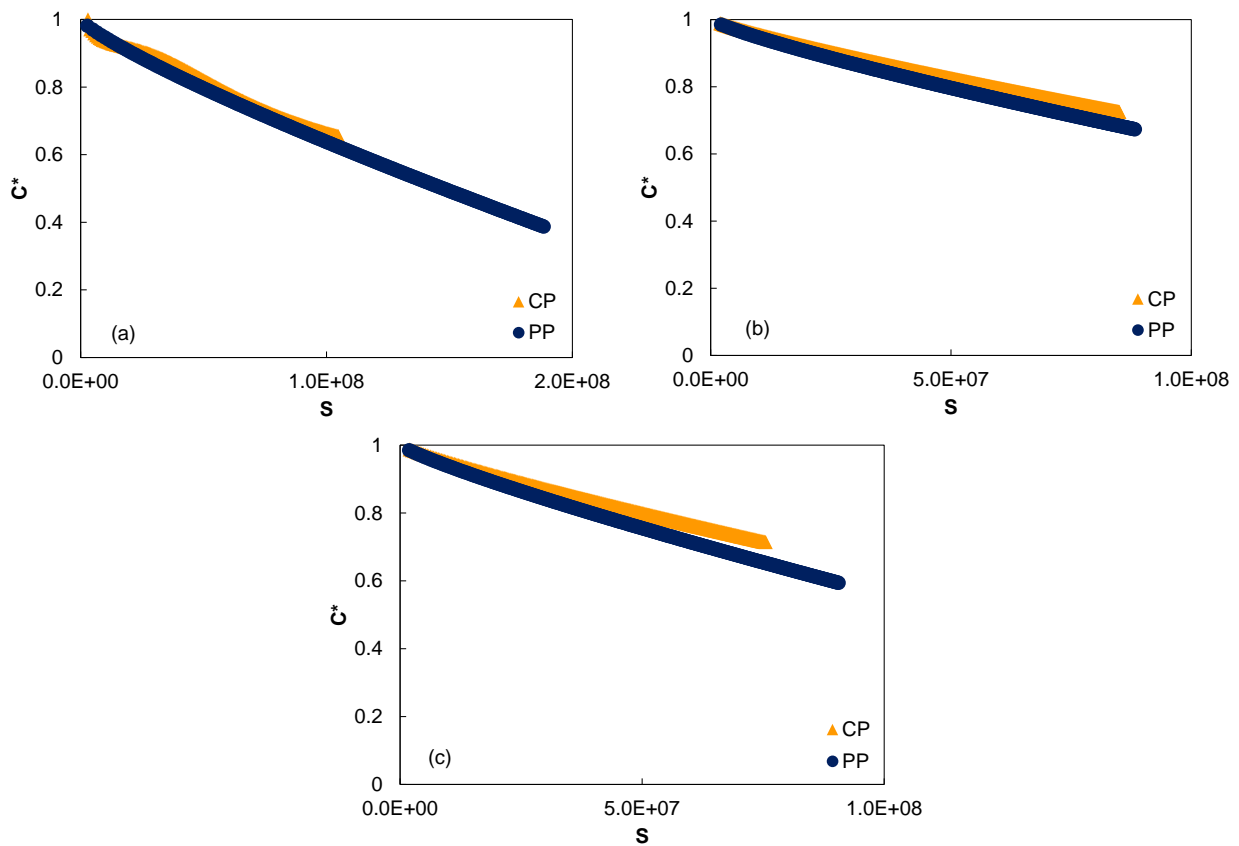


Figure 6-14. Comparison of damage curves from cone and plate and parallel plate testing for (a) PG 64-22 TS 4% strain (b) PG 70-22 TS 3% strain (c) PG 58-28 TS 4% strain at 20°C.

The comparison between failure criteria obtained from cone and plate testing and parallel plate testing is shown in Figure 6-15. Note that the failure criteria obtained from parallel plate testing was obtained after calibrating the damage characteristic curve model parameters.

Subsequently, C^* versus N was predicted at the specimen edge and the bisectional approach was used to determine the failure point. The results demonstrate reasonable agreement between the failure criteria obtained using cone and plate and parallel plate TS tests. However, fatigue life predictions are needed to determine the significance of the observed discrepancy in failure criteria.

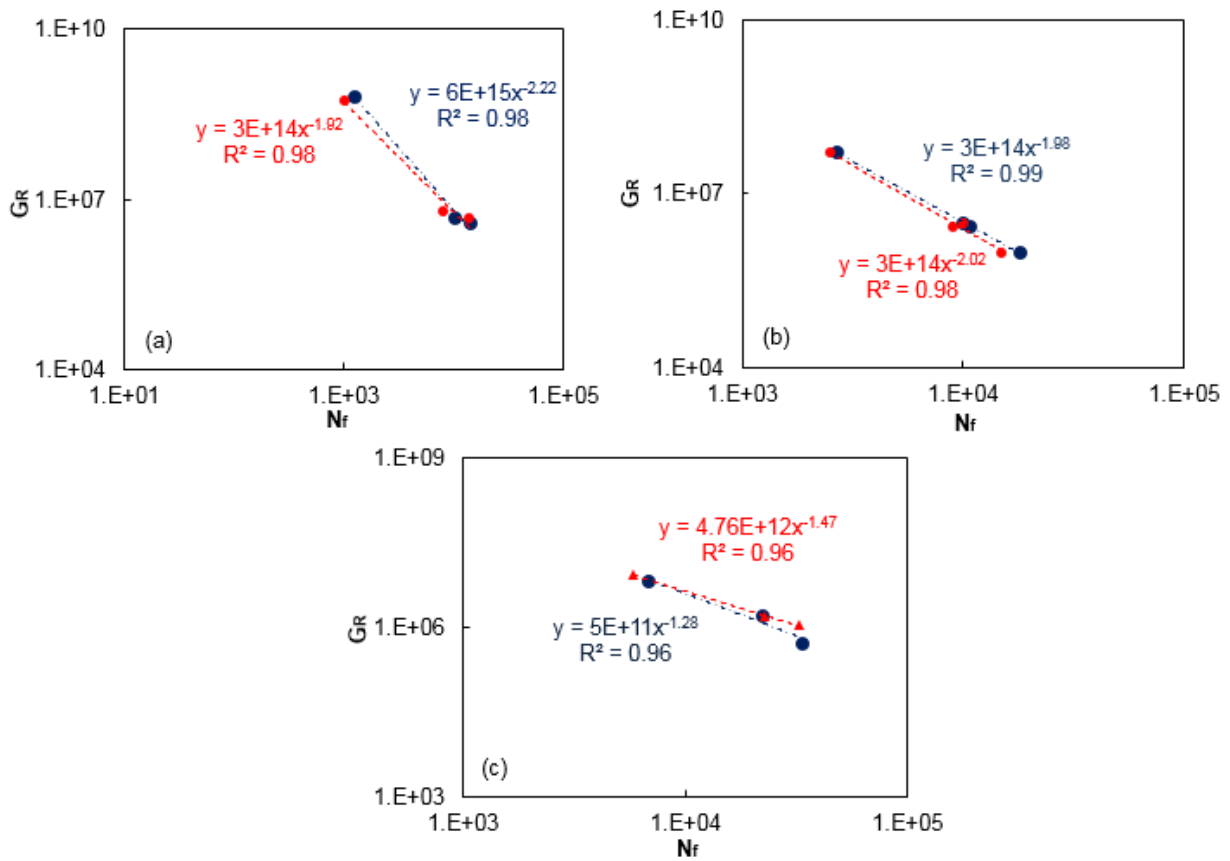


Figure 6-16. Comparison of failure criteria from cone and plate and parallel plate testing for (a) PG 64-22 (b) PG 70-22 (c) PG 58-28.

6.5.5.2 Validation

To validate the prediction method for inclusion of nonlinear radial stress gradient in S-VECD analysis, fatigue lives (N_f) were predicted using the S-VECD and failure criteria calibrated using parallel plate test results and compared to fatigue lives measured from cone and

plate tests. Figure 6-15 shows that the methodology developed to interpret parallel plate test results allows for accurate fatigue life prediction at a given strain amplitude.

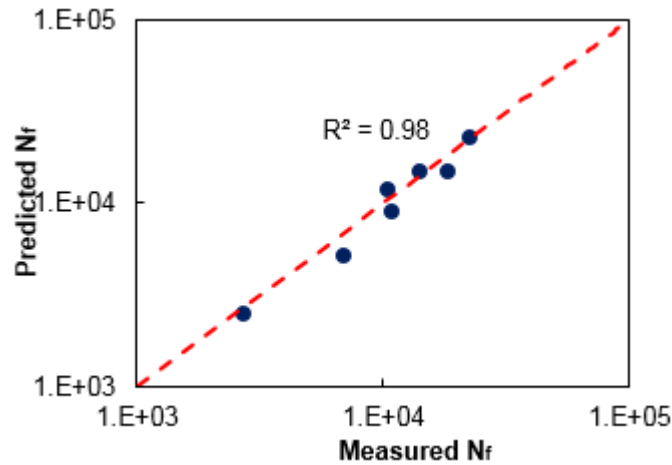


Figure 6-15. Comparison of predicted fatigue lives using parallel plate versus measured fatigue lives in cone and plate.

6.6 Conclusions

The following conclusions can be drawn from this study:

1. The nonlinear dynamic shear modulus of asphalt binders can accurately be obtained using parallel plate Repeated Stress Sweep (RSS) test results if the correction proposed by Ng et al. (2011) is applied to obtain the true edge stress. The RSS can be used to elucidate dynamic shear moduli at intermediate temperatures up to approximately 6 percent strain amplitude.
2. The S-VECD model applies to cone and plate TS test results. Cone and plate testing can be used to accurately calibrate S-VECD model parameters.
3. Alternatively, the torque evolution in parallel plate TS tests can be used to calibrate S-VECD model parameters accurately. The S-VECD model calibrated using parallel plate test results provides accurate prediction of fatigue life under variable strain amplitude conditions.

CHAPTER 7 CONCLUSIONS AND RECOMMENDATIONS

The main contribution of this research are summarized as below:

- The derivation and assessment of a Simplified Viscoelastic Continuum Damage (S-VECD) modeling framework to asphalt binder fatigue test results including assessment of the model's ability to capture the effects of loading history, temperature, and loading mode was performed in a rigorous manner.
- The developed framework was validated through comparison to asphalt mixture S-VECD model results derived from cyclic direct tension tests and measured pavement performance obtained from the Federal Highway Administration (FHWA 2006) Accelerated Loading Facility (ALF).
- An improved framework to select asphalt binder fatigue test temperatures was developed based on climatic Performance Grade (PG) that reflects critical climatic conditions and will ensure cohesive cracking failure.
- Repeated Stress Sweeps (RSS) can be used to determine dynamic shear moduli accurately at intermediate temperatures for strain amplitudes less than six percent. However, implementation of the RSS test requires a trial and error procedure to determine the stress sweep conditions that will yield data where damage and NLVE behavior can be distinguished. Therefore, it is recommended that future research be dedicated to developing a practical alternative to RSS testing.
- Nonlinear viscoelasticity should be considered when applying S-VECD modeling to asphalt binder fatigue.

- The S-VECD model, derived using RSS and TS test results, can be used to back-calculate the nonlinear dynamic shear modulus in Linear Amplitude Sweep (LAS) test results. The back-calculation approach allows for determining the nonlinear dynamic shear modulus at higher strain amplitudes than can be elucidated using RSS testing.
- Nonlinear dynamic shear moduli cannot be determined using LAS testing alone, thereby making consideration of nonlinear viscoelasticity in S-VECD modeling impractical for routine specification use. The linear viscoelasticity-based S-VECD model applied to LAS test results, while less accurate, and still provides a good indication of the relative fatigue performance of binders. Therefore, two levels of testing to characterize the fatigue resistance of asphalt binder are proposed in Table 7-2, with varying levels of accuracy and practicality. For the secondary level, the LAS testing coupled with linear viscoelasticity-based S-VECD analysis is recommended and merits further consideration for incorporation into future binder fatigue specifications. The primary level includes the nonlinear S-VECD model and is recommended if rigorous modeling is conducted using asphalt binder fatigue test results (e.g., within a multi-scale model to predict pavement fatigue).
- An improved means for interpreting parallel plate DSR cyclic fatigue tests was developed that considers the nonlinear radial gradient in stress response. To apply the method, the torque evolution in parallel plate TS tests is used to calibrate S-VECD model parameters. The S-VECD model calibrated using parallel plate test results provides accurate prediction of fatigue life under variable strain amplitude conditions.

REFERENCES

- AASHTO, MPI-93 IA Edition (2008). Standard Specification for Performance Graded Asphalt Binder. *AASHTO Provisional Standards*, Washington, DC.
- AASHTO, M332 (2014). Standard Specification for Performance-Graded Asphalt Binder Using Multiple Stress Creep Recovery (MSCR) Test. *American Association of State Highway and Transportation Officials*, Washington, DC.
- AASHTO, M320 (2016). Standard specification for performance graded asphalt binder. *American Association of State Highway and Transportation Officials*, Washington, DC.
- AASHTO, PP 61-09 (2009). Standard practice for mixture conditioning of hot mix asphalt. *American Association of State Highway and Transportation Officials*, Washington, DC.
- AASHTO, R 3 (2006). Standard practice for mixture conditioning of hot mix asphalt. *American Association of State Highway and Transportation*, Washington, DC.
- AASHTO, TP 107-14 (2014). Determining the Damage Characteristics Curve of Asphalt Mixtures from Direct Tension Cyclic Fatigue Test. *American Association of State Highway and Transportation Officials*, Washington, DC.
- AASHTO, TP 101 (2014). Estimating Damage Tolerance of Asphalt Binders Using the Linear Amplitude Sweep. *AASHTO Provisional Standards*, Washington, DC.
- Airey, G. D., B. Rahimzadeh and A. C. Collop (2004). Linear rheological behavior of bituminous paving materials. *Journal of Materials in Civil Engineering*, 16(3): 212-220.
- Al-Khateeb, G. G. and K. A. Ghuzlan (2014). The combined effect of loading frequency, temperature, and stress level on the fatigue life of asphalt paving mixtures using the IDT test configuration. *International Journal of Fatigue*, 59: 254-261.
- Anderson, D., Y. Hir, M. Marasteanu, J.-P. Planche, D. Martin and G. Gauthier (2001). Evaluation of fatigue criteria for asphalt binders. *Transportation Research Record: Journal of the Transportation Research Board*, 1766: 48-56.
- Anderson, D. A., D. W. Christensen, H. U. Bahia, R. Dongre, M. Sharma, C. E. Antle and J. Button (1994). Binder characterization and evaluation, volume 3: Physical characterization. *Strategic Highway Research Program, National Research Council*, Report No. SHRP-A-369.
- Bahia, H. U., D. Hanson, M. Zeng, H. Zhai, M. Khatri and R. Anderson (2001). Characterization of modified asphalt binders in superpave mix design. Report No. 459, *National Cooperative Highway Research Program Report, National Research Council*, ISSN 0077-5614.

Bahia, H. U., H. Zhai, K. Bonnetti and S. Kose (1999). Non-linear viscoelastic and fatigue properties of asphalt binders. *Journal of the Association of Asphalt Paving Technologists*, 68: 1-34.

Bahia, H. U., H. Zhai, M. Zeng, Y. Hu and P. Turner (2001). Development of binder specification parameters based on characterization of damage behavior. *Association of Asphalt Paving Technologists Technical Sessions*, 70: 442-470.

Bodin, D., J. Terrier, C. Perroteau, P. Hornych and P. Marsac (2010). Effect of temperature on fatigue performances of asphalt mixes. *Proceedings of the 11th International conference on asphalt pavements*.

Bonaquist, R. F. (2011). Mix design practices for warm mix asphalt. Report No. 691, *National Cooperative Highway Research Program Report, National Research Council*.

Branco, V. T. F. C. (2008). A unified method for the analysis of nonlinear viscoelasticity and fatigue cracking of asphalt mixtures using the dynamic mechanical analyzer. *PhD Dissertation, Texas A&M University*.

Chehab, G., Y. Kim, R. Schapery, M. Witczak and R. Bonaquist (2002). Time-temperature superposition principle for asphalt concrete with growing damage in tension state. *Journal of the Association of Asphalt Paving Technologists*, 71: 559-593.

Christensen, D. W. and D. A. Anderson (1992). Interpretation of dynamic mechanical test data for paving grade asphalt cements. *Journal of the Association of Asphalt Paving Technologists*, 61: 67-116.

Daniel, J. S. and Y. R. Kim (2002). Development of a simplified fatigue test and analysis procedure using a viscoelastic, continuum damage model. *Journal of the Association of Asphalt Paving Technologists*, 71: 619-650.

de Souza Mendes, P. R., A. A. Alicke and R. L. Thompson (2014). Parallel-plate geometry correction for transient rheometric experiments. *Journal of Applied Rheology*, 24(5): 52721.

Delgadillo, R. (2008). Nonlinearity of asphalt binders and the relationship with asphalt mixture permanent deformation. *PhD Dissertation, University of Wisconsin - Madison*.

Drakos, C., R. Roque and B. Birgisson (2001). Effects of measured tire contact stresses on near-surface rutting. *Transportation Research Record, Journal of the Transportation Research Board*, 1764: 59-69.

Farrar, M., T. Turner, J.-P. Planche, J. Schabron and P. Harnsberger (2013). Evolution of the crossover modulus with oxidative aging: Method to estimate change in viscoelastic properties of asphalt binder with time and depth on the road. *Transportation Research Record: Journal of the Transportation Research Board*, 2370: 76-83.

Status of the Nation's Highways, Bridges, and Transit: Conditions and Performance (2006). *US Department of Transportation*.

Gibson, N. H. (2010). Summary of Binder Fatigue Findings from FHWA-ALF. Irvine, California, *Presented at the Binder Expert Task Group Meeting*.

Haggag, M., W. Mogawer and R. Bonaquist (2011). Fatigue evaluation of warm-mix asphalt mixtures: Use of uniaxial, cyclic, direct tension compression test. *Transportation Research Record, Journal of the Transportation Research Board*, 2208: 26-32.

Hellström, L. H. O., M. A. Samaha, K. M. Wang, A. J. Smits and M. Hultmark (2014). Errors in parallel-plate and cone-plate rheometer measurements due to sample underfill. *Measurement Science and Technology*, 26(1): 015301.

Hintz, C. and H. Bahia (2013). Understanding mechanisms leading to asphalt binder fatigue in the dynamic shear rheometer. *Road Materials and Pavement Design*, 14: 231-251.

Hintz, C., R. Velasquez, C. Johnson and H. Bahia (2011). Modification and validation of linear amplitude sweep test for binder fatigue specification. *Transportation Research Record, Journal of the Transportation Research Board*, 2207: 99-106.

Hintz, C., R. Velasquez, Z. Li and H. Bahia (2011). Effect of oxidative aging on binder fatigue performance. *Journal of the Association of Asphalt Paving Technologists*, 80: 527-548.

Huang, Y. H. (1993). *Pavement analysis and design*. Pearson, New York, NY.

Jin, X., R. Han, Y. Cui and C. J. Glover (2011). Fast-rate–constant-rate oxidation kinetics model for asphalt binders. *Industrial & Engineering Chemistry Research*, 50(23): 13373-13379.

Johnson, C., H. Bahia and H. Wen (2009). Practical application of viscoelastic continuum damage theory to asphalt binder fatigue characterization. *Asphalt Paving Technology-Proceedings*, 28: 597-638.

Johnson, C. M. (2010). Estimating asphalt binder fatigue resistance using an accelerated test method. *PhD Dissertation*, University of Wisconsin - Madison.

Kim, Y.-R. and D. Little (2004). Linear viscoelastic analysis of asphalt mastics. *Journal of Materials in Civil Engineering*, 16(2): 122-132.

Kim, Y. (2012). MEPDG inputs for warm mix asphalt. *Final Report to NCDOT*, Report No. FHWA/NC/2012-01.

Kim, Y., S. Lee, Y. Seo and O. El-Haggan (2005). Impact of Price Reductions on the Long-Term Pavement Performance of HMA Mixes in North Carolina. *Final Report to NCDOT*, Report No. FHWA/NC/2005-09.

Kim, Y. and B. Underwood (2010). S-VECD fatigue test protocol and analysis software. *Asphalt Mixture and Construction Expert Task Group Meeting*, Irvine, California.

Kim, Y. R. and D. N. Little (1990). One-dimensional constitutive modeling of asphalt concrete. *Journal of Engineering Mechanics*, 116(4): 751-772.

Kluttz, B., C. Castorena, S. Puchalski and A. Andriescu (2014). Recent developments in asphalt binder linear amplitude sweep (LAS) test. *51st Peterson Asphalt Research Conference*, Laramie, Wyoming.

Koenders, B., D. Stoker, C. Bowen, P. De Groot, O. Larsen, D. Hardy and K. Wilms (2000). Innovative process in asphalt production and application to obtain lower operating temperatures. *2nd Eurasphalt & Eurobitumen Congress*, Barcelona, Spain, Citeseer.

Kose, S. (2002). Development of a virtual test procedure for asphalt concrete. *PhD Dissertation*, University of Wisconsin - Madison.

Kose, S. and H. Bahia (2002). Analysis of high volume fraction irregular particulate damping composites. *Journal of Engineering Materials and Technology*, 124(2).

Kose, S., M. Guler, H. Bahia and E. Masad (2000). Distribution of strains within hot-mix asphalt binders: applying imaging and finite-element techniques. *Transportation Research Record, Journal of the Transportation Research Board*, 1728: 21-27.

Kutay, M. E., N. H. Gibson and J. Youtcheff (2008). Conventional and viscoelastic continuum damage (VECD)-based fatigue analysis of polymer modified asphalt pavements. *Journal of the Association of Asphalt Paving Technologists*, 77: 395-433.

Kvasnak, A., A. Taylor, J. Signore and S. Bukhari (2010). Evaluation of gencor green machine ultrafoam GX. *Final Report to NCAT*, National Center for Asphalt Technology Report 10-03.

Lee, H.-J. and Y. R. Kim (1998). Viscoelastic continuum damage model of asphalt concrete with healing. *Journal of Engineering Mechanics*, 124(11): 1224-1232.

Lee, J.-S. and Y. Kim (2014). Performance-based moisture susceptibility evaluation of warm-mix asphalt concrete through laboratory tests. *Transportation Research Record, Journal of the Transportation Research Board*, 2446: 17-28.

Macosko, C. W. (1994). *Rheology: principles, measurements, and applications*. Wiley, New York, NY.

Martono, W. a. H. U. B. (2008). Considering Pavement Temperature and Structure in Defining Asphalt Binder Fatigue. *ASCE 18th engineering Mechanics Conference*.

Masad, E., C.-W. Huang, G. Airey and A. Muliana (2008). Nonlinear viscoelastic analysis of unaged and aged asphalt binders. *Construction and Building Materials*, 22(11): 2170-2179.

Masad, E., N. Somadevan, H. U. Bahia and S. Kose (2001). Modeling and experimental measurements of strain distribution in asphalt mixes. *Journal of Transportation Engineering*, 127(6): 477-485.

Monismith, C., J. Epps, D. Kasianchuk and D. McLean (1970). Asphalt mixture behavior in repeated flexure. Report TE 70-5, Institute of Transportation and Traffic Engineering, University of California, Berkeley.

Nelson, G., A. Shenoy, Q. Xicheng, S. Aroon, A. Ghazi, A. Adrian, S. Kevin, Y. Jack and H. Thomas. Performance testing for superpave and structural validation. *Federal Highway Administration*.

Ng, T. S., G. H. McKinley and R. H. Ewoldt (2011). Large amplitude oscillatory shear flow of gluten dough: A model power-law gel. *Journal of Rheology*, 55(3): 627-654.

Norouzi, A. and Y. Kim (2015). Mechanistic evaluation of fatigue cracking in asphalt pavements. *International Journal of Pavement Engineering*, 18: 530-546.

Park, S. W., Y. R. Kim and R. A. Schapery (1996). A viscoelastic continuum damage model and its application to uniaxial behavior of asphalt concrete. *Mechanics of Materials*, 24(4): 241-255.

Petersen, J., R. Robertson, J. Branthaver, P. Harnsberger, J. Duvall, S. Kim, D. Anderson, D. Christiansen and H. Bahia (1994). Binder characterization and evaluation: *Volume 1. Rep. No. SHRP-A-367, Strategic Highway Research Program*, National Research Council, Washington, DC.

Prowell, B. D., E. Brown, R. M. Anderson, J. S. Daniel, A. K. Swamy, H. Von Quintus, S. Shen, S. H. Carpenter, S. Bhattacharjee and S. Maghsoodloo (2010). Validating the fatigue endurance limit for hot mix asphalt. *TRB's National Cooperative Highway Research Program (NCHRP) Report 646*, National Research Council.

Rowe, G. (1993). Performance of asphalt mixtures in the trapezoidal fatigue test. *Asphalt Paving Technology*, 62: 344-344.

Sabouri, M. and Y. Kim (2014). Development of a failure criterion for asphalt mixtures under different modes of fatigue loading. *Transportation Research Record, Journal of the Transportation Research Board*, 2447: 117-125.

Safaei, F. and C. Castorena (2016). Temperature Effects of Linear Amplitude Sweep Testing and Analysis. *Transportation Research Record: Journal of the Transportation Research Board*, 2574: 92-100.

Safaei, F., C. Castorena and Y. R. Kim (2016). Linking asphalt binder fatigue to asphalt mixture fatigue performance using viscoelastic continuum damage modeling. *Mechanics of Time-Dependent Materials*, 20(3): 299-323.

- Safaei, F. and C. Hintz (2014). Investigation of the effect of temperature on asphalt binder fatigue. *Proceedings of the International Society for Asphalt Pavement Conference*.
- Safaei, F., J.S. Lee, L. A. H. d. Nascimento, C. Hintz and Y. R. Kim (2014). Implications of warm-mix asphalt on long-term oxidative ageing and fatigue performance of asphalt binders and mixtures. *Road Materials and Pavement Design*, 15: 45-61.
- Schapery, R. (1984). Correspondence principles and a generalized J integral for large deformation and fracture analysis of viscoelastic media. *International Journal of Fracture*, 25(3): 195-223.
- Schapery, R. (1990). A theory of mechanical behavior of elastic media with growing damage and other changes in structure. *Journal of the Mechanics and Physics of Solids*, 38(2): 215-253.
- Shan, L., S. Tian, H. He and N. Ren (2017). Internal crack growth of asphalt binders during shear fatigue process. *Fuel*, 189: 293-300.
- Shaw, M. T. and Z. Z. Liu (2006). Single-point determination of nonlinear rheological data from parallel-plate torsional flow. *Applied Rheology*, 16(2): 70-79.
- Soenen, H., C. De La Roche and P. Redelius (2004). Predict mix fatigue tests from binder fatigue properties, measured with a DSR. *Proceedings of the 3rd Eurasphalt and Eurobitume Congress*, Vienna.
- Soenen, H. and B. Eckmann (2000). Fatigue testing of bituminous binders with a dynamic shear rheometer. *Proceedings of the 2nd Eurasphalt and Eurobitume Congress*.
- Thompson, M. and S. Carpenter (2009). Perpetual pavement design: An overview. *Proceedings of the 2009 International Conference on Perpetual Pavement*.
- Underwood, B. S. (2011). Multiscale constitutive modeling of asphalt concrete. *PhD Dissertation*, North Carolina State University, Raleigh, NC.
- Underwood, B. S. (2016). A continuum damage model for asphalt cement and asphalt mastic fatigue. *International Journal of Fatigue*, 82: 387-401.
- Underwood, B. S. and Y. R. Kim (2015). Nonlinear viscoelastic analysis of asphalt cement and asphalt mastics. *International Journal of Pavement Engineering*, 16(6): 510-529.
- Underwood, B. S., Y. R. Kim and M. N. Guddati (2006). Characterization and performance prediction of ALF mixtures using a viscoelastoplastic continuum damage model. *Journal of the Association of Asphalt Paving Technologists*, 75, 577-636.
- Underwood, B. S., Y. R. Kim and M. N. Guddati (2010). Improved calculation method of damage parameter in viscoelastic continuum damage model. *International Journal of Pavement Engineering*, 11(6): 459-476.

Wang, C., C. Castorena, J. Zhang and Y. Richard Kim (2015). Unified failure criterion for asphalt binder under cyclic fatigue loading. *Road Materials and Pavement Design*, 16: 125-148.

Weissenberg, K. (1947). A continuum theory of rheological phenomena. *Nature*, 159(4035): 310-311.

Wen, H. and H. Bahia (2009). Characterizing fatigue of asphalt binders with viscoelastic continuum damage mechanics. *Transportation Research Record, Journal of the Transportation Research Board*, 2126: 55-62.

Wu, S., Q. Ye and N. Li (2008). Investigation of rheological and fatigue properties of asphalt mixtures containing polyester fibers. *Construction and Building Materials*, 22(10): 2111-2115.

Zapata, C. E. and W. N. Houston (2008). Calibration and validation of the enhanced integrated climatic model for pavement design. *National Cooperative Highway Research Program (NCHRP) Report 602*, National Research Council.